DESIGN, DEVELOPMENT AND OPTIMIZATION OF A FLEXIBLE NANOCOMPOSITE PROXIMITY SENSOR

by

Reza Moheimani

A Dissertation

Submitted to the Faculty of Purdue University

In Partial Fulfillment of the Requirements for the degree of

Doctor of Philosophy

School of Mechanical Engineering

West Lafayette, Indiana

May 2022

THE PURDUE UNIVERSITY GRADUATE SCHOOL
STATEMENT OF COMMITTEE APPROVAL

Dr. Hamid Dalir
School of Mechanical Engineering

Dr. Marcial Gonzalez
School of Mechanical Engineering

Dr. Saeed Mohammadi
School of Electrical and Computer Engineering

Dr. Andres Tovar
School of Mechanical Engineering

Approved by:
Dr. Nicole L. Key

This dissertation is dedicated

to my parents, Alieh and Saeid for their unconditional love, support and sacrifice

ACKNOWLEDGMENTS

The work presented in this report would not have been possible without the support and encouragement of many people. First, I would like to express my utmost appreciation to my advisors, Prof. Hamid Dalir and Prof. Marcial Gonzalez, for the continuous support, guidance, and encouragement throughout my study and research.

I thank the rest of my advisory committee: Prof. Saeed Mohammadi, and Prof. Andres Tovar, for their help, insightful comments, and valuable guidance.

I would like to thank all my past and present friends at the School of Mechanical Engineering for their help and support. Furthermore, I would like to extend my sincere respect and appreciation to my former colleague Dr. Nojan Aliahmad, who helped me to better understand electrostatic physics through his vast knowledge and intuition. I am also grateful for the inspiring support of my friends, Iman Fakhari and Saman Taheri, for their direction as to learn Machine Learning basics and optimization methods.

Most importantly, I would like to express my thanks to my beloved parents and my sister and brother for their support and encouragement throughout my time at Purdue. They have always been the strongest support to me, and they deserve my deepest appreciation for their love, devotion, and sacrifices.

TABLE OF CONTENTS

LIST OF TABLES

LIST OF FIGURES

NOMENCLATURE

Symbol	Units	Description
$V_0(x)$	V	Voltage distribution on the polymer substrate
λ_P	C.m^{-3}	Charge density per unit length stored on the polymer
λ_o	C.m^{-3}	Charge density per unit length stored on the object
I	Amp	Electrical current
ρ	Ohm.m	Resistance per unit length of the polymer substrate
d	cm	Object distance from sensor
z	cm	Height
a_n, b_n	-	Constant coefficient in the Fourie series
b	cm	The width
ε_0	Farads m^{-1}	Permittivity in vaccum
I_0	Amp	Currents passing through the substrate at $x = 0$
I_l	Amp	Currents passing through the substrate at $x = l$
l	cm	Length of substrate
V_{exc}	V	Voltage amplitude of the excitation
V_0	V	voltage distribution on the polymer substrate
R_{eq}	ohm	Equivalent resistance of the system
C_{eq}	Farad	Equivalent capacitance of the system
CNT	-	Carbon Nanotubes
TPU	-	Thermoplastic Polyurethane
IOT	-	Internet of things
CPS	-	Capacitive proximity sensors
MEMS	-	Micro-Electro-Mechanical System
CDC	-	Capacitance-to-digital converter
PCB	-	Printed Circuit Board
LCR	-	Inductance, capacitance, Resistance
PET	-	Polyethylene terephthalate
FPCB	-	Flexible printed circuit board
CNC	-	Cellulose nanocrystals
GO	-	Graphene oxide
$PDMS$	-	Polydimethylsiloxane
CMC	-	Carbon micro-coils
AgNWs	-	Silver nanowires
MWCNT	-	Multiwall carbon nanotube
ms	-	Millisecond
PET	-	Polyethylene terephthalate

ABSTRACT

Sensing systems have evolved significantly in recent years as a result of several advances in a number of sensor manufacturing approaches. The proximity measuring of approaching objects is a challenging, costly, and critical operation that permits the detection of any impediments without coming into touch with them and causing an unfavorable occurrence. However, developing a flexible proximity sensor capable of operating throughout a wide range of object motion continues to be a difficulty. The current work describes a polymer-based sensor that makes use of a nanostructure composite as the sensing element. The sensor will be used in healthcare and automotive applications in the near future. Composites comprising Thermoplastic Polyurethane (TPU) and Carbon Nanotubes (CNTs) are capable of sensing the presence of an external item at a great distance. The sensor model's performance was then enhanced further by microfabricating an integrated model with a certain shape. The design and production techniques for the TPU/CNTs proximity sensor are basic, and the sensor's performance demonstrates repeatability, as well as high electrical sensitivity and mechanical flexibility. The sensing process is based on the comparison of stored charges at the composite film sensor to the sensor's base voltage. The sensor operates reliably across a detection range of 2-20 cm. Tunneling and fringing effects are used to explain substantial capacitance shifts as sensing mechanisms. The structure's fringing capacitance effect has been thoroughly examined using ANSYS Maxwell (Ansoft) FEA simulation, as the measurements perfectly confirm the simulation's sensitivity trend. A novel mathematical model of fringe capacitance and subsequent tests demonstrate that the distance between an item and the sensor may be determined. Additionally, the model argues that the change in capacitance is significantly influenced by sensor resistivity, with the starting capacitance varying between 0.045pF and 0.024pF in the range 103-105 mm. This analytical model would enable the sensor's sensitivity to be optimized.

Additionally, a new generation of durable elastomeric materials is commercially accessible for 3D printing, allowing the development of an entirely new class of materials for wearable and industrial applications. By using functional grading and adjusting to diverse users, the mechanical reaction of soft 3D-printed objects may now be modified for increased safety and comfort. Additionally, electronics may be included into these 3D printed lattice and wearable structures to

offer input on the movement of objects associated with healthcare devices as well as automotive components. Thus, in order to investigate the influence of additive manufacturing on the sensitivity of TPU/CNT sensors, samples with equal thickness and size but varied orientations are printed and compared to hot-press samples. Among the many 3D printed patterns, the [0,0] direction has the highest sensitivity, and may be used as an optimum method for increased sensitivity. In contrast to the hot-press samples, the 3D-printed TPU/CNT film features a crystalline network, which may aid in the passage of surface charges and hence increase capacitance changes.

To have a better understanding which feature, and parameter can give us the most sensitivity we need to do an optimization. This will be accomplished by collecting experimental and computational results and using them as a basis for establishing a computationally and experimentally supported Genetic Algorithm Assisted Machine Learning (GAML) framework combined with artificial neural network (ANN) to develop TPU/CNT nanocomposite flexible sensors in which material characterizations will be coupled to strain, tactile, electronic and proximity characteristics to probe intermolecular interactions between CNTs and polymers. The proposed framework provides enhanced predictive capabilities by managing multiple sets of data gathered from physical testing (material characterization and sensor testing) and multi-fidelity numerical models spanning all lengths scales. The GAML-ANN framework will allow the concurrent optimization of processing parameters and structural features of TPU/CNT nanocomposites, enabling fabrication of high-performance, lightweight flexible sensor systems.

Our suggested nanocomposite sensor establishes a new mainstream platform for ultrasensitive object perception, demonstrating a viable prototype for wearable proximity sensors for motion analysis and the automobile sector.

1 PREFACE

1.1 Background and Motivation

Recent research has focused on the inclusion of flexible sensors into textiles or direct connection to the human body as wearable smart devices and human robotic systems[1-6]. Numerous flexible and stretchable sensors have been developed for a variety of applications using Micro-Electro-Mechanical System (MEMS) technology. Strain sensors [7-12]detect body motion, tactile sensors[13-19] monitor three-axis object handling/manipulation, and proximity sensors [17, 18, 20, 21] assist in detecting things within a specified range. Numerous electronic platforms require the incorporation of proximity sensors. A proximity sensor frequently operates in response to a change in an electromagnetic or electrostatic field[22-26]. Capacitive proximity sensors (CPSs) detect proximity due to changes in the electric field surrounding and above the CPS. CPSs are thus an extension and improvement over capacitive pressure sensors, which capture changes in capacitance only in response to physical contact (pressure). CPSs are non-moving and have been widely adopted in certain industries, including as smart phones, due to their small weight, low cost, and great sensitivity. However, conventional flexible proximity sensors have a restricted detection range (5cm) [27, 28] while proximity sensors based on metal or silicon substrates are brittle, unable of withstanding substantial deformations, and incapable of adapting to curved surfaces.

Multiple electronically conductive polymers and elastomers with low modulus, such as polyethylene terephthalate (PET), polyimide (PI), or polydimethlysiloxane (PDMS), have been proposed as composite substrates for the fabrication of resistive and capacitive sensors/arrays, but have met with limited success [2, 29-32]. Flexible electrodes such as metal nanowires [15, 31, 33] carbon nanotubes (CNTs)[14, 34-36], and graphene [37-39]have been investigated as conductive layer/electrode building blocks. A different concept of CPS involves printing metal interdigitated electrodes on polymer substrates, although interfacial adhesion between the polymer and the electrodes has been shown to be extremely difficult [5, 13, 40].

Recent theoretical and experimental research conducted in our lab indicate that integrating carbon nanotubes into thermoplastic polyurethane (TPU) significantly outperforms other published flexible carbon nanotube composite structures[32, 41]. However, constructing a flexible

nanocomposite with the requisite performance and functionality has remained elusive, owing to a lack of fundamental understanding of microstructure creation at molecular to larger scales. Integrating carbon nanotubes into polymer composites frequently requires inefficient time/cost processes that result in inhomogeneous CNT dispersion, [42] weak interfacial bonding between polymer and carbon nanotube [14], and damage to the side-walls of carbon nanotubes, altering their intrinsic properties[14, 43-45]. To address these limitations, a transformational technique in the processing and manufacturing of carbon nanotube-based polymer nanocomposite flexible capacitive sensors is required. However, no application of carbon nanotubes in TPU-based nanocomposites for proximity sensing has been documented. This document shows how a TPU-CNT film can detect objects/obstacles across a wide range of distances, both experimentally and analytically. Additionally, this study examines how this film sensor may be expanded to the realm of additive printing, which allows for a greater variety of unique designs and sensitivity, resulting in a potential prototype for wearable proximity sensors for motion analysis and the automobile industry.

1.2 Outline of the Research

This research investigates the mechano-electrical characterization of a carbon nanotube (CNT)-based composite sensor and application to creative industries. In this chapter, the advances of capacitive proximity sensors are introduced in various fields. This chapter discusses industrial and commercially used proximity sensors and sensing mechanisms. Then, the recent development of nanofiller-based sensors is discussed. In addition, the limitations and challenges associated with the existing methods are discussed. Subsequently, CNT-reinforced composite sensors and their applications are described. This section discusses the importance of polymeric nanocomposite (PNC) sensors along with some literature reviews on the polymer matrix, carbon nanotubes (CNTs), fabrication processes, numerical modeling methods, and different techniques for improving sensitivity of the nanocomposite sensors. TPU is studied for this project as it fulfills the requirement of elasticity, ease of processing, affordability, and flexibility.

In chapter two, a flexible ultrasensitive polymer-based proximity sensor was presented. The TPU was reinforced by adding CNTs and delivered the potential to adjust the sensitivity based on electrical behavior of CNTs. Manufacturability and measurement of our new sensor will be

discussed in this chapter. Fringing capacitance effect of the structure has been systematically analyzed by ANSYS Maxwell (Ansoft) simulation, as to the experimental validation.

In the chapter three, an analytical model was delivered for our sensor in cartesian coordinates to validate our experimental measurements. The model accurately follows experimental measurement and give us the flexibility to optimize the sensor functionality.

In the chapter four, we investigate on 3D printing strategies of additive manufacturing effect in the sensitivity of TPU/CNT sensor, samples are 3printed out by 3 with similar thickness and size but different orientations in order to be compared with hot-press samples. We also look over the feasibility of design modeling of creative structures like (haptic glove and car bumper) made out of this material.

In the chapter five, the multi-objective optimization of a nanocomposite proximity sensor was conducted considering two objective functions, namely, sensitivity and cost. Six design variables including thickness, width, length, frequency, permittivity, and impedance of the film sensor are considered. The results provide a wide range of geometrical data leading to the maximum sensitivity at the minimum cost of conductive nanoparticles. The innovative contribution of this research is the combination of GA and ANN, which results in a fast and accurate optimization scheme. Finally, we review all work done as a summary chapter and talk about the future of work.

1.3 Literature Survey

1.3.1 Mechanisms and Characteristics of Performance

Sensors are mostly utilized to detect a change in a physical or chemical stimulus (such as heat, pressure, etc.,) and convert it to a measurable and recordable signal [29]. Sensors are classed according to the amount of external power required, the distance to the object, the reference used, and the sensing technique used (refer Figure 1.1). There exist several ways to further classify sensors, some of them are discussed as follows:

- Contact versus non-contact sensors: A contact sensor, such as a strain gauge or temperature sensor, needs physical contact with the stimuli, while a non-contact sensor, such as an optical or magnetic sensor, does not.

- Active vs passive sensors: Active sensors need an external power source to work, but passive sensors create their internal electrical signal and do not utilize a power source [29].
- Absolute and relative sensors: An absolute sensor responds to a stimulus on an absolute scale; for example, a thermistor always reads the absolute temperature; a relative sensor measures the stimulus in relation to a fixed or variable reference; for example, a thermocouple measures the temperature difference.

To detect and quantify the amplitude of inputs (such as strain, pressure, temperature, and humidity), they must first be transformed to a quantifiable and processable signal. Our focus in this research would be on non-contact detection which categorized as proximity detection.

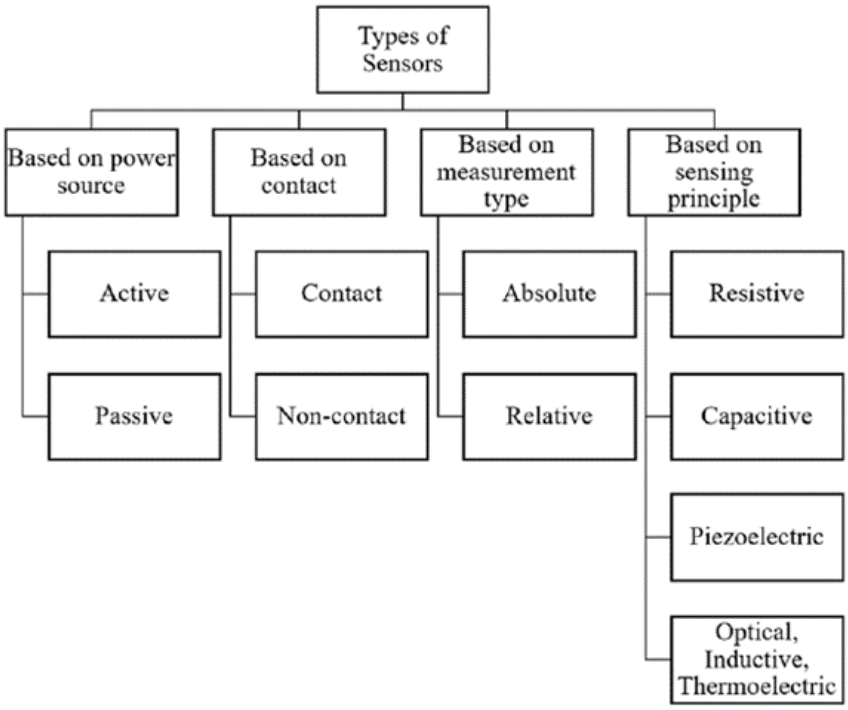

Figure 1.1 Classification of sensors [29]

Flexible electronics have recently experienced extensive applications in Internet of Things (IoT), human machine interfaces, robotics, safety protection, human motion tracking, and healthcare systems, among other applications. With the IoT increasingly making its way into thousands of homes, the area of flexible electronic wearable gadgets has also entered a new phase [1]. On one hand, traditional ceramic/metallic sensors suffer from the limitations of fragile materials and a limited detecting range. On the other hand, the fast advancement of visualization

technology, as well as the enormous market for smart devices, have raised the bar for flexible and wearable sensors, requiring excellent performance, mass manufacturing, low weight, and flexibility, among other characteristics [2]. Additionally, flexible wearable technologies have a tremendous promise for health monitoring and nursing applications. Clearly, flexible sensors with great performance will be vital for the implementation of flexible wearable devices [3]. As such, flexible nano composites may lead the gates for implantable and stretchy devices.

Numerous flexible and stretchy sensors have been created for a variety of applications using Micro-Electro-Mechanical System (MEMS) technology. Strain sensors, for example, detect body motion [4], tactile sensors monitor three-axis item handling/manipulation [5] and proximity sensors assist in detecting things within a certain range [6]. Among all these applications, proximity detection is a key task that aims to identify information about objects that are physically near another object without requiring physical contact. Numerous electronic platforms and industries need the use of proximity sensors. These sensors are critical components of systems ranging from human-machine interfaces to healthcare, smart homes, shipping industry, and soft robotics [46]. In addition to detecting external stimuli, proximity sensors are anticipated to detect instantaneous and continuous activities such as vibration, inertia, shear force, and normal force[16, 42, 47-50], in order to meet the requirements of smooth multi-functional interactions. These applications are highly demanded to be expanded in the near future.

1.3.2 Proximity Detection

Proximity Sensing refers to detection and measurement of the distance to nearby objects without physical contact. Such techniques have been in existence for decades in fields such as consumer electronics, defense, automotive, food processing, and manufacturing industries. Multiple types of proximity sensors relying on ultrasonic, infrared, magnetic and capacitive interfaces cater to the vast need for proximity sensing mechanisms. The proximity sensors' market is expanding with growth in demand from applications that rely on proximity sensing. Sensor-based technologies such as infotainment systems, multimedia enhancements, 3-Dimensional gesture recognition system along with other control systems used in consumer electronics has attracted a lot of audiences. Based on the sensor application, the market is further segmented into categories such as automotive, robotics and manufacturing industry. Manufacturing is a key task in the consumer product industry. Manufacturers produce a variety of products from raw materials

in the form of metal, ore, wood, oil, and fabrics. Resource extraction and subsequent processes involves a lot of labor and mostly repetitive tasks. Such an environment serves as a suitable breeding ground for robots[13-16, 34]. Automation has started to become commonplace in the manufacturing and service industries.

Advancements in robotics are critical in driving this change. Companies are investing more time and money into developing technology than manpower which has enabled man to create jobs that never existed 20 years ago. Another popular application of sensors is to maintain a safe working environment in industries. Machines in industries are equipped with advanced sensors such as strain [17], [18]chemical [18] and other non-contact proximity sensors. Specific sensors or combinations of sensors are used to meet the application's requirement. Sensors provide an analog or digital output which serves as a decision-making tool for the interrogating system. A sensor with a binary output is referred to as a detector. Proximity detectors can be used in places where, for instance, an obstruction in the sensor's field of view can trigger an immediate shut down in case of an emergency [19]. Catering to complex tasks and performance requirements need sophisticated sensors that efficiently extract information from their surrounding environment and provide reliable information to the parent robot to act safely.

1.3.3 Capacitive based proximity sensing

To sense things, a proximity sensor often searches for changes in the electromagnetic field. Since proximity sensors are activated via electromagnetic or electrostatic environment changes, they can be categorized into capacitive [14, 48, 51], electrostatic [26, 52], magnetic [7, 15, 53], electromagnetic radiation (infrared) [16], and light (visual) sensors [17]. Another way to classify proximity sensors is to categorize them according to their operating principles as capacitive [18], piezoresistive [53] triboelectric and piezoelectric [20, 21]. In comparison to triboelectric and piezoelectric sensors, capacitive and piezoresistive sensors have received substantial research, and many similarities in their mechanics are apparent [22]. Piezoelectric and triboelectric sensors, on the other hand, have the apparent benefits of not requiring an external power source and being more responsive to dynamic stimuli. The main characteristics of each proximity detection technique are summarized in Table 1.1.

Table 1.1. A comparison of the most frequently used proximity detection techniques

Sensing Technique	Detected Objects	Sensing Element	Operational Range	Standard Detective Circuit	Tangible Limitation
Optical	Non-conductive and conductive	Lighting resource	Frequency and condition dependent	Converter (V–I)	Lenses and object preparation needed
Ultrasonic	Non-conductive and conductive	Sound producer	Frequency and condition dependent	Digital to analog converter or Sensor modules	Object dependent
Inductive	Only Conductive	Metal coil	Coil size dependent	Impedance analyzer, LCR oscillator,	-
Capacitive	Non-conductive and conductive	Conductive electrode	Conductive electrode fabrication/size dependent	Charge amplifier, RC low pass filter, capacitance meter	-

Inductive sensing can detect only conductive objects, and the maximum scanning range is about equal to the sensing coil's diameter. While both optical and ultrasonic techniques are capable of detecting non-conductive and conductive items, implementing the complicated light source or sound producer on fabric is challenging. Additionally, the detection range is depending on the object's surface polish and material qualities. Because the capacitive mechanism detects both conductive and non-conductive items, it is well suited to identifying humans and passive objects. Additionally, the capacitive technique is easy to set up and requires fewer components than other sensing systems. It is the most suited mechanism for a printed implementation since it allows for the use of a simple conductive electrode of any form as the sensing element. A basic sensing element of any form is helpful for creative applications since the sensor may be customized to any artistic shape required by the designer. Capacitive proximity sensors (CPSs) have been used in a variety of applications to date, including determining the aging of composite insulators [23], determining the permittivity and thickness of dielectric plates and shells [24], measuring tire strain in automobiles [25], force sensing in biomedical applications [26], liquid level detection [27], and harvest yield monitoring [28].

A capacitor is an inert electrical device that stores energy as an electrostatic field. A capacitor's fundamental structure consists of 2 conducting electrodes separated by a thin dielectric material, as shown in Figure 1.2, where changes in the dielectric constant (ε_r), electrode area (A), and electrode spacing (D) all have a direct effect on capacitance through the following relationship:

$$C = \varepsilon_0 \varepsilon_r \frac{A}{D} \tag{1.1}$$

in this equation, ε_0 is the proximity associated with the free space.

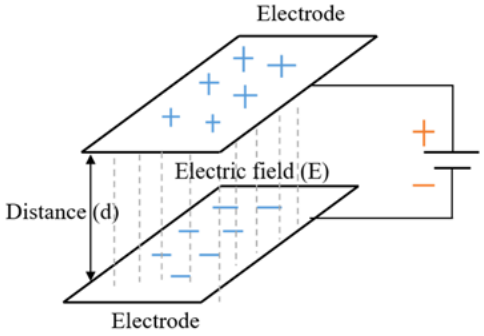

Figure 1.2. Schematic representation of capacitor in a parallel plate configuration.

The three governing factors in the capacitance formula for a parallel plate capacitor used as a sensor are dielectric constant (ε_0), overlapping area (A), and spacing (D). Meanwhile, the dielectric constant may alter owing to the presence of various chemical fluids or variations in humidity [8]. In addition to parallel plate capacitors, spherical and cylindrical capacitors are also employed in many applications. Capacitive sensors that sense pressure based on change in separation are also utilized [11], [12]. Capacitive touch sensors may operate on the surface capacitance or projected capacitance principle [13], [14]. A surface capacitive sensor, as shown in Figure 1.3, is composed of a conductive coating on one side and a contact on the other. A tiny voltage signal is supplied to all the corners of the coated side, creating a consistent electrostatic field, which creates a capacitor when a conductive item or human finger contacts the uncoated side.

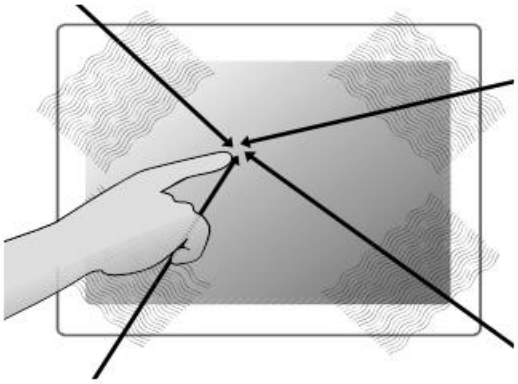

Figure 1.3. Capacitive-based surface touch sensor schematic [15].

By monitoring the capacitance at each responsive electrode, projected capacitive technology [16] detect touch. When a finger or conductive stylus comes into contact with an electrode, the electromagnetic field is disturbed, and the capacitance is altered. This may be subdivided further into self- and mutual capacitance, as shown in Figure 1.4. In self capacitance architecture, one electrode forms a separate capacitor with the environment, and when a conductive object (i.e., a human finger) contacts the sensor's cover material, the electromagnetic field is disturbed and the capacitance with respect to ground changes, generating an additional touch capacitance [17]. A self-capacitance sensor measures the current flowing between each electrode and ground [18]. On the other hand, mutual capacitance necessitates the use of two electrodes in such a way that an approaching finger takes some charge (refer to Figure 1.5), hence lowering the capacitance between the electrodes. The mutual capacitance structure is advantageous for detecting proximity, touch, and pressure, as discussed in [19].

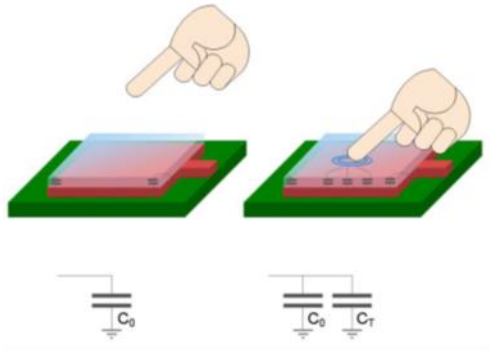

Figure 1.4. Schematic representation of self-capacitance sensing. on left: untouched sensor pad with parasitic capacitance C_0. On right: touched sensor pad with extra touch capacitance[17].

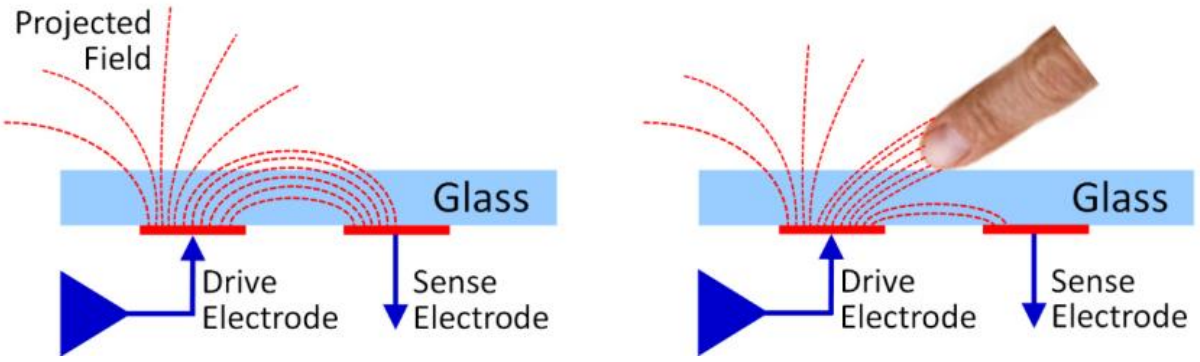

Figure 1.5. Schematic representation of mutual capacitance in between two electrodes [14], [18].

Table 1.2 shows a few applications for the capacitive sensors implemented in previous literature. The capacitance of the circuit changes as the sensible object moves away from the electrodes. While capacitive displacement sensing may be used to measure distance, displacement, and position, the detection range is limited by the item's size and dielectric constant. Additionally, by putting multiple electrodes in a regular pattern, we may discern the object's position, movement direction, and certain interaction intents expressed by the movement trajectories of a human body. Numerous applications for this sensing mode have been suggested, including electrical capacitance tomography [34], capacitive voltage sensors [35], capacitive humidity sensors [36], and capacitive gas sensors [37]. For example, electrical capacitance tomography is largely utilized for non-invasive imaging, with capacitance measurements used to determine the dielectric permittivity distribution inside inaccessible domains [34]. Additionally, based on the underlying features of the electrodes and certain transformation associations between the electrode distortion and the observed physical variables, it is easy to infer the force, acceleration, or actions as the muscle moves from the displacements. The capacitance changes generated by electrode deformation are used to determine acceleration [35], angles [36], force [37], displacement [38], and muscle action for interaction [39].

Table 1.2. Some of the practical applications associated with capacitive sensors

Reference	Application
[11]	Electrical capacitance tomography
[15]	Capacitive voltage sensors
[14]	capacitive humidity sensors
[36]	capacitive gas sensors
[32]	Displacement detection
[51]	muscle action for interaction

In [40–43], CPSs are offered as a viable cost-effective and non-destructive alternative to optical sensors for a broad variety of applications involving the examination of geometrical and physical properties. Their sensitivity, on the other hand, is affected by moisture and temperature. Additionally, parasitic capacitance and noise from external disturbances may affect the capacitive sensors' response, necessitating proper shielding of the device and design of the reading out circuits. Capacitive proximity sensing methods have been extensively used for the nondestructive evaluation of materials with poor conductivity [44].

Capacitive sensing methods have been also utilized to monitor the structure-healthy state of a concrete slab retrofitted with composites by detecting the local fluctuation in the dielectric characteristics of the materials under test [45]. The proximity capacitive approach was used by EI-Dakhakhn et al. [54] to identify empty cells in grouted masonry buildings. A concentric coplanar capacitive sensor was designed for quantitative material property assessment of multi-layered dielectrics [47], and the suggested approach for detecting water incursion in random constructions was experimentally confirmed. Additionally, the outer insulating layer of electric wires is often made of a low-conductivity substance. Capacitive sensing methods have been used to characterize the insulation qualities of cables. Chen et al. [55]developed a capacitive probe for determining the permittivity of wire insulation, and tests established the possibility of determining the state of wiring insulation deterioration using quantitative capacitive approaches. The introduction of proximity-coupled interdigital sensors to detect insulation degradation in power system cables confirms that the proximity capacitive approach is sensitive to the existence of holes and water trees in a power line cable [49]. Sheldon et al. [56] designed an interdigital capacitive sensor to detect aircraft wire aging damage and experimentally confirmed the capacitance fluctuation caused

by aviation fluid immersion. Figure 1.6 shows a couple of CPSs used in traditional applications as well as creative industries.

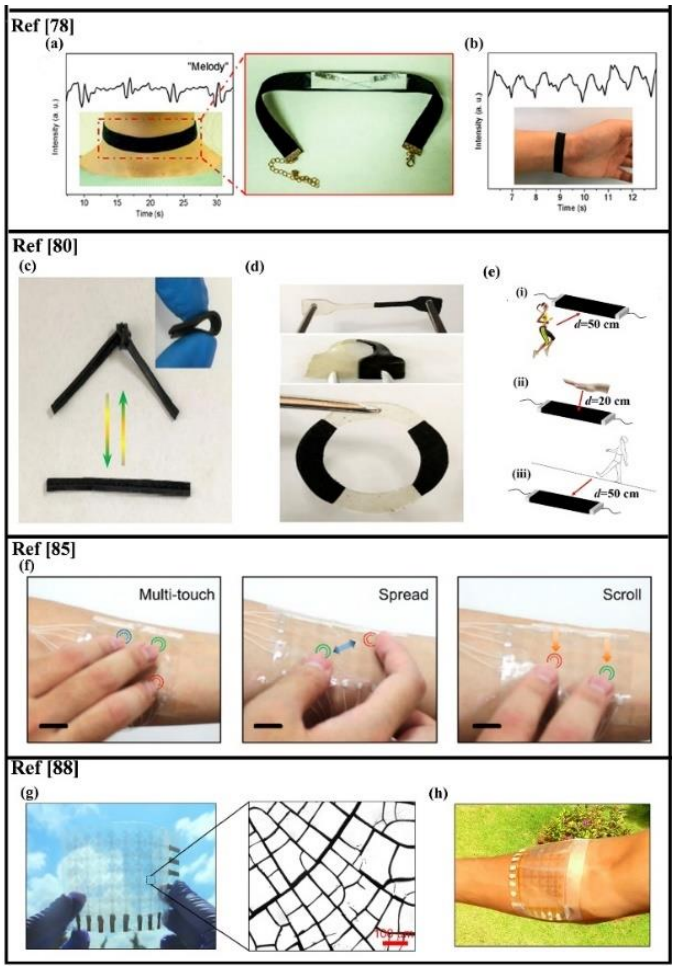

Figure 1.6. Application of proximity sensors proposed by Refs [78, 80, 85, 88]: (a) Signal of relative capacitance as measured by a choker sensor while the phrase "melody" is repeated four times, (b) Recording pulse signal when a fiber-sensor is attached to the wrist, (c) Optical images demonstrating the resulting flexible conductive films, (d) PAM (white) and PAM-FGO (black) fragments in optical photos of the healed specimens, (e) The PAM-FGO film-based proximity sensors allow for remote monitoring of human movements, (f) Image of a graphene electrode-based wearable capacitive touch sensor, (g) Optoelectronic characteristics of capacitive sensor, (h) Bendability and wearability of the proposed sensor.

1.3.4 Design, Materials, and Fabrication of CPSs

The most often used electrode configurations for capacitive sensing are planar parallel plate electrodes and co-planar electrodes (also called capacitive proximity sensors). Capacitive proximity sensors operate on the basis of the electric field's fringing effect. In comparison to the

traditional parallel plate capacitor, capacitive proximity sensors have several advantages, including one-sided access (the other side can be open to the environment), easy control of signal strength via dimension changes, multiple physical implications in the same structure (magnetic, acoustic, and electric), and a broad frequency range of operation. As a result, they are extensively employed in a variety of sectors, including humidity sensing, monitoring material qualities, chemical sensing, biosensing, and electrical insulating properties sensing [51, 52].

According to research, the electrode designs and parameters have a significant effect on capacitive sensor performance metrics such as signal intensity, diameter, sensitivity, and noise-to-signal ratio, which all impact the detecting capabilities of capacitive proximity sensors. Numerous improvements have been made to the performance of capacitive proximity sensors [53, 54]. Numerous sensor designs were explored, including square-shaped, maze, spiral, and comb patterns. It was found that complex sensor patterns may increase the effective electrode area, hence increasing sensor signal and sensitivity[55, 56]. Rivadeneyra et al. [57] designed a serpentine structure that combines meandering and interdigitated electrodes to increase signal strength and sensitivity. For humidity measurement, a capacitive sensor with an interdigital electrode arrangement and an enhanced height was built [57]. In comparison to the conventional interdigital electrode sensor, the suggested sensor demonstrated increased sensitivity due to the confinement of horizontal electric field lines in the polyimide sensing layer. Syaifudin et al. [58, 59]investigated the effect of electrode configuration on capacitive proximity sensor performance and discovered that the optimal number of negative electrodes between two adjacent positive electrodes can increase chemical detection sensitivity. A few petal-like electrode devices were constructed for water detection in an automated windshield system [60].

To enhance the flexibility and wearability of CPSs, flexible electrodes and dielectric layers made of polymer elastomers such as polyethylene terephthalate (PET) [61], polydimethylsiloxane (PDMS) [62], polyvinyl alcohol (PVA) [63], polyimide (PI) [64], polyvinylidene fluoride (PVDF), and Eco-flex [65] are frequently used [66]. Their pressure sensitivity, on the other hand, still needs improvement. As a result, a straightforward approach for introducing conductive fillers into the dielectric layer of polymer elastomers has been widely researched [67]. Due to the percolation threshold hypothesis [68], the inclusion of a conductive filler may raise the dielectric constant under applied pressure, resulting in a change in capacitance [69]. Additionally, the sensor's non-contact detection mode enables it to recognize and monitor the form and location of an item

without physical touch and to interact with the surrounding environment, highlighting the sensor's particular capabilities in the context of the COVID-19 epidemic. Zhang et al. [70] produced a stretchy dual-mode sensor array capable of detecting a 4% relative capacitance fluctuation at a non-contact distance of 10 cm. Sarwar et al. [71] described a transparent touch sensor was developed on a hydrogel electrode with a maximum capacitance corresponding difference of 15% in absolute value. However, due to the structure and material properties of the classic film- or resin-based capacitive sensor, their low air permeability is incompatible with sweat evaporation, thus impeding the capacitive sensor's long-term deployment in the area of wearable electronics. As a result, flexible capacitive sensors with a high degree of breathability are still required to increase comfort and durability.

Textile-based capacitive sensors have been claimed to increase the permeability of flexible capacitive sensors owing to their low weight, flexibility, deformability, comfort, and softness [72, 73]. By depositing PDMS on the surface of the conductive fiber as a dielectric layer and vertically stacking the two PDMS-coated fibers, Lee et al. [60] created a highly sensitive CPSs. Chen et al. [75] electrospun the nylon dielectric constant and electrode to create a CPS that can detect human joint motion with high accuracy. As a result, textile based CPSs are favored for achieving durability, flexibility, multifunctional sensing capabilities, and comfort all at the same time, making them an important research topic in the field of flexible and wearable CPSs.

Nonetheless, the construction process of some CPSs is barely documented particularly for fabric based CPSs with multifunctional sensing. Table 1.3 summarizes some of the studies that report the construction process of their proposed sensor in a detailed manner.

Table 1.3. Summary description of few CPS studies with manufacturing details, CDC (capacitance-to-digital converter), PCB (Printed Circuit Board), LCR (Inductance, capacitance, Resistance)

Reference	Application	Shape/Size	Measuring Range	Shielding	Error or Resolution	Method of measurement
[44]	Inductive and capacitive sensors integration	20mm×5mm	10mm	×	-	Resonance
[45]	Ultrasonic and capacitive integration	60mm×30mm×0.1mm	200mm	✓	30mm	CDC:AD7143
[63]	Two arrays of 16*16 electrodes	5mm×100mm Rectangle	170mm	✓	-	200kHz charging circuit
[64]	Woven-polyester fabric, printed on a standard	180mm×180mm×3mm Spiral	80mm	×	0.5mm	CDC:MTCH112
[67]	Temperature and capacitive sensor combined	7mm×3mm×0.1mm Rectangle	17mm	✓	-	CDC:AD7746
[73]	Moving target detection CPS	310mm×190mm	60mm	✓	5mm	LPF, C/V circuit
[76]	Symmetrical distribution of electrodes—circular shape	45mm×45mm Circular	55mm	✓	0.3—4.6%	LCR meter
[47]	Equally distributed sensors (120^{o})	85mm×40mm Single	336mm	✓	3.3mm	Neural Network

In this context, 3-D honeycomb, which consists of a supporting yarn layer and two independent mesh knitted textiles, has been suggested because of great wearing comfort and compression, making it a viable material for flexible CPSs [76]. In this context, Ref [77] described the construction of a bimodal fabric-based CPS using a practical and affordable manufacturing process. The suggested sensor was made out of a 3D honeycomb fabric dielectric surface (weight: 220 g/m2, thickness: 3 mm) and bottom and top conductive Ni-plated woven electrodes, giving it a high sensitivity for non-contact detection with a detection distance of 10cm and a maximum relative capacitance change of 15%. Furthermore, at the short distance range (≤3 cm), a maximum sensitivity of 0.022 cm-1 is obtained. When a hand is hovered at various distances, the capacitance fluctuations are consistently maintained, proving the proposed sensor's stable non-contact detecting response. Furthermore, when the finger is hung above the sensor array unit, the capacitance change rate of the corresponding sensor unit is 9%. This demonstrates that the proposed fabric-based sensor array can precisely detect the finger and provides outstanding non-contact spatial response.

In another study, the authors described a hierarchically porous silver nanowire-bacterial cellulose fiber that can be used to sense both pressure and closeness of human fingers [78]. The conductive fiber was made by continuous wet spinning at a speed of 20 m/min, and it had a diameter of 52 cm, an electrical conductivity of 1.3 104 S/cm, a tensile strength of 198 MPa, and an elongation strain of 3.0% at break. To create the fiber sensor element, which is thinner than a human hair, the fibers were coaxially coated with a 10 cm thick poly (dimethyl siloxane) dielectric elastomer. The capacitance variations between the conductive cores in response to closeness were monitored using two fiber-based sensors that were arranged diagonally. The suggested sensor was found to be very sensitive to objects up to 29 cm away. In addition, the fiber may be simply sewed into clothes as pleasant and stylish heartbeat and voice pulse sensors. A fiber sensor array may be used to play music and correctly identify the closeness of an item without the need for a touchpad. A two-by-two array was also shown for detecting faraway objects in two- and three-dimensional space.

A recent study looked at the usage of a noninvasive omnidirectional CPS developed in-house as a possible option for human–machine interaction applications [79]. The performance of the proposed sensor was compared to that of infrared, time-of-flight, and ultrasonic sensors, all of which are routinely employed in comparable applications. The suggested sensor is based on a heterodyning approach employed in theremin, which consists of two digital oscillators, one of which is coupled to a sensing (conductive) plate (primary/sensing). If a grounded item enters the detecting range, the oscillator's total capacitance rises, affecting the frequency of the produced square wave. In our tests, we employed a 10×10 cm thin copper PCB square as a sensor plate. The detecting plate is linked to the main oscillator, which has a fixed 10 k resistor in the feedback line. Any grounded item put within the sensing range will add capacitance to this oscillator, causing it to shift frequency to some amount. A measuring system is built to verify the performance, as shown in Figure 1.7. The camera is used to compute the displacement of the user's hand from the sensor module in this arrangement. They concluded that the sensing mechanism may be extended to all directions surrounding the detecting element by using an omnidirectional CPSs, such as the one described in their study. In addition, the suggested capacitive sensor's range (4–11 cm) is greater than that of comparable capacitive sensing technologies. The power usage was further decreased by duty-cycling the power supply to 5mW while still allowing 50 readings per second to be acquired.

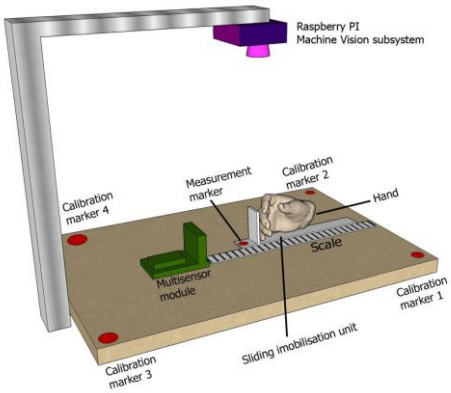

Figure 1.7. Measurement setup proposed by Ref [79] for CPSs.

To advance contactless measurement, a few research have been conducted on incorporating the proximity sensing function of nanofillers into applications for other kinds of sensors, such as touch, pressure, and strain sensors, which are gaining growing popularity in wearable electronics. Table 1.4 summarizes the key characteristics of modern CPSs coated on a variety of flexible polymeric substrates using nanostructured particles/fillers. As previously stated, only a few number of flexible nanocomposite polymeric CPSs with a broad detection range exist.

Table 1.4. Summary description of few CPS studies with manufacturing details. A summary of the fundamental properties of flexible capacitance-type proximity sensors enhanced with nanomaterials.

Reference	**Active materials and substrate**	**Response Time (1 pF)**	**Shape/Size**	**Sensitivity** $\left[\frac{\Delta C}{c_0} mm^{-1}\right]$	**Operation Range**	**Error or Resolution**	**Other Features**
[16]	CNC-m-rGO-epoxy GO (conducting particles)	-	1×2 cm^2 Thickness 0.16 mm	7.8 (Skin) 0.0 (Copper and plastic rod)	0.6 cm	0.6 mm	Durability of the touch sensor (100 cycles at the distance of 0.02 cm) Excellent stability and repeatability, Average recovery time (3 s)
[10, 82]	PET-PDMS-AgNWs PDMS (dielectric layer) AgNWS (electrodes)	<40 ms	7.5×2.5 cm^2 1 mm Thickness	0.06–0.12 (Skin)	9 cm [10] 14 cm [82]	4.8 mm	All pressure sensing Reversibility (up to 100 kPa) [82] and (50% strain) [10], Stability (2 h), Bending stability (310 cycles and r_b =3 cm) [10]

Table 1.4 continued

[33]	AgNW-PDMS AgNWS (electrodes) PDMS (dielectric layer)	<40 ms	800×2500 μm^2 3 μm Thickness	0.16 (Skin)	15 cm	5 mm	Durability (200 cycles in 100 kPa), All pressure sensing Reversibility
[63]	PCB	-	0.7×0.3 cm^2 16 × 16 sensor array	0.18 (Steel)	8 cm	1% output frequency	switched-charge amplifier and sampling/filtering for noise rejection,
[67, 87]	CMC-MWCNT-silicone CMC (elastomer composite sheet)	-	3.3×3.3 cm^2 FPCB electrode layer Thickness 0.6 mm	0.10 (Copper)	6 cm	2 mm	Inductive and capacitive sensing modes, Repeatability and reversibility (5cycles), Durability (3000 cycles for 150 kPa), Maximum detection 1.5% [67] and 8% [87]
[74]	PDMS Copper Electrodes	-	600×600 μm^2 16×16 capacitor array	0.5 (Plastics, PVC, Acrylic, HDPE)	17 cm	0.5 mm	Dual-mode functioning custom circuit board, many possible variations of the electrode configuration
[78]	AgNW−BC/PDMS fibers	<75 ms	53 μm Diameter Thickness 10 μm	0.19 (Skin)	30 cm	1 mm	Proximity and Pressure, bacterial cellulose coated with PDMS, Wet spinning for compressibility
[79]	-	<16 ms	-	-	5-10 cm	-	Energy efficient using duty-cycling power supply, boot-up self-adjustment mechanism via digital potentiometer, Wide variety of applications
[81]	Fabinks TC-C4001, Polyester woven	<30 ms	0.4×0.4 cm^2 Thickness 30 μm	0.79 (Skin)	0.1–40 cm	0.5 mm	76% less conductive ink via loop design, Microchip MTCH112 to simplify the circuit
[85]	Graphene, acrylic PET, PET (mesh-structured), Graphene (electrodes), Acrylic polymer (dielectric layer)	<60 ms	6×4 cm^2 8×8 Channels 0.03 mm	0.66 (iron) 0.10 (skin)	1 cm (Iron) 7 cm (Skin)	5 mm	Touch sensing Searchability~9–16% (r_b =0.15 cm)

Table 1.4 continued

[88]	PET-PDMS CP coating	<100 ms	10×10 cm^2 15 grid lines, Effective line width 3.3 mm	0.5 (Skin)	13 cm	-	High flexibility (2cm), Transparent (90%), Can detect several stimuli, Pressure touch, Minimal noise

In Ref [80], a new form of conductive flexible film is developed using self-healing polyazomethine (PAM) and functionalized graphene oxide (FGO) as conductive fillers. PAM-FGO conductive films were made by using imine bonds to crosslink the PAM polymer chains with the FGO. With a skin-like elongation of 200 percent and elastic moduli of 0.75 MPa, the conductive films produced demonstrated excellent flexibility. Furthermore, the papered conductive films showed excellent intrinsic self-healing capability that benefited from dynamic covalent interactions, with important role in enhancing of mechanical properties and electrical conductivity as high as 95 percent, respectively, after healing the fractured sample for 24 hours at 25 degrees Celsius. Importantly, strain sensors based on the PAM-FGO conductive film showed ultrahigh sensing sensitivity, with GF up to 641, and could detect human large-scale movements and delicate physical signals with accuracy. Because of its ultrasensitive capabilities, proximity sensors based on the organic film field-effect transistor architecture could record human movements from a distance of up to 1 m. This research can pave the way for the creation of multifunctional soft materials. Sensors based on the FGO-PAM film have a wide range of applications in wearable electronics, health diagnostics, human-machine interface, and security protection.

Ref [81] describes the dispenser printing of a CPS on a woven cloth made entirely of polyester. Three electrode designs, spiral, filled, and loop, are reviewed and contrasted in order to determine a trade-off between ink consumption and maximum detection distance. To facilitate operation, a simple detecting circuit based on a proximity sensor chip is constructed. Three patterns with identical exterior dimensions were used to investigate the effect of sensing electrode design on performance. A commercially available CPS integrated circuit (IC), the Microchip MTCH112, is chosen to obtain the proximity sensor functionality. The MTCH112 supports a maximum input capacitance of 41 pF and may be set to offer two independent CPSs channels or one sensor channel plus an active guard electrode to mitigate the effects of external electrical noise. The linearity of

the sensing circuit is determined to be 0.8 after testing printed CPS with varied diameters ranging from 1 cm to 40 cm. A broad detection range indicates that the proximity sensor is capable of interacting with humans in big-scale creative applications.

Using an extremely transparent material, Ref [82] investigated the continuous response of pressure and proximity sensing. The sensor functions by detecting the capacitance change between two transparent silver nanowire electrodes. A sandwich construction was used to construct the capacitive sensor. The substrate was a polyethylene terephthalate (PET) sheet with parallel electrode stripes printed on it. Two of these PET substrates were connected together using an elastic polydimethylsiloxane dielectric layer with orthogonal top and bottom electrode stripes (row-and-column electrodes). Throughout their tests, the authors encountered a constant issue: the development of ghost points for multi-point object recognition, which occur from virtual intersections in places other than the actual locations of the items. To examine the sensor's reaction performance, the capacitance fluctuations as a finger approached and moved away for four cycles was depicted; the device demonstrated excellent reversibility and stability with a rapid response, allowing for accurate proximity detection. In this context, Figure 1.8 summarizes the platform setup, the sensor construction, and the results associated with some of the references studied so far.

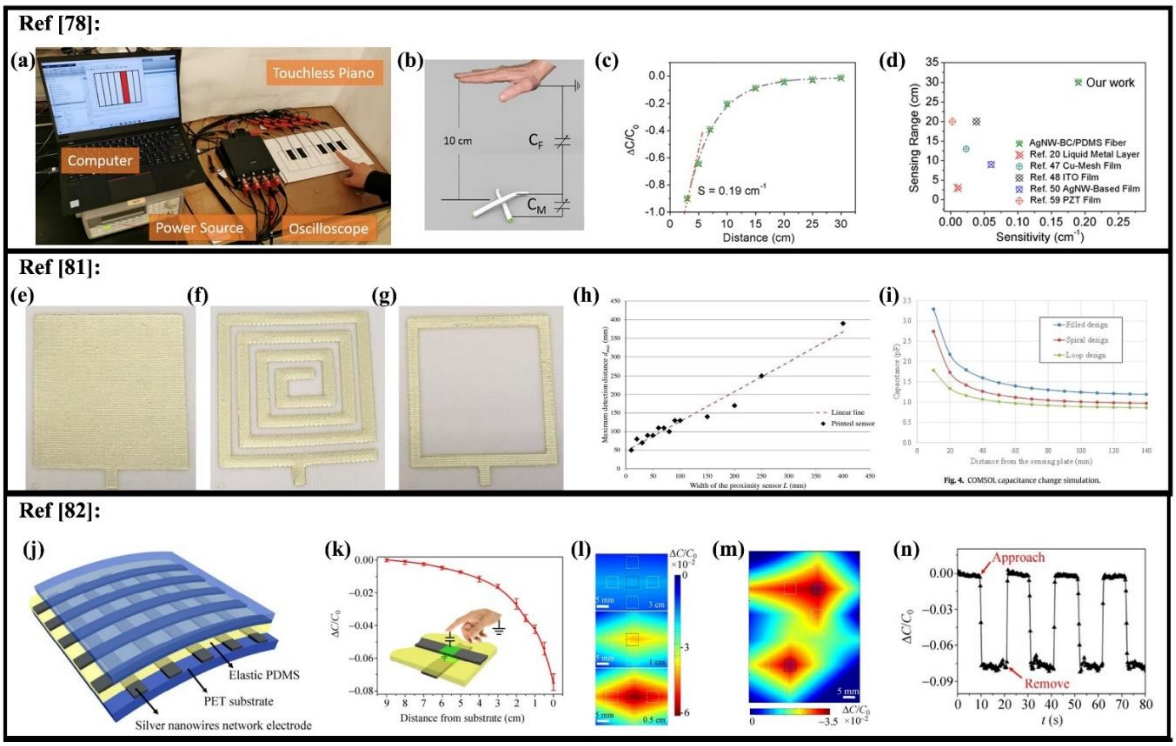

Figure 1.8. Measurement setup and the results proposed by Ref [78, 81, 82, 89]: (a) Touchless piano being played optically with a human finger hovering 40 mm above the keyboard, (b) Schematic representation of sensor sensing, (c) Increase in relative capacitance with response to an approaching object, (d) Performance comparison of the proposed setup with previous works, (e) Printed proximity sensors on fabric with filled design, (f) Printed proximity sensors on fabric with spiral design, (g) Printed proximity sensors on fabric with loop design, (h) Maximum detection distance as a function of the proximity sensor width, (i) Capacitance change simulation via COMSOL, (j) Sandwich structure of CPS, with the AgNWs stripes serving as the row and column electrodes, placed orthogonally on the top and bottom PET substrates, (k) Capacitance variation as a function of vertical distance from the intersection, (l) Contour graphics depicting the estimated capacitance change profile of a center pixel and its four closest neighbors with varying degrees of sensitivity, (m) Proximity sensing depiction of 2 metal bars, the intersections of which are denoted by dashed black boxes, (n) Relative capacitance change vs response time during 4 cycles, (o) A schematic representation of a TPU/carbon nanotube proximity sensor configuration, (p) Noise minimization using semi-planner 45^o probes, (q) Mutual capacitance becomes apparent when an item is moved near to the sensor. Shunting the initial electric lines results in a highly strong and distributed fring field between the object, film, and probes, resulting in a dramatic decrease in capacitance (r) Comparing the maximum sensitivity of various weight percentages of CNTs.

1.3.5 Theoretical Analysis

A successful CPS design is contingent upon a grasp of basic concepts and the trade-offs between sensitivity, resolution, and signal intensity. Because the structure of the sensor might

affect the measurement, it is critical to optimize the electrode parameters in order to achieve the greatest design priority for a practical application. As a result, some familiarity with capacitive sensing theory is essential. Traditionally, a capacitor consists of a pair of parallel electrodes separated by a dielectric. When a voltage differential is introduced between two electrodes, an electric field is created between them. This electric field occurs not only between the electrodes, but also extends the overlap region. A fringe field is an expanded field. In general, the fringe field of a parallel electrode capacitor may be ignored if the distance between the electrodes is much shorter than the diameters of the electrodes. The electric field is stretched into a larger region as the electrodes progressively open. A CPS is produced when the fringe field between the electrodes becomes dominant [5]. However, current formulations for the fringe field often result in complex mathematical models from which it is impossible to compute a given CPS effectively [26]. When an item approaches a CPS, the relative difference in capacitance in between circuit element and earth (self-capacitance) or between electrodes (mutual capacitance) is determined. The item is treated as a virtual electrode in the self-capacitance mode. As a result, the sensor may be conceptualized as a parallel capacitor connected between the electrode and the object. Self-capacitance and object distance may be approximated as follows:

$$C_{self-capacitance} = \frac{\varepsilon_r \varepsilon_0 A}{d} \tag{1.2}$$

It is worth noting that CPSs are vulnerable to changes in the form, size, material, and relative location of the objects while operating in the mutual capacitance mode, making it impossible to obtain a definite expression given these objective factors. In general, CPS modeling is focused with the simplified characteristics of objects or electrodes. For example, the object may be reduced to an endless plane, or the electrodes may be considered point particles (or point mass). Although many capacitive systems include numerous transmit/receive electrodes, for modeling purposes, simply a pair of transmit/receive electrodes is employed to simplify the analytical models. There are three approaches for modeling the proximity sensor: the image method, the conformal map method, and the Laplace's equation solution method. This part discusses these three modeling techniques in detail.

The concept behind this approach is that solving Laplace's equation yields the electric potential distribution, which can be used to compute the fringe capacitance between electrodes enclosing the field. In this regard, Chen and Luo [37] demonstrated a proximity detection

algorithm using a ring-shaped sensor with one circular inner electrode and one annular outside electrode, as shown in Figure 1.9(a).

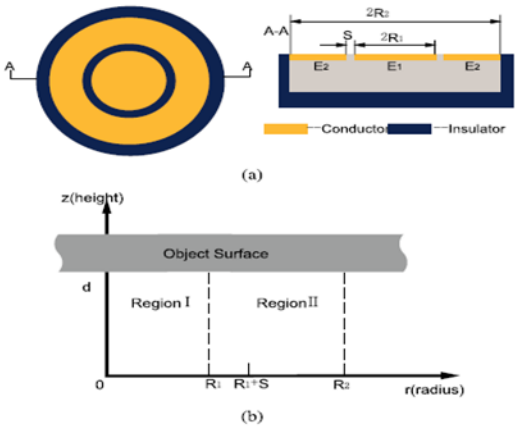

Figure 1.9. Proximity sensor schematic with ring-shaped sensor design [37]: The sensor's top and cross-sectional views.

The inner circular and outer annular electrodes have radiuses of R_1 and R_2, respectively, and have an electrode gap of *s*. Between the object and electrode surfaces, the space-charge density is 0. Thus, Laplace's equation's solution may be expressed as:

$$\nabla^2 V(x, y, z, t) = 0 \tag{1.3}$$

where $V(x, y, z, t)$ implies the electric field of the sensing space. Eq 1.4 shows the Laplace's equation within the cylindrical system:

$$\frac{\partial^2 V}{\partial r^2} + \frac{1}{r}\frac{\partial V}{\partial r} + \frac{\partial^2 V}{\partial z^2} = 0, \tag{1.4}$$

Despite the fact that these theoretical analyses are based on idealistic presumptions and rigorous boundary conditions, and the responses on capacitance cannot be exactly expressed due to a variety of influencing factors (e.g., parasitic effects on the environment), these modeling methods can assist readers in fully grasping the principle of capacitive displacement sensing in three distinct ways, and also serve as a guideline for parameter optimization of a capacitive displacement sensor. This paper examines cartesian coordination, which has received little attention so far.

1.3.6 Application of Nanocomposite Sensors

Sensors are important devices for monitoring the condition of the mechanical systems and manufacturing processes. They can convert an external stimulus into a measurable signal. The demand for development of new sensors and monitoring techniques continuously increases as the industry moves towards development of the fourth industrial revolution (Industry 4.0) and higher levels of automation for improving the quality of the manufactured goods. Polymeric nanocomposite (PNC) sensors have been widely used for different applications, especially sensing, due to their specific properties and low cost. PNCs are considered as a new class of materials, which are made of combined polymer and non-organic nano-scale fillers.

As previously stated, there are several methods for achieving touch sensing. Resistive [6,7], capacitive [8,9], piezoelectric [10,11], surface acoustic [12,13], and infrared signals are some of the processes. Additionally, the triboelectric nanogenerator (TENG) has been used for multifunctional touch sensing [15]. Capacitive sensing is believed to be the most dependable of them since it enables multitouch with the necessary resolution and little cross talk. [2] A patterned grid electrode has been extensively used in this way. Kim et al.[16] used multitouch to patterned indium zinc oxide (IZO) electrodes. Jin et al. detected touch, pressure, and curvature using three AgNW films separated by PDMS. [17] Nie et al. [18] demonstrated a multifold enhancement in capacitive touch sensing using a flexible, transparent inotropic film.

1.3.7 Materials for stretchable and flexible electronics

To create a sensing film, we must impart electrical conductivity to an intrinsically insulating polymeric substrate. Electrical conductivity is a measure of charge carrier mobility and is a critical criterion for a device's overall electrical performance. Materials may be classed as insulators or conductors based on their electrical conductivity [60]. The majority of polymeric materials, which are composed of long, chain-like molecules, are excellent conductors of both heat and electricity. The material selection process is crucial for the creation of flexible polymeric sensors. Polymer-based materials have been widely employed to fabricate flexible sensors 25 because to its inherent flexibility and customizable chemical and mechanical capabilities due to their molecular level synthesis. Two critical components of the nano-base composite sensor are addressed in this section. Another intriguing technique for fabricating stretchable and transparent

electrodes is the use of carbon-based nanomaterials. Carbon-based nanomaterials, such as carbon nanotubes (CNTs, 1D) and graphene (2D), have been extensively studied as electrodes and semiconducting channels in flexible and transparent electronics [68–70] due to their exceptional Young's modulus (1.0 TPa) and tensile strength (130 GPa), [71] as well as their high breakdown current density of 109 A cm^2. [72,73] Additionally, they exhibit an exceptional optical transmittance of up to 97 percent in monolayer form. [74,75] Their electrical and mechanical qualities may be enhanced by stacking many layers or by using a pre-strained wavy structure, albeit at the expense of transmittance.

1.3.8 TPU as nanocomposites sensors

As one of the high-elasticity materials, thermoplastic polyurethane (TPU) is distinguished by its high elasticity, low-temperature flexibility, and abrasion resistance. Liu et al. demonstrated for the first time the strain sensing behavior of two-dimensional graphene filled thermoplastic polyurethane (TPU) conductive composites, achieving a two-dimensional conducting network through the flake-like graphene's plane–plane contact. For various strain patterns, we found high sensitivity and sensing stability, as well as strong recoverability and repeatability during cyclic loading stabilization. However, since various applications need varying degrees of strain sensing behavior, conductive polymer composites (CPCs) with customizable strain response patterns are required.

TPUs with a programmable macromolecular structure [18,19] have the potential to become the material of choice for piezoresistive strain sensors owing to their superior mechanical strength and elasticity, as well as their ease of melt processing in contrast to other elastomers/rubbers. To date, an increasing amount of attention has been dedicated to the piezoresistive behavior of TPU nanocomposites including carbon-based nanofillers or conductive metal nanoparticles [20-28]. This research shown that when TPU nanocomposites are deformed under tensile strain, contact between neighboring conductive fillers may be lost, resulting in a resistance-strain response. However, no investigation has been conducted on the usage of TPU for capacitive proximity sensors.

1.3.9 Carbon nanotubes as nanofillers

Carbon nanotubes (CNTs) are great nanofillers since they provide remarkable mechanical [12], electrical [34] and thermal properties [35]. They have remarkable physical properties, including high tensile strength, high stiffness, high Young's modulus, high aspect ratio and good thermal conductivity [36]. They have been widely studied in researches since their discovery. This section discusses the methodologies for fabricating stretchable and transparent electrodes using carbon nanotubes or graphene.

Carbon Nanotubes: A carbon nanotube is a one-dimensional cylindrical substance with an aspect ratio of up to 132 million [76]. As indicated before, a conducting network composed of 1D materials with higher aspect ratios often exhibits greater optical transmittance and lower electrical resistance than a network composed of materials with lower aspect ratios at the same area fraction [77]. CNTs may be synthesized using a variety of scalable processes, including chemical vapor deposition (CVD), laser ablation, and arc discharge [78]. During the early stages of developing carbon nanotubes as stretchable and transparent electrodes, CVD-synthesized carbon nanotube forests were drawn to stretch and align them for high optical transmittance [79]. They were then put to pre-strained elastomer substrates in order to create wavy shapes. As a result of the drawing procedure, these CNT networks exhibited anisotropic optical properties dependent on the direction of the drawing [80]. Solution-based procedures are more scalable than these synthesis–drawing–transfer approaches [79,80]. CNT dispersions may be deposited using conventional solution-based deposition procedures [78]. Due to the random distribution of CNTs in solution-deposited CNT networks, they may be extended omnidirectionally. Lipomi et al. published spray-coated carbon nanotube random networks on a PDMS substrate [81]. The CNT networks demonstrated a low sheet resistance of 328 Ω sq−1 at 80% optical transmittance, as well as excellent stretchability of up to 150 percent. They showed the use of this CNT-based electrode to create a pressure and strain sensor. CNT electrodes with grid topologies may be synthesized utilizing solution-based techniques by regulating the surface energy. Ahn et al. used a self-assembly process to fabricate solution-based single-walled carbon nanotube (SWCNT) nano-mesh films [82]. To create an aligned SWCNT network, a SWCNT solution was poured between a substrate and a prepatterned PDMS template. At the same degree of optical transmittance, this network demonstrated tenfold lower sheet resistance (264 Ω sq−1) than random networks (78 percent). A network that is aligned has more unoccupied space than a network that is random, suggesting that it has a better optical

transmittance. Electrical resistance rose by 35% when they were stretched 30% in the diagonal direction.

Jiang et al. recently announced the development of a carbon-welded SWCNT network for transparent electrodes [83]. They achieved an electrode with a low sheet resistance of 41 Ω sq−1 at 90% transmittance by introducing ferrocene vapor throughout the production process. Wang et al. announced the development of meter-scale SWCNT sheets for use in flexible and transparent electrodes [84]. Using a floating catalyst CVD technique, they performed continuous roll-to-roll synthesis–deposition–transfer of SWCNT networks. They showed 101-stage ring oscillators using their SWCNT material, which had a low sheet resistance of 65 Ω sq−1 at 90% transmittance.

CNTs have one-dimensional (1D) structure and high aspect ratios (around 100-1000) which make them unique materials for developing conductive PNCs compared to other metallic particles[65]. There are two types of CNTs, namely single wall carbon nanotubes (SWCNTs) and multi wall carbon nanotubes (MWCNTs), depending on the number of concentric layers of carbon in the nanotube. SWCNTs and MWCNTs contain different properties and they can be used for different applications depending on required properties. Therefore, investigating the physical properties of MWCNTs are more complex compared to SWCNTs [43]. The length of CNTs varies between some nanometers (*nm*) to some micrometers (μm), and their dimeter ranges from 0.2 to 2 *nm* for SWCNTs while it is between 2 to 100 *nm* for MWCNTs. CNTs can be dispersed in molecular scale inside a polymer matrix due to their original size. Therefore, it results in composites with substantial electrochemical and electromechanical properties that makes them a unique option for sensor applications [15]. Electrical conductivity of PNCs can increase significantly using even low concentrations of CNTs [39].

A CNT-PNC becomes suitable for sensing applications when the CNT concentration reaches a region called the percolation threshold as it provides a network that is fragile and susceptible to breakage due to the external forces [13, 28]. Outside of this region there is no significant change in electrical conductivity with the PNC behaving as an insulator below the region and a conductor above it. The overall conductivity of a CNT-PNC varies by the filler volume fraction, the connectivity and topology of the network, i.e. the CNT dispersion, the CNT orientation, and the interaction between the polymer and the filler [43-45]

CNT-PNCs can be used for different sensing application, such as pressure [10], biomolecules and flow sensor [11], chemical [17-19], gas sensors [20], and mechanical force or strain [21-25].

Piezoresistive properties of CNTs can be used for strain measurement. The piezoresistivity of CNT-PNCs is attributed to different contributing factors, i.e. (a) altering the conductive network due to variation in the number of contacts between the CNT nanoparticles (b) change of the tunneling resistance caused by variation of the distance between the CNT nanotubes and (c) deformation of CNTs [34], where the first two factors contribute significantly more [40]. It is shown that CNT-PNCs based strain sensors can contain higher sensitivities compared to the conventional strain gauges [12]. However, there are some challenges associates with piezoresistive CNT-PNC based strain sensors, including dispersion of CNTs inside the polymer matrix and CNT alignment. Different fabrication methods of CNT-PNCs are discussed in the next section.

1.3.10 Development of the nanocomposite sensor with capacitor

Nanocomposite properties vary by changing the nanofiller's type, concentration, alignment, aspect ratio and volume fraction as well as the polymer matrix. Therefore, studying the effect of different parameters on the nanocomposite properties through only experiments is an expensive and time-consuming procedure. Numerical and analytical modeling of nanocomposites, however, can help to decrease the cost and time associated with performing experiments and to understand and predicts the properties of the nanocomposites. Therefore, quite a few theoretical models have been developed to identify different properties of the nanocomposites, including electrical conductivity, piezoelectricity, electromechanical properties, and percolation threshold of the nanocomposites. However, the number of numerical research in this area is fewer compared to the experimental studies.

Figure 1.10. Schematic of transparent stretchable proximity sensors. a) demonstrating the tactile sensory neuron's integration of the spatial and temporal characteristics of a pattern in an action–perception loop, b) Photograph showing a three-dimensional sensor on the palm of a hand with an approaching finger.

Additionally, capacitive physical sensors have been designed to measure capacitance changes caused by physical deformation or movement. Typically, these sensors are utilized in conjunction with pressure, touch, and tactile sensors [139,140]. Research has been made to construct stretchy, transparent capacitive physical sensors [32,141,142]. The capacitive sensor is made up of two electrodes connected by a dielectric substance. Physical deformation, such as that generated by applied pressure or contact, alters the dielectric's dimension, resulting in a change in capacitance. Additionally, the proximity of a subject (e.g., a finger) affects the device's fringe electric fields, enabling physical detection [143]. Kang et al. demonstrated a graphene-based three-dimensional capacitive touch sensor by incorporating mechanical stretchability into a mesh-structured PET substrate [142]. PET with a mesh structure may expand up to 8% and 15% along the x- and y-axes, respectively. The top and bottom graphene electrodes were shaped into arrays, and the overlapping area (six layers of graphene) had an 84.6 percent transmittance. They exhibited multitouch and three-dimensional touch functionalities even when stretched to 15% tensile strain. On the other hand, the majority of measurements in the CNT-based capacitive sensor business are deformation-based (pressure/strain sensors); nevertheless, this study will concentrate on proximity distance measurement. To advance contactless measurement, a few studies have been conducted on incorporating the proximity sensing function of nanofillers into applications for other types of sensors, such as tactile, pressure, and strain sensors [23, 49-51, 65-67], which are gaining increasing popularity in wearable electronics. Table 1.5 discusses the major characteristics of modern capacitive proximity sensors (CPSs) placed on various flexible polymeric substrates with nanostructured particles/fillers. As previously stated, there are just a few flexible nanocomposite polymeric CPSs with a broad detection range.

Table 1.5. Review of main characteristics of flexible capacitance-type proximity sensors reinforced by nanomaterials

Active materials & Substrate	Sensitivity $[\%\frac{\Delta C}{C_0}mm^{-1}]$	Response time (1 pF)	Resolution	Size/shape (area)	Operational range	Other industrial features
[37] Graphene/PET/acrylic PET (mesh-structured) Graphene (electrodes) Acrylic polymer (dielectric layer)	0.67 (Iron) 0.11 (Finger)	< 60 ms	5 mm	4 x 6 cm^2 8 × 8 array (64 channels) Thickness 0.03 mm	10mm (Iron) 70 mm (Finger)	Touch sensing Searchability ~ 8-15% (r_b=1.5 mm)
[31, 61, 62] PDMS/AgNWs/PET PDMS (dielectric layer) AgNWS (electrodes)	0.06-0.12 (Finger)	< 40 ms	5 mm	2.5 x 7.5 cm^2 Thickness 1 mm	90 -140mm	All pressure sensing Reversibility [31, 62] (up to 100kPa) & [62](50%strain) [31]Durability (200 cycles for 100kPa) [61]Stability (2hrs) [61]Bending stability (300cycles & r_b=30 mm)
[63, 64] CMC/MWCNT/silicone CMC (elastomer composite sheet)	0.10 (Copper)	---	2 mm	3.2 x 3.2 cm^2 FPCB electrode layer Thickness 0.6mm	60 mm	Inductive and capacitive sensing modes [64]Repeatable & reversibility (5cycles) [64]Durability (3000 cycles for 150kPa) CMC (0%-1.5%-3%-5%-8%) Maximum detection 1.5% [63] and 8% [64]
[65] CNC/m-rGO/epoxy GO (conducting particles)	7.8 (Finger) zero (Copper & Plastic rod)	---	0.5 mm	2 x 1 cm^2 Thickness 0.16mm	6 mm	Touch sensor Durability (100cycles at the distance of 0.2 mm) Good stability, high reproducibility Suitable recovery time (3 second)
PET: Ultrathin Polyethylene Terephthalate, FPCB: flexible printed circuit board, CNC: cellulose nanocrystal, GO: Graphene Oxide, PDMS: polydimethylsiloxane, AgNWs: silver nanowires, CMC: carbon microcoils, MWCNT: multiwall carbon nanotube, ms: millisecond						

1.4 Summary and outlook

A literature review on the capacitive properties of nanocomposite sensor development was provided in this chapter. Different studies on the nanoparticle-based prototyping of proximity

function were reviewed. Importance of identifying the electrical/mechanical properties in order to have an accurate film sensor was discussed. In addition, different types of sensors mechanism and their applications were presented. Some analytical models proposed for proximity sensors identification consider the Laplace equation in cylindrical coordinate and are capable of determining the fringe capacitance. However, these models are usually complicated and need the experimental data to be calibrated and verified. The FE modeling and analytical works for determining the capacitive properties mostly suffer from modeling errors and sometimes there are discrepancies between the numerical results and test measurements. Mostly, CNTs or other nanofillers were used for its piezoresistive properties embedded in flexible substrates.

In addition, a literature review was provided on polymeric nanocomposites (PNCs), which are a combination of polymers and nanofillers, as new class of materials. They can be used for different applications such as energy harvesting, actuation and sensing due to their specific characteristics, including flexibility, high mechanical properties and piezoelectric and piezoresistive properties. TPU is the most important flexible polymer that can be used for making PNCs. In addition, carbon nanotubes (CNTs) are among the most important nanofillers that provide remarkable mechanical, electrical, and thermal properties and can be used for creating a piezoresistive PNC applicable for sensing. Two main methods, i.e. melt mixing and solution mixing techniques, can be used for fabricating the TPU-CNT nanocomposites. The limitations associated with each method were elaborated in this chapter.

New fabrication experimental methods are provided in the next chapter for determining the capacitive proximity properties of polymeric sensor. In addition, this study develops new nanocomposite sensors with capacitive properties and high range of detection. Most of the available commercial proximity sensors have limited in silicon/metallic type and range of detection and can only be used for either strain, pressure, or tactile measurements. Finally, new mathematical models are developed to extract the governing equation of our sensor while sensing an object. The methods developed in this study for flexible nanocomposite are designed to eliminate the limitations and problems regarding the existing approaches. Therefore, the difficulties associated with fabrication, detection and object identification are addressed. The established identification techniques can be coupled with additive manufacturing to improve the sensitivity of the film sensor and implement in creative industries.

2 THERMOPLASTIC POLYURETHANE FLEXIBLE CAPACITIVE PROXIMITY SENSOR REINFORCED BY CNTS FOR APPLICATIONS IN THE CREATIVE INDUSTRIES

Acknowledgment: This is a post-peer-review, pre-copyedit version of an article published in Nature Scientific reports. The final authenticated version is available online at: https://www.nature.com/articles/s41598-020-80071-0

Author contributions

R.M. developed and executed the research study, simulations, material preparation, mechanical characterization, and wrote the manuscript. NO.A. contributed to the preparation of experiment setup, electrical characterization, discussion, and interpretation of results and helped in the writing. NA.A. contributed to preparation of materials and SEM characterization, percolation discussion. M.A. and H.D. supervised the findings and coordinated various aspects of the project.

2.1 Introduction

Electronic technologies including sensors are one of the key components in smart devices. Flexible sensors have been highly explored recently for incorporation into textiles or for direct connection to the body of a human/robot for wearable smart devices [23, 33, 66-69] and human robotic systems [70-72]. Furthermore, flexible sensors can be implemented as artificial skin and medical prosthetic, chiefly delivering a sensing interface while transmitting information to prevent from damage between human beings and robots as well as the nature[60, 73, 74] . Multiple flexible or stretchable sensors have been developed by Micro-electro-mechanical system (MEMS) micromachining techniques for different purposes. For instance, strain sensors [75-77] can detect body motion, tactile sensors [44, 78-83] enable to monitor three-axis handling/manipulation of objects, while proximity sensors [61, 82-84] avoid any possible accident of humans and robots to unknown obstacles. Among them, proximity sensors are extremely appealing candidates for nondestructive realizing of collision prevention in industry. Thereafter, it is necessary to be able to detect the presence of the object without making contact. To benefit the contactless measurement, studies have been extended on integration and incorporation of proximity sensing function in many electronic platforms. A proximity sensor often looks for the change in the field of either electromagnetic or electrostatic, whose sensing techniques are such as ultrasonic, optical, magnetic induction, and capacitive measurement [85-89]. Capacitive proximity sensors (CPSs) have been widely deployed for their advantages over other sensors thanks to their lightweight, relatively economical, fast detection of a wide range of materials, and readily embedded on both

flat and curved working substrates (flexible and variable structure design). To date, the reported target objects for capacitive proximity sensors have been restricted to human finger and conductors, with limited distance resolution [37, 90]. These sensors are typically based on metal and silicon substrates in a simple printed circuit board (PCB), constituting a number of circuits and complex layered matrix arrays. Other limitations are addressed such as being too brittle to endure large deformation and not flexible enough to cover curved surfaces. Therefore, flexible conductive materials are required in CPSs. Accordingly, sensor dielectric layer is required to be fabricated using various electronically conducting polymers, elastomers with low modulus, such as polyethylene terephthalate (PET), Polyimide (PI), or Polydimethylsiloxane (PDMS) [45, 91, 92]. These flexible polymers are frequently proposed as the composite's substrates for preparation of resistive and capacitive sensors/arrays [62, 93-96]. Furthermore, the development of flexible conductive electrodes is reported to be essential for increasing the sensitivity of flexible capacitive sensors. Accordingly, metal nanowires/nanoparticles[31, 61, 62, 97], carbon nanotubes CNTs [42-47], and graphene [30, 48] have been widely explored as the conductive layers/electrodes. Although metal interdigitated electrodes have been designed and engineered on polymer substrates to employ flexible capacitive micro-sensors, interfacial adhesion between the metal electrodes, polymer and electrode on the film are reported to be very challenging [32, 40].

Among the three dominant emerging nanoscale materials addressed in the literature, CNTs, as active sensing elements, have been the center of attention as an alternative to conventional materials because they have remarkable interfacial, mechanical and electrical properties [52-55]. With respect to metal nanomaterials, CNTs have superior merits of good flexibility, facility to be designed into various morphologies, which benefit their applications in wearable strain/pressure sensors [56]. For instance, elastomer composites with incorporation of CNTs show great potential with promising features for electronic device platforms [42, 57]. Recently, vertically aligned CNTs (VACNTs) have been modeled as interdigitated electrodes on a silicon substrate for capacitive sensing [58]. CNTs have also been utilized as the sensing nanofillers for providing conductive polymer composites, which can eliminate the possible interfacial adhesion issues and crack propagation problems of metal film layers patterned on polymer substrates [33]. Different processes have been typically employed to fabricate CNT–polymer nanocomposites sensors, such as mechanical stirring, vacuum filtration, nanoimprint lithography and inkjet printing [55]; however, shaping CNTs in a uniform line pattern as sensing elements are reported to be very

complex by these methods [59, 60]. Although CNT can provide unique properties to a polymeric structure, it is still a challenge to integrate CNTs within the structure for further applications [61-63]. Furthermore, numerous processes of polymer micromachining have been newly developed to employ in polymer-based flexible sensors [64, 65].

On the other side, most measurements in CNT-based capacitive sensor industry are being focused on a deformation-based nature (pressure/strain sensors); however, this paper intends to investigate more on proximity distance measurement. To benefit the contactless measurement, a couple of studies have been carried out on incorporation of nanofiller based proximity sensing function to the applications for other types of sensors like, tactile, pressure and strain sensors [23, 49-51, 66-68], becoming an increasing prevalence in wearable electronics. The details of main features of recent capacitive proximity sensors (CPSs) deposited on different flexible polymeric substrates with nanostructured particles/fillers are discussed in the Table 2.1. As indicated, there are only very few numbers of flexible nanocomposite polymeric CPSs with a large range of detection.

Table 2.1. Review of main characteristics of flexible capacitance-type proximity sensors reinforced by nanomaterials

Active materials & Substrate	Sensitivity $[\%\frac{\Delta C}{C_0}\,mm^{-1}]$	Response time (1 pF)	Resolution	Size/shape (area)	Operational range	Other industrial features
[37]Graphene/PET/acrylic PET (mesh-structured) Graphene (electrodes) Acrylic polymer (dielectric layer)	0.67 (Iron) 0.11 (Finger)	< 60 ms	5 mm	4 x 6 cm^2 8 × 8 array (64 channels) Thickness 0.03 mm	10mm (Iron) 70 mm (Finger)	Touch sensing Searchability ~ 8-15% (r_b=1.5 mm)
[31, 61, 62]PDMS/AgNWs/PET PDMS (dielectric layer) AgNWS (electrodes)	0.06-0.12 (Finger)	< 40 ms	5 mm	2.5 x 7.5 cm^2 Thickness 1 mm	90 -140mm	All pressure sensing Reversibility [31, 62] (up to 100kPa) & [62](50%strain) [31]Durability (200 cycles for 100kPa) [61]Stability (2hrs) [61]Bending stability (300cycles & r_b=30 mm)

Table 2.1 continued

[63, 64]CMC/MWCNT/silicone CMC (elastomer composite sheet)	0.10 (Copper)	---	2 mm	3.2 x 3.2 cm^2 FPCB electrode layer Thickness 0.6mm	60 mm	Inductive and capacitive sensing modes [64]Repeatable & reversibility (5cycles) [64]Durability (3000 cycles for 150kPa) CMC (0%-1.5%-3%-5%-8%) Maximum detection 1.5% [63] and 8% [64]
[65]CNC/m-rGO/epoxy GO (conducting particles)	7.8 (Finger) zero (Copper & Plastic rod)	---	0.5 mm	2 x 1 cm^2 Thickness 0.16mm	6 mm	Touch sensor Durability (100cycles at the distance of 0.2 mm) Good stability, high reproducibility Suitable recovery time (3 second)

PET: Ultrathin Polyethylene Terephthalate, FPCB: flexible printed circuit board, CNC: cellulose nanocrystal, GO: Graphene Oxide, PDMS: polydimethylsiloxane, AgNWs: silver nanowires, CMC: carbon micro-coils, MWCNT: multiwall carbon nanotube, ms: millisecond

This study offers an innovative capacitive proximity sensor enabling sensing objects within a wide range. The nanocomposite ultrasensitive proximity sensor has a simple nanostructure compared with previous studies, but with complex microstructure in which CNTs are melt-mixed in the mold substrate thermoplastic polyurethane (TPU). For the first time, the effect of CNT content is studied on the proximity sensitivity of the flexible capacitive sensor. The sensitivity distribution of the sensor is simulated with Finite Element Modeling (FEM) electrostatic simulation software, and thus, voltage distribution and capacitance reduction behavior are also being examined in the following experiments. The current proximity sensor leaps ahead of the currently used CPSs with their limited sensing distance and provides users with a direct, quick, and easy manufacturing way to interact based on electromechanical principles.

2.2 Materials and Method

2.2.1 Material Preparation

TPU and MWCNT were used as the constituents of the nanocomposite sensors. TPU (Elastollan 1185A polyurethane, with a density of 1.12g/cm3) and TPU/MWCNT masterbatch (A 5wt% of TPU/MWCNT contains NC7000 MWCNT with 90% purity, having an average diameter and length of a single CNT, 9.5nm and 1.5μm, respectively) were ordered and mixed for different dilution of CNTs. In this work, the content of CNTs filament was produced and varied from 1wt % to 5wt % MWCNT by diluting a 5wt % masterbatch of TPU/MWCNT with pure TPU through a 16 mm twin-screw extruder with L/D ratio of 40 (FilaFab PRO 350 EX, D3D Innovations Limited, UK). To obtain TPU-CNT films with 0.5 mm thickness, pellets of TPU-CNT were then cut from filaments and later compression-molded in a hot press machine (Carver Inc., Wabash, Indiana) at a pressure of 5 MPa at 190 °C for 60 seconds. The films were cooled down to the room temperature and utilized to fabricate the sensors and for characterizations. Samples were cut from the films in 60×20 mm squares. Figure 2.1. shows the final product and the flexibility of the film sensor along with the experiment setup.

2.2.2 Proximity measurements and sensor readout

Distances ranging from 20 to 220 mm were applied by using a probing station (Keithley 4200-SCS, Tektronix, USA). The TPU-CNT film was fixed over a glass substrate to eliminate noise and the sensing object (brass bar- 10 mm (height)×20 mm (width)×200 mm (length)) started approaching the sample with a speed of 6.6 mm/s after 60s. Samples were dried in an oven at 60 C for 10 h before testing. The impedance analysis was performed by the modular instrumentation using a probing station. To detect the maximum change in the capacitance, the samples were pre-soaked with 5V direct current (DC) to saturate and reduce the tunneling effect and also to polarize the polymer and form the surface charge. Furthermore, a 30mv alternate current (AC) swiping signal was applied to measure the capacitance of the film with varying frequencies to achieve maximum stability of the working window for the fabricated sensors. As demonstrated in Figure 2.1 (a), (b), the experimental setup and how change of capacitance to the initial capacitance ($\Delta C/C_0$) were analyzed. The sensor probes were mechanically co-planner with an angle of 45 degree to eliminate the noise and reduce the penetration depth inside the film. The entire three set

of tests were done for each CNT content. Other conditions, including temperature and humidity, were strictly controlled to obtain a precise measurement.

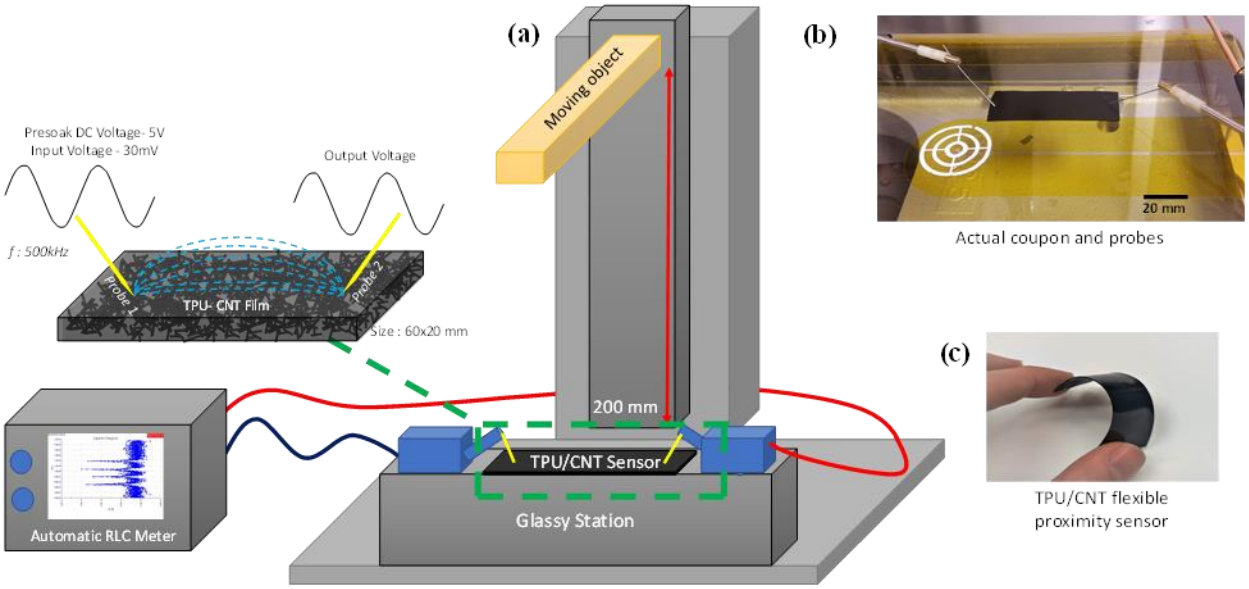

Figure 2.1. Schematic illustration of a TPU/CNT proximity sensor setup. (a) Distances ranging from 20 to 220 mm were applied by using a probing station (Keithley 4200-SCS, Tektronix, USA). The film was fixed over a glassy substrate to eliminate the noise and the sensing object (brass bar-10 ×20 ×200 mm) approached the sample with a speed of 0.66 mm/s. To detect the maximum change in the capacitance, the samples were pre-soaked with 5V direct current (DC) to saturate and reduce the tunneling effect. Furthermore, a 30mv alternate current (AC) swiping signal was applied to measure the capacitance of the film with varying frequencies. Negative change plot in capacitance showing sensitivity on RLC meter screen. (b) The sensor probes were mechanically semi-planner with an angle of 45 degree to reduce noise and the penetration depth inside the film. (c) Sensor being bent to show the thickness and the flexibility.

2.2.3 Electrical Testing

To investigate the percolation behavior of the bulk TPU/CNTs nanocomposites, the in-plane conductivity of hot-pressed nanocomposites was measured on 60 mm by 20 mm square samples with 0.5 mm thickness. The narrow strip of two ends of samples were then coated with conductive silver adhesive to erase the influence of contact resistance, and then the bulk electrical resistivity was calculated by measuring the resistance using Keithley 2400 4-probes. Electrical conductivity of each sample is being calculated by using: $\sigma = L/RS$, where σ is the volume conductivity, R is the volume resistance, S is the cross-section area of the strip, and L is the length between the electrodes.

2.2.4 Finite Element Analysis

3D and Finite Element Modeling were performed using electromagnetic field simulation software (Ansys Maxwell 2018). Material properties with affiliated modules including relative permittivity and bulk conductivity of 2wt%. TPU/CNT sample were experimentally measured and assigned to the software. Furthermore, boundary conditions, vacuum domain (15cm ×10 cm ×10cm) and excitation (i.e. applied voltages) are implemented, accordingly. Electric field streamlines in the vacuum domain on the symmetric plane passed through, where a voltage difference of 5V is applied between the two probes of tungsten (the driving and the sensing electrodes). Maximum length of the element with an efficient computational time was optimized about 1 mm. Regarding mesh objectivity, the mesh was refined about 30% in every run for ten iteration. The mesh density is set to be "extremely fine"; and the mesh number ends up in 302,982.

2.3 Results and Discussion

TPU-CNT films can be a replacement for conventional proximity sensors, due to its simpler fabrication process, flexibility, and durability. Proximity detection is defined by the change in the amount of measured capacitance of the TPU-CNT film due to the presence of an object in the electric field around it. Figure 1 (a)--(c) illustrates the measurement setup and how data was analyzed. The sensor probes are mechanically semi-planar with an angle of 45 degree to eliminate the noise and reduce the penetration depth inside the film. To identify physics of the sensation, this sensing film constitutes two types of capacitors including a capacitor between nearby probes (self-capacitance -C_s) and fringe capacitance (mutual capacitance- C_m), caused by the overlapping fringing field between the surface of the object, film and probes. As shown in Figure 2.2 (a), the electric field line does not fully horizontally match with the linear distance between the probes. When an object is not close to the film, the fringe capacitance between each probe with object is negligible. At closer distances to the probes, the fringe field between film and the sensing object becomes significant, as seen in Figure 2.2 (b). Theoretically, shunting of the electric field changes the overall capacitance of the film. Gauss' law for electricity states that the electric flux through any closed surface is proportional to the total charge enclosed by the surface, $\int \vec{E}.d\vec{A} = \frac{\mathrm{Q}}{\varepsilon_0}$.

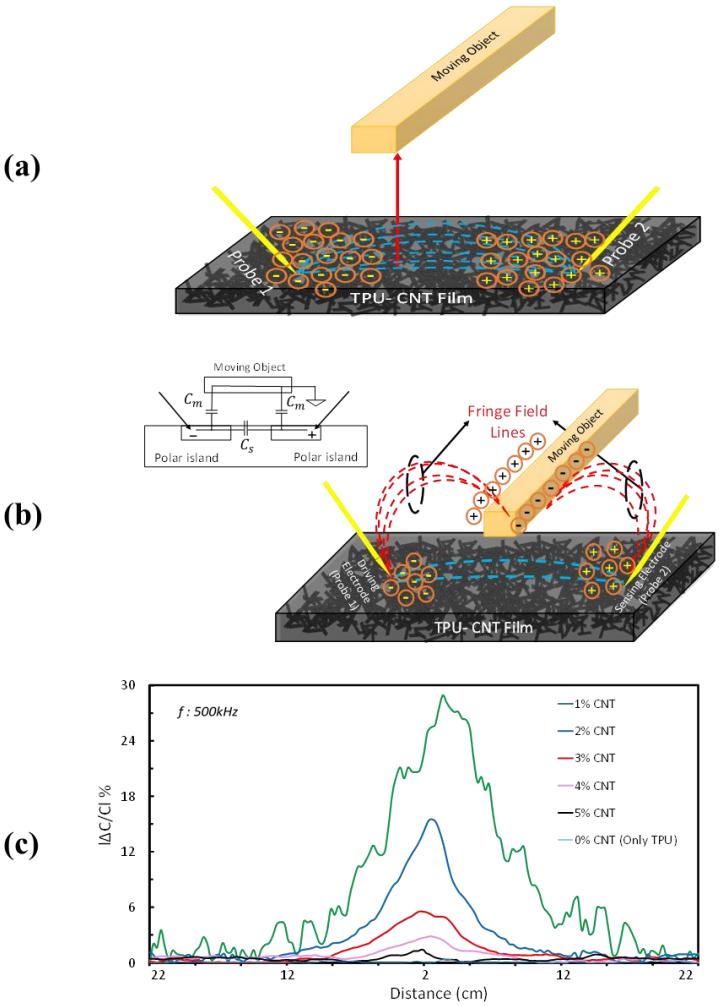

Figure 2.2. Electrical field lines of proximity sensor and maximum sensitivity. a) Moving object at the farthest distance from sensor (i.e., 220mm), no electrical field lines exist between probs and object. Bent electric filed lines (self-capacitance) are shown. b) Moving object at the closet distance to sensor (i.e., 20mm), mutual capacitance becomes clear. Shunting of the initial electric lines causes very strong and scattered fringe field between object, film and probes, and capacitance drops radically. c) Maximum sensitivity comparison of different wt %. CNTs. Absolute percentage change of capacitance to the initial capacitance is plotted against distance.

Hence, electric field strength emanating from film capacitor is shunted and weakened by the object, thereby lowering the charges stored in the film capacitor. Furthermore, the mutual capacitance of sensor increases due to the reduced distance between probes and object while the capacitance of the actual film (self-capacitance) drops due to the change in the charge balance (C = Q/V). Thus, while right probe (sensing electrode) and the moving object are DC grounded, certain amount of charges migrates from the grounded probe to the moving object, resulting in the

reduction of stored surface charges on the film and subsequently overall capacitance reduction (Figure 2.2 (a),(b)). Having an optimal nanocomposite sensor, five different CNT contents are studied. Figure 2.2 (c) shows sensitivity (ΔC/C %) of proximity sensor with respect to the weight percent of CNT. However, Pure TPU does not show any noticeable capacitance change under the test. Absolute percentage change of capacitance to the initial capacitance was plotted against distance. Measurement is aimed to be performed within a range of 20 cm. The object starts moving closer to the sensor from a distance of 22 cm and eventually stops off at 2 cm. Due to the surface charge migration (fringe effect), the capacitance radically drops for the distances lower than 2 cm. Below 2 cm, sensor acts more like a tactile capacitive sensor which is not the purpose of this study. Although changes in the capacitance occur relatively from 22 cm for CNTs 1 wt%., the limit for visible proximity sensing is about 12 cm, which becomes prominent at 2 cm. We also directly calculated the sensor's sensitivity to the detection distance. Our calculations suggest that the sensor's capacitance output will vary on the order of 10 fF per centimeter. Given that the sensor operates on the sensitivity order of 100 fF, this represents a sensitivity of 0.3 %/mm, meaning that it should be fairly sensitive to distance variation in a long detection range. The response time of this sensor is about 30ms, which is comparable with reported values in Table 2.1.

The improved sensitivity of the very sensor possibly arises from the nanostructured architecture, which have a higher density of the electric field originating from larger polarization of the polymer by the presence of highly conductive nano tubes. Thus, the field can be enhanced while the nano particles are acting as an embedded conducting network within the polymer structure, and it leads to improvement of polarization inside the nonconductive polymer.

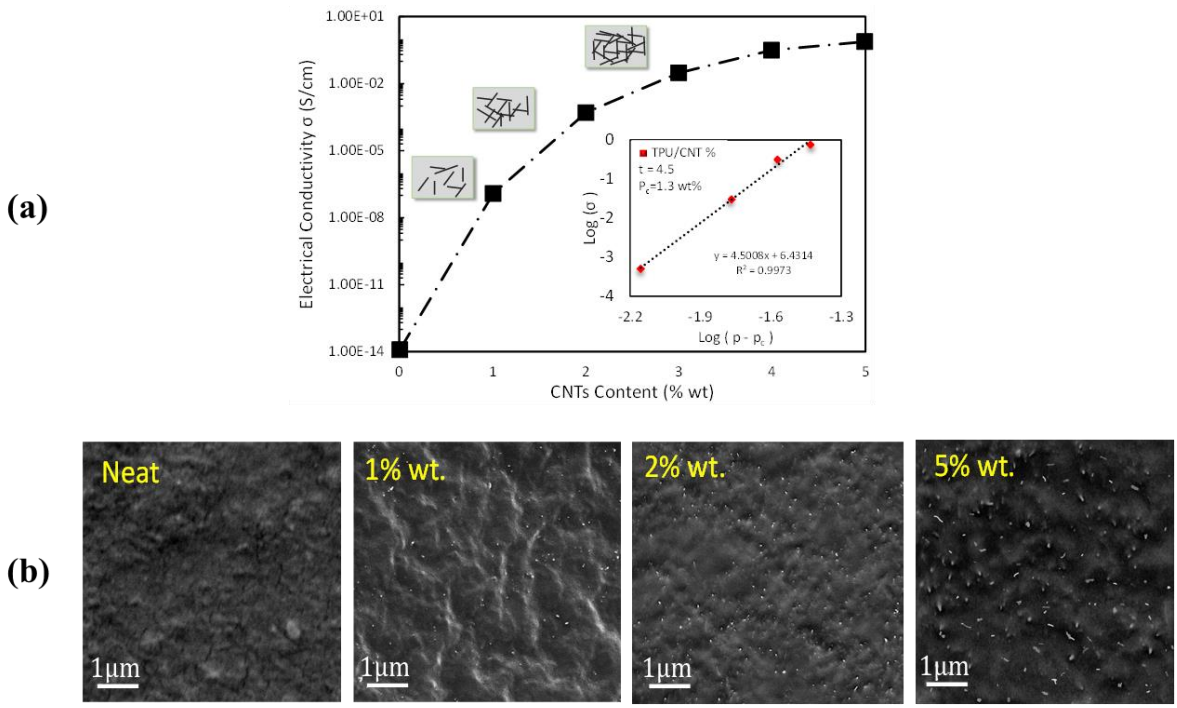

Figure 2.3. Electrical conductivity and CNTs distribution a) Electrical conductivity of TPU/CNT samples vs. CNT content wt % are employed to do calculation of percolation threshold. b) SEM distribution images of cross-section fracture surface of the neat, 1wt. %, 2wt.% and 5wt.% MWCNTs in TPU nanocomposite. White dots and lines are the carbon nanotubes within the polymer matrix.

As seen from Figure 2.2 (c), the sensitivity graph shows 2wt% with quite high sensitivity but less noticeable noise among other CNT contents. The physics behind the observed noise data (Figure 2.2 (c)) is that this number of nanoparticles provides a certain number of conductive pathways due to the percolation of CNTs inside the TPU structure. In percolation threshold, not only the electrical conductivity of the composite enhances remarkably but it also rises the chance of trapping charges by applying a presoak voltage. Hence, the conductivity of the film can be generally described in terms of modified classical percolation behavior using eq. (2-1):

$$\sigma = \sigma_0 (p - p_c)^t \qquad (2\text{-}1)$$

where p_c is the percolation threshold, t reflects the dimensionality of the conductive networks in the composite, and p is the volume fraction of the fillers which depends on the electrical conductivity of the composite film at a given filler loading (σ) and the proportionality constant (σ_0) that is related to the intrinsic conductivity of the filler. The values of p_c and t of composite films were determined by fitting of the experimental data. The conductivities of the TPU film containing

CNT as a function of filler content is plotted in Figure 2.3 (a). A fairly high percolation threshold of 1.3 wt% and a scaling exponent t is 4.5 was estimated in the TPU-CNT nanocomposites. In addition, the films containing CNT alone are observed to show a rapid increase in electrical conductivity by about 7 orders of magnitude (from 5.06×10^{-14} to 1.2×10^{-7}Scm−1) when the CNT content was increased from neat to 1 wt%. This sharp change of conductivity indicates the formation of percolating network in the polymer matrix. Although the inherently high conductivity and high aspect ratios of CNTs allow them to form electrical pathways more easily in the polymer matrix, the morphology of the conductive filler also plays an important role in the geometry of the conductive network in the matrix.

Here, Scanning Electron Microscope (SEM) analysis is utilized to investigate the morphology of CNTs conductive networks in the TPU matrix. Figure 2.3 (b) illustrates cross-section microstructure of TPU-CNTs by SEM for neat TPU, 1, 2 and 5wt% CNTs contents. White dots and lines represent CNTs within the polymer matrix. It can be seen that CNTs exhibit relatively homogeneous dispersion in the TPU matrix, and there is no serious aggregation phenomenon. Furthermore, after percolation process conductive pathways becomes more solid and apparent, and not only lower standard deviations (i.e., noise) but a good sensitivity also is expected. At CNT content of 5 wt%, the dispersion of CNTs becomes denser and most of CNT contact each other, forming a denser CNT network structure in the whole TPU matrix.

Additionally, another remarkable trend is that proximity sensitivity of the TPU-CNT sensors lowers by increasing the CNT content (from 1wt% toward 5wt% CNTs). TPU has been known as a high polar polymer which can be used as a perfect dielectric. TPU in the form of multi-block copolymers also contains of more high polarity segments (called hard-short segments), which leads to formation of surface charge and consequently higher polarization in the presence of an electric field. Addition of CNTs inside the TPU structure, makes the film semi-conductive and increases the polarity. As consequently observed, the initial capacitance of the TPU/CNT film has been increased by adding CNTs content. However, the maximum sensitivity ($\Delta C/C$ %) has been observed at the lower content of CNTs (1wt %). This phenomenon allows us to conclude that the maximum sensitivity would be possibly achieved around the percolation threshold (1.3%wt CNT) and afterward, the sensitivity drastically drops. This decreasing trend can be interpreted by the performance of both matrix and nanoparticles. By addition of CNT, clusters of non-conductive TPU and highly conductive CNT form higher capability of polarization. Consequently, adding

higher percentage of CNT[98-101] increases the conductivity and initial capacitance, but lowers slope of polarity growth. Within higher CNT concentrations, larger polar islands are being formed on the TPU film in presence of an electric field (fig. 2a). Thus, by approaching the object with limited charges (fringe field-fig. 2b.) to the TPU-CNT samples with higher polarity, less percentage change of capacitance has been measured due to less difference in the transferred charges. This supports the observation of less sensitivity in samples with higher CNT concentration.

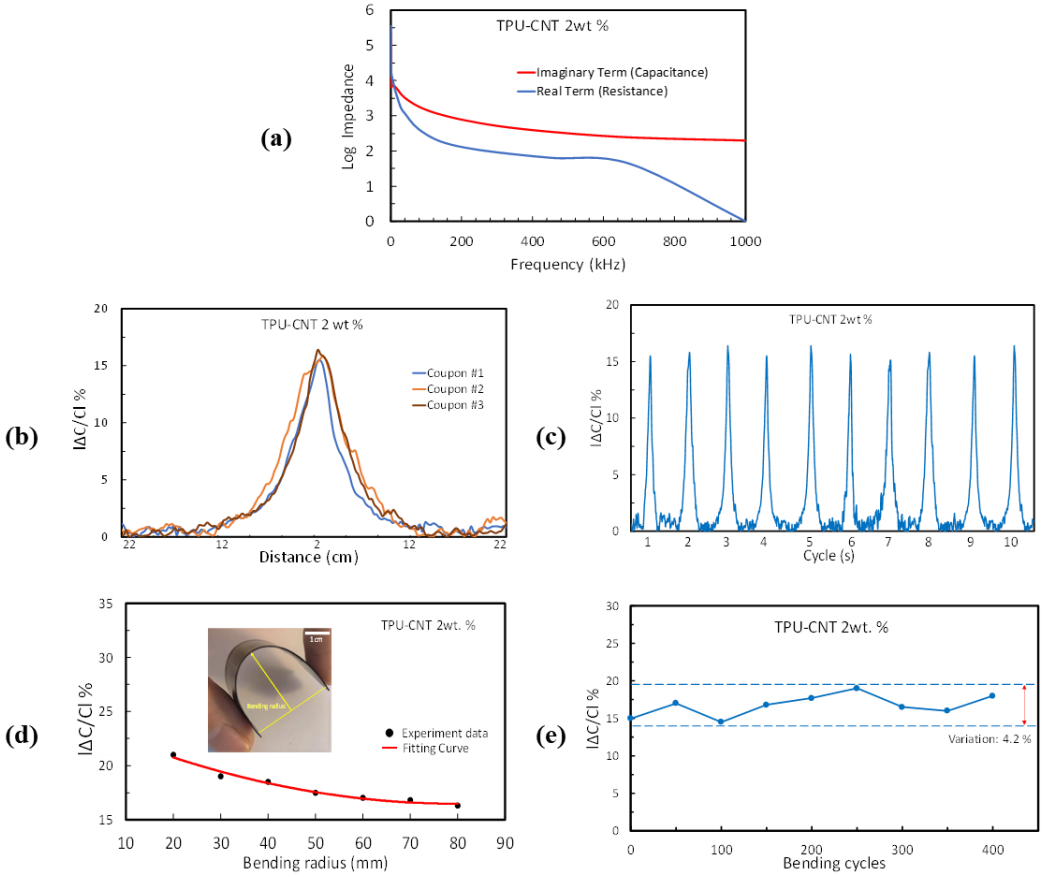

Figure 2.4. Sensor characterization with 2wt%. CNT a) Nyquist stability plot of the impedance sensing to the magnetic field at different exciting frequencies. From EIS, the stable region of frequency response for imaginary and real are initiated around 500kHz. b) Reproducibility response of sensors for three different coupons of similar manufacturing process. c) Repeatability response with several identical approaching cycles along with repeatable peaks. d) Relative change in capacitance of the sensor film under various bending radii of 20–80 mm. e) Mechanical flexibility of the proximity sensor - Relative change in capacitance measured for 400 bending/relaxing cycles at a bending radius of 20mm.

To achieve the maximum stability for the capacitance measurements, in Figure 2.4, Nyquist plots were utilized to demonstrate the impedance sensitivity with respect to the frequency for TPU-CNT 2wt% sample as to determine the stable region of frequency. As it can be observed from Electrochemical Impedance Spectroscopy (EIS), the stable region of frequency response for imaginary impedance (capacitance) is initiated at around 500 kHz. On the other hand, that of the real impedance (resistance) is detected between 400 to 600 kHz. Therefore, to achieve the maximum stability and efficiency, 500 kHz was chosen the sensor operating frequency. This frequency provides maximum stability for the impedance while the frequency response does not alter the resistance of the film or change the capacitance of the sensors. This would improve in minimization of measurement errors (i.e., noise) and provide maximum sensitivity for the film sensor. Despite higher frequencies may render more sensitivity and relatively lower noise, energy consumption drastically increases. The standard deviation for the values was high in the low-frequency region. Reproducibility and repeatability sensing responses of 2wt%. CNTs are shown in Figure 2.4 (b), (c). Reproducibility response of the sensor is assessed for three different coupons of similar manufacturing process. Subsequently, cycling response has been analyzed and its peaks are apparently very self-repeating (Figure 2.4 (c)).

An important improvement of polymeric proximity sensors, in order to widen their applicability, is sufficient mechanical flexibility to allow for stable operation under bending conditions. Figure 4d shows a photograph of the flexible proximity sensor subjected to bending. The flexibility of the sensor was examined by measuring capacitance changes with respect to its before-bent sample under applying various bending radii. The capacitance increases as the bending radius decreases and reaches ≈21% at a maximum bending (radius of 20 mm). At the lower bending curvature (higher radii) of 2 wt.% TPU-CNT sensor, the percentage magnitude of capacitance change becomes closer to the before-bent one (≈15%) – shown earlier in Figure 2.2 (c). So, the capacitive response of highest radius (lowest external bending) is insignificant (4.7 %) respect to that of lowest radius (highest bending). In another word, the capacitance recovered to its initial value with no permanent changes, demonstrating robust mechanical flexibility of the TPU-CNT sensor. To evaluate the durability of the sensor against bending, we conducted cyclic tests with repeated bending and relaxing (see Figure 2.4 (e)). The variation of the capacitance change is lower than 4.2 % over 400 cycles of bending at a radius of 20 mm, and thus the capacitive output of the sensor remained stable to the repeated bending.

As earlier mentioned, the sensing mechanism is based on the object interference with the electrical field between two probes. The interference disturbed and reduced the number of electric field lines (i.e., self-capacitance) and consequently, stored charged decreased radically on the polymer. To assure that the capacitance change comes from the fringe phenomenon, a simple 3D model is simulated in Ansoft Maxwell. Figure 2.5 (a) demonstrates the measurement setup in which object, material properties, boundary conditions, vacuum domain and excitation (i.e. applied voltages) are implemented (further details are available in FEM sesction2.). This figure shows the electric field streamlines in the vacuum domain on the symmetric plane passed through, where a voltage difference of 5V is applied between the two probes of tungsten. Primitivity and bulk conductivity of 2wt%. CNT sample are approximately employed as the material input property of TPU-CNT. Capacitance measurements have been illustrated in Figure 2.5 (b), for different distances between the grounded object and the substrate (i.e. electrostatic simulation). Applying the voltage to the TPU-CNT film sensor, the formation of potential gradients around the substrates is observed. By introducing the object inside the formed electric field, the disturbance of the field has been detected and used as the sensing mechanism. As observed in Figure 2.5 (b), while the object is at very far distance (>80mm), there is minimal change in the potential surfaces (stored charges) and the field is uniform. By lowering the distance, the field shape changes and high potential surface forms between the object and the surface of the film in z direction and thus leads to the migration of surface charges and formation of fringe fields around the object. Although the object is smaller than the TPU-CNT sensing film, the fringe fields have been created on both extremities of the object. The fields change the polarization (the charge balance) of the TPU-CNT film and outcome in formation of unexpected store charged between the object and the film. By reduction of the distance (<40mm), the field creates a new capacitor between the film and the object and the stored charge on the film are being interrupted, and this eventually leads to more reduction in the capacitance of the film sensor. While the electric field between the probes and the object (mutual capacitance-Cm) are responsible for the reduction of electrodes capacitance (self-capacitance), their change is not being measured neither in the simulation model nor in the experiments. In a short, the overall capacitance changes of the sensor (self-capacitance) is majorly under the influence of object movement and the resistivity of film sensor. As displayed in Figure 2.5 (c), capacitance decreases when the object-sensor distance goes from 120mm to 20mm.

Furthermore, the experimental result closely follows the Maxwell simulation trend in logarithmic scale and simulation is capable of identifying the fringing effect.

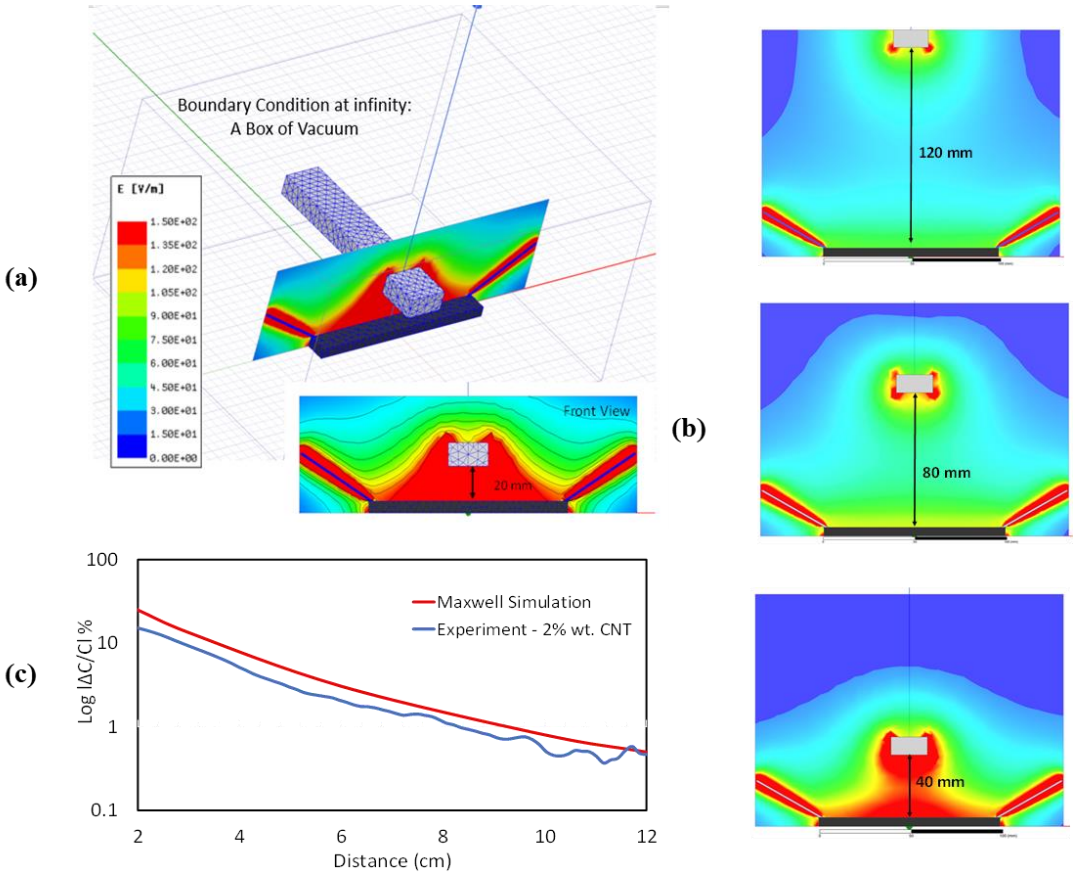

Figure 2.5. Schematic representation of simulation results of the basic fringe field cell a) A simple 3D model in Ansoft Maxwell along with implemented material properties, boundary conditions, vacuum domain, mesh and voltage distribution of sensor at closest proximity to the sensor (20mm) inside a vacuum box b) Voltage distribution between two probes in range of 120mm to 30mm. Capacitance between two probes is mainly determined by fringe effects. c) Experimental and Maxwell simulation comparison of capacitance change as a function of distance.

2.4 Conclusion

A flexible ultrasensitive polymer-based proximity sensor was presented. The TPU was reinforced by adding CNTs and delivered the potential to adjust the sensitivity based on electrical behavior of CNTs. The developed sensor was sensing based on the change of the capacitance that was mainly quantified by fringe effects. Although 1wt%. CNTs showed highest sensitivity, 2wt% CNTs exhibited lowest noise along with the significant sensitivity. Fringing field and tunneling effects (polarity) were addressed as two main explanations of observing the changes trend of the

capacitance(sensitivity). As the object approached the sensor, electric field partially started to be distracted and accumulated over the object. Local surface charges migrated from the film sensor and consequently the self-capacitance declined. Additionally, tunneling network pathways resulted in higher amount of polarization (less transferred charge) justified higher sensitivity in the samples with lower wt%. of CNTs. Frequency of 500 kHz was selected as the optimum to minimize noise as well as power consumption. We further discussed extraordinary flexibility under the bending loading and durability during loading/unloading process with the variation of below 5%. The sensor can sense the object movement with a fast response time/range, high repeatability and cycling feasibility.

Lastly, the numerical simulation results were capable of accurately following the fringe effect and showed decreasing trend of capacitance as previously shown in the experiments. Overall, the detection performance of our described proximity sensor implies potential applications in the field of smart flexible devices which is the best platform to realize and monitor the movement of objects. The flexibility, high sensitivity, and notable stability of the proposed sensor, along with extremely simple fabrication process, offer an alternative to the current controlled electrical proximity sensors for incorporation into wearable gadgets and future smart electronic devices.

3 MATHEMATICAL MODEL AND EXPERIMENTAL DESIGN OF NANOCOMPOSITE PROXIMITY SENSORS

Acknowledgment: This is a post-peer-review, pre-copyedit version of an article published in journal of IEEE Access. The final authenticated version is available online at:
https://ieeexplore.ieee.org/abstract/document/9169895

Author contributions
R.M. developed and executed the research study, simulations, material preparation, mechanical characterization, and wrote the manuscript. A. P. discussion, and interpretation of results and helped in the writing. M.A. and H.D. supervised the findings and coordinated various aspects of the project.

3.1 Introduction

The evolution of sensor engineering has made a spectacular development for years in many existing and emerging applications, including robotic technologies, human-machine interfacing, bioelectronic devices, and electronics skins [46, 68, 73, 75, 102-108]. Multiple flexible or stretchable sensors have been developed by Micro-electro-mechanical system (MEMS) micromachining techniques for different purposes. For instance, strain sensors can detect body motion [75, 107, 109], tactile sensors enable to monitor three-axis handling/manipulation of objects [81, 108, 110], while proximity sensors avoid any possible accident of humans and robots to unknown obstacles [10, 102, 103]. Although most measurements made in sensor industry are of a deformation-based nature, proximity distance measurement becomes an increasing prevalence in wearable electronics which need to interact with human being and environment safely. Hence, it is necessary to be able to detect the presence of the object without making contact. To benefit the contactless measurement, a couple of studies have been carried out on incorporation of proximity sensing function to the applications for other types of sensors like, tactile, pressure and strain sensors [10, 47, 49, 103, 111]. Therefore, it becomes desirable to integrate proximity sensors in many electronic platforms as much as possible. Up to now, various types of proximity sensors have been manufactured in market such as ultrasonic, infrared, magnetic induction, and capacitive sensors. Among the different detection mechanisms, capacitance-based proximity sensors have been deployed more than the others thanks to their simple device design, easy readout, integration

and unbiased functionality respect to different color and texture while detecting [47, 50, 107, 112-114].

Technically, the mechanism of capacitive proximity sensors (CPS) is usually governed by two principles which are based on either a traditional parallel-plate capacitor or fringe capacitance (also named planar capacitive sensors). Though parallel-plate proximity sensor has a straightforward mechanism and wide applications, it exhibits some major limitations, including the approaching object must be conductor, sensitivity drops drastically while the gap between two plates increases, and eventually this type is not applicable when the media of measurement is inaccessible(one plate is spinning or in the water)[115]. Recently, a large number of CPSs applying the principle of fringe capacitance have been proposed. Here, a CPS, a device that consists of two live electrodes located on either side of conductive substrate, transduces stimuli movement to capacitance signal. Furthermore, an object, which is aimed to be detected in the vicinity of the sensor, does not have to be part of the structure, and it can also be either a conductor or nonconductor [9, 111, 113-117].

Lately, modeling, implementation and analysis of CPS were extensively presented on the variation of the fringe. In capacitive displacement sensing perspective, as an object approaches a CPS, the relative change in capacitance between two electrodes (mutual capacitance mode) is recorded. There are three methods for modeling of the proximity sensor: the technique of images[118], the technique of conformal map[119], and the method of solution of Laplace's equation. However, very few analyses have been examined on the latter one due to its nonlinear feature. Mostly, studies are limited to empirical formula and numerical simulation to anticipate an analytical formula for varied geometry of proximity sensors. Noltignk [120] firstly reported CPS functioning based on the fringe effect. They theoretically analyzed two quite large types of sensing structure, constructed in the ring-shaped and rectangular electrode. Chuang et al. [121] presented a fringe capacitance formula of microstructures with derivation of an empirical formula for the capacitance. The empirical formula is obtained by using curve fitting on numerous ANSYS numerical simulation within dimension ranges of plate and ground. To detect damage location in power system cables, PCSs with an interdigitated structure showed the great potential for nondestructive monitoring of the insulation status [31]. Due to the inherent difficulty in developing exact analytical formulas for such a complicated geometry, authors suggested an empirical equation based on Ansoft Maxwell simulation and experimental measurements [31].

Although empirical models describing planar capacitive sensor exist, they do not provide actual insight into the interaction of the electric field with the moving object nor do they explain the actual interaction of different parameters in the sensing mechanism. With this in mind, to explore the fringe effect of parasitic capacitance for nanoscale metal–oxide–semiconductor field-effect transistor (MOSFETs), several full/semi analytical models have been established by the conformal mapping method [32-35]. They were also able to estimate, optimize, and compare the fringe capacitance through simulation results without any fitting parameters.

From a proximity detection model and simulation results with a ring-shaped sensor presented by Chen & Lue[115, 117], the solution of cylindrical Laplace's equation was employed and the electric potential distribution from which the fringe capacitance between electrodes bounding the field was calculated. It was found that the dominant parameter in the sensor response is the electrode spacing. Furthermore, it was also stated that the fringe capacitance is proportional to the effective electrode length, defined in this case as the average length of the two electrodes. However, the existing formulations for the fringe field often result in complicated mathematical models from which it is difficult to accurately calculate a given CPS and an extant model can only apply to ideal situations.

Much research are under their way developing the range of proximity measurement from micrometers to millimeters [36, 37]. To date, the reported target objects for capacitive proximity sensors have been restricted to human finger and metal conductors, with limited distance resolution (below 100mm) [38, 39]. These sensors are mostly based on metal and silicon substrates in a simple printed circuit board (PCB), constituting a number of circuits and complex layered matrix arrays. Other limitations are addressed such as being too brittle to endure large deformation and not flexible enough to cover curved surfaces. Recently, sensor arrays have been made using various polymers such as Parylene, Polyimide (PI), or Polydimethlysiloxane (PDMS) [40-42]. These are frequently proposed as the substrates for resistive and capacitive flexible sensors/arrays [18, 22, 43-45]. Capacitive sensing approaches are less susceptible to temperature variation respected to resistive sensing techniques [22]. However, metal interdigitated electrodes have been designed and fabricated on polymer substrates to implement flexible capacitive micro-sensors[40, 46]. Interfacial adhesion between the metal electrodes, polymer and electrode length on the film were reported to be very challenging [40].

As active sensing elements, nano fillers like Carbon Nanotubes (CNTs) have been the center of attention as an alternative to conventional materials because they have remarkable mechanical/electrical properties [47-50]. Particularly, polymers with incorporation of CNTs show great potential with promising features for electronic device platforms. In this regard, vertically aligned CNTs (VACNTs) have been modeled as interdigitated electrodes on a silicon substrate for capacitive sensing [51]. CNTs have also been utilized as the sensing nanofillers for providing conductive polymer composites, which can eliminate the problems of metal film layers patterned on polymer substrates [41]. Different processes have been typically employed to fabricate CNT–polymer nanocomposites sensors, such as mechanical stirring, vacuum filtration, nanoimprint lithography and inkjet printing [50]; however, shaping CNTs in a uniform line pattern as sensing elements are reported to be very complex by these methods [52, 53]. Most of these studies have fabricated planar polymer nanocomposites as strain sensors. Although CNT can provide unique properties to a polymeric structure, it is still a challenge to integrate CNTs within the structure for further applications [54-56]. Furthermore, numerous polymer micromachining processes have been recently developed to implement polymer-based flexible sensors [57, 58]

Therefore, in this paper, nanocomposite ultrasensitive proximity sensor exhibits a simple flexible nanostructure compared with previous studies, but with complex microstructure in which CNTs are melt-mixed in the mold substrate thermoplastic polyurethane (TPU). Adding CNTs with different volume rations to the polymer has made continuous variation of the composite electrical conductivity possible which is used to achieve the sensor with controllable sensitivity in this study. The results are made on the basis of a mathematical closed-form model, and a set of experiments corresponding to the mathematical is accomplished to confirm the accuracy of the simulation results. The hypothesis of a fringing electric field sensor is described in our coplanar capacitance sensor in cartesian coordinate. The sensor is designed to be fabricated using flexible polymeric substrate and two thin electrodes located on both ends. This new design not only simplifies the sensing structure and increases the practical sensing area, but it also offers the opportunity to bring the two electrodes closer or farther together. Calculated and experimental results are presented through the analysis of capacitance behavior and finally voltage distributions of the modeled sensor are simulated over the area between the sensor and the object for different distances and resistivities.

3.2 Fabrication and Design

3.2.1 Material preparation and synthesis of TPU-CNT composites

TPU (Elastollan 1185A polyurethane with a density of 1.12g/cm3) and TPU/MWCNT masterbatch (A 5wt% of TPU/MWCNT containing NC7000 MWCNT with 90% purity, a diameter and length of about 9.5 nm and 1.5 μm, respectively) were purchased and diluted. TPU filaments containing 1 and 2 wt % MWCNT were produced by diluting a 5wt % masterbatch of TPU/MWCNT with pure TPU through twin-screw extruder (LabTech Engineering Company LTD., Thailand). The extrusion was performed at 210 °C and 60 rpm. To make TPU-CNT films, pellets were made through cutting TPU-CNT filaments and later compressed in a hot press machine (Carver Inc., Wabash, Indiana) at 2.25 metric tons at 185 °C for 60 seconds. The films were cooled down to the room temperature and utilized to fabricate the sensors and for characterizations. Samples were cut into strips with a size of about 50×20 mm squares and a thickness of about 0.5-0.6 mm. (Figure 3.1)

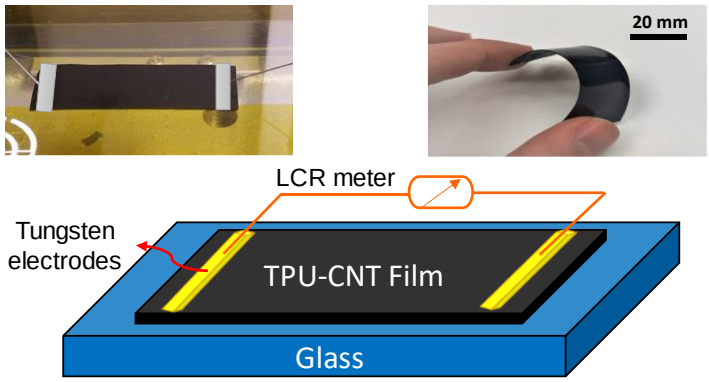

Figure 3.1. Schematic view of the measurement setup and a flexible TPU-CNT film.

3.2.2 Proximity Measuring System Configurations

The narrow strip of two ends of samples were coated with CircuitWorks CW2400 conductive silver epoxy to eliminate the noise effects like the penetration depth inside and transverse direction over the film. Tungsten pin probes were then placed on the film ends with a separation of 50 mm and an angle of 45 degree. As shown in figure 1, sensor probes were mechanically changed to coplanar electrodes due to the silver paste, and technically located on the sensor ends. Capacitance measurements were carried out by using a probing station (Keithley 4200-SCS, Tektronix, USA). Sensing conductive object approached the fixed TPU-CNT film with a constant speed of 6.6 mm/s

after 60s waiting time. To detect the maximum change in the capacitance, the samples were pre-soaked with 5V direct current (DC) to saturate and reduce the tunneling effect. Furthermore, a 30mv alternate current (AC) swiping signal was applied to measure the capacitance of the film with a frequency of 500 kHz to achieve maximum stability of the working window for the fabricated sensors. From the measurements, the value of resistivity of samples varies from 0.1 to 10^5 Ω.m.

3.3 Mathematical Model

Many capacitive proximity sensing and displacement measurement techniques are built on the use of a field - either electric or magnetic - to detect the presence or position of an object. Technically, an intruding (moving) object performs as a barrier, hindering the electric field and thus reducing the capacitance between electrodes. Thus, this change in capacitance can be reported as the sensitivity of sensor. A schematic view of the proposed sensor together with a moving object and the fringe effect concept were shown in figure 2. As can be seen, two-line electrodes are placed at distance on the polymer-based nanocomposite substrate. When a voltage is applied between the electrodes some amount of current will start flowing inside the substrate resulting in a voltage and charge distribution on the substrate. Moreover, some fringing fields will be developed outside the substrate which contribute on the stored charge on the polymer surface. The current passing to the electrodes is monitored and by dividing the current by the exciting voltage the effective capacitance cam be measured. As an object gets close to the sensor it distorts the fringing fields and consequently changes equivalent(self) C_{eq} and mutual C_m capacitances. These changes in capacitance may be measured and calibrated to measure the distance of the object from the sensor. Figure 3 illustrates a schematic view of the sensor which is composed of two conductive electrodes connected to a polymer substrate. Although the mutual capacitance C_m is increasing by the presence of an object, it is not of a great importance of this study. To measure the amount of capacitance between the electrodes (C_{eq}), they are connected to a LCR meter apparatus. When the LCR meter starts to work a sinusoidal voltage of arbitrary frequency is applied between electrodes and therefore opposite charges are stored on them. By definition, the amount of capacitance equals the amplitude of current passing through the LCR meter which stores charges on the electrodes divided by the amplitude of the derivative of the applied voltage with respect to time. It should be noted that only the component of the electrical current which has 90 degrees of difference with the

applied voltage should be considered in calculation of the capacitance. That is because due to finite resistivity of the polymer base there will be a component of current which is in phase with the applied voltage, as well.

(a)

(b)

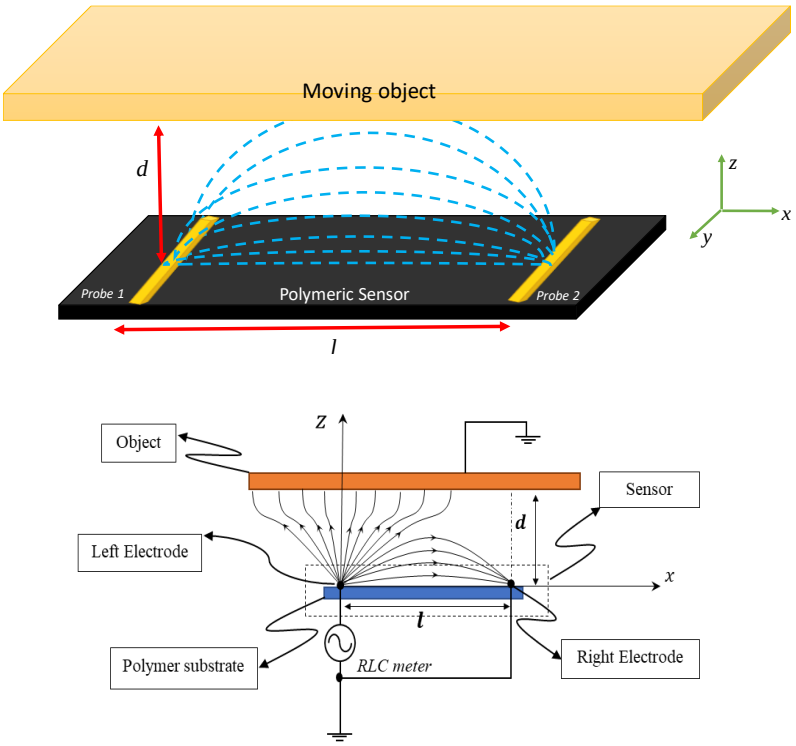

Figure 3.2. Schematic illustration of sensor mechanism for fringe-based TPU-CNT proximity sensor a) 3D model when object is at the farthest distance and not affecting the fringe fields. b) 2D model showing how the fringe field lines are being distracted.

When the object is far enough from the base polymer substrate, all the lines representing the electric field begin from the left electrode and end in the right one or vice versa. That occurs while as soon as the object which is supposed to be conductive and grounded gets close to the sensor, some electric field lines change their route and will end in the object instead of the electrodes. It is noteworthy that the following solution does not hold for an object with floating potential. In that case, different behavior should be expected, and the capacitance increases while the object approaches the sensor and subsequently sensitivity would be proportional to the dielectric constant of the object. Due to this fact as Gauss's law indicate the amount of stored charge on the right-hand side electrode decreases and therefore the measured capacitance declines too. This characteristic of the system may be used to recognize the external object which is approaching the sensor. Experimental measurements show this behavior of the system clearly. In

addition to experimental observations, here an analytical analysis of the system will be accomplished with a couple of goals. Firstly, an analytical solution helps to higher level of understanding of what happens in the system and secondly quantization of the changes of capacitance with respect to the distance of the object not only helps in calibration of the sensor but also will be beneficial in design of different sensors for various applications.

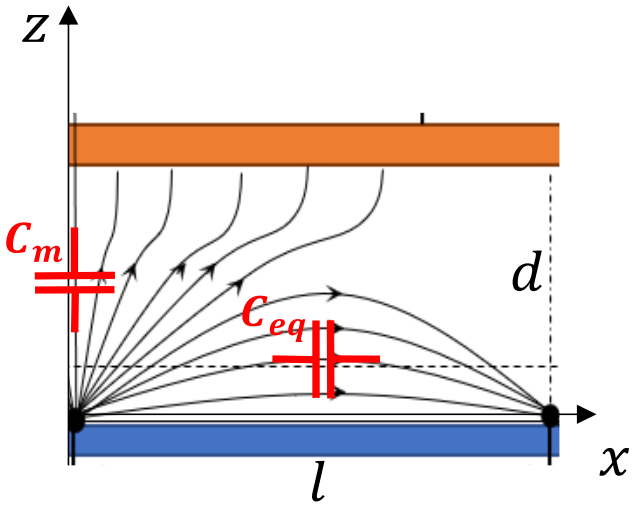

Figure 3.3. Cross section of the rectangular-shaped sensor model with cartesian coordinate system; two different capacitances which specify the sensitivity are shown. C0 is being measured by LCR meter as a polymer capacitance.

Due to large dimensions of the system in y -direction, changes of voltage along this axis may be neglected. Therefore, the problem can be modeled as a 2-D one. In what follows we derive the voltage distribution in a rectangular region determined by the following relation:

$$0 \le z \le d, 0 \le x \le l \tag{3.1}$$

The boundary conditions include:

$$\begin{cases} z = 0 \\ 0 \le x \le l \end{cases} \quad V = V_0(x,t) \quad (a$$

$$\begin{cases} z = d \\ 0 \le x \le l \end{cases} \quad V = 0 \quad (b$$

$$\begin{cases} 0 \le z \le d \\ x = 0 \end{cases} \quad \frac{\partial V}{\partial x} = 0 \quad (c \tag{3.2}$$

$$\begin{cases} 0 \le z \le d \\ x = l \end{cases} \quad \frac{\partial V}{\partial x} = 0 \quad (d$$

where $V_0(x)$ denotes the voltage distribution on the polymer substrate. Since there is no free stored charge in the part of space enveloped between the polymer substrate and the surface of object, the following equation governs the distribution of voltage in this region:

$$\nabla^2 V(x,y,z,t) = 0 \tag{3.3}$$

As mentioned above, the problem can be modeled as 2-D, therefore, the above equation turns into:

$$\frac{\partial^2 V(x,z,t)}{\partial x^2} + \frac{\partial^2 V(x,z,t)}{\partial z^2} = 0 \tag{3.4}$$

According to the boundary conditions given in equation (3.2), the solution to the above equation can be written as the following Fourier series:

$$V(x,z,t) = a_0 + b_0 z + \sum_{n=1}^{N} \left(a_n \exp\left(\frac{n\pi z}{l}\right) + b_n \exp\left(-\frac{n\pi z}{l}\right)\right) \cos\left(\frac{n\pi x}{l}\right) \tag{3.5}$$

In order that the given boundary conditions, be satisfied by the above solution one should have:

$$\begin{gathered} \sum_{n=1}^{N} (a_n + b_n) \cos\left(\frac{n\pi x}{l}\right) = V_0(x,t) \\ \sum_{n=1}^{N} \left(a_n \exp\left(\frac{n\pi d}{l}\right) + b_n \exp\left(-\frac{n\pi d}{l}\right)\right) \cos\left(\frac{n\pi x}{l}\right) = -a_0 - b_0 d \end{gathered} \tag{3.6}$$

Substituting $z = 0$ and d into equation (3.5) then integrating both sides with respect to x from 0 to l, results in:

$$a_0 = \frac{1}{l}\int_0^l V_0(x,t)dx \,, b_0 = -\frac{1}{ld}\int_0^l V_0(x,t)dx \tag{3.7}$$

Similarly, multiplying both sides of equation (6) by $\cos\left(\frac{n\pi x}{l}\right)$, then integrating with respect to x from 0 to l, one obtains:

$$\begin{gathered} a_n + b_n = \frac{2}{l}\int_0^l V_0(x,t) \cos\left(\frac{n\pi x}{l}\right) dx \\ a_n \exp\left(\frac{n\pi d}{l}\right) + b_n \exp\left(-\frac{n\pi d}{l}\right) = 0 \end{gathered} \tag{3.8}$$

Solving the above equation for a_n and b_n, results in:

$$a_n = \frac{2\int_0^l V_0(x,t) \cos\left(\frac{n\pi x}{l}\right) dx}{l\left(1 - \exp\left(2\frac{n\pi d}{l}\right)\right)}, \tag{3.9}$$

$$b_n = \frac{2\int_0^l V_0(x,t)\cos\left(\frac{n\pi x}{l}\right)dx}{l\left(1-\exp\left(-2\frac{n\pi d}{l}\right)\right)}$$

Therefore, provided that the voltage distribution (V_0) on the polymer substrate is known, its distribution in the region between the polymer substrate and the object surface (V) may be calculated according to equations (3.5), (3.7), and (3.9). Using Gauss's law the charge density per unit length stored on the polymer and object surfaces will be:

$$\lambda_P = -b\varepsilon_0 \left.\frac{\partial V(x,z)}{\partial z}\right|_{z=0} \qquad (a$$
$$\lambda_O = b\varepsilon_0 \left.\frac{\partial V(x,z)}{\partial z}\right|_{z=d} \qquad (b \tag{3.10}$$

Additionally, according to law of conservation of charge, one has the following relation governing electrical current I inside the substrate:

$$\frac{dI}{dx} = \frac{d\lambda_P}{dt} \tag{3.11}$$

Substituting equation (3.10-a) into equation (3.11) one obtains:

$$\frac{dI}{dx} = -b\varepsilon_0 \left.\frac{\partial^2 V(x,z,t)}{\partial z \partial t}\right|_{z=0} \tag{3.12}$$

According to Ohm's law, considering resistance per unit length of the polymer substrate to be represented by ρ, the substrate current may be related to its voltage derivative as:

$$\frac{dV_0}{dx} = \rho I \tag{3.13}$$

Substituting equation (3.12) into the above equation, results in:

$$\frac{\partial^2 V_0(x,t)}{\partial x^2} = -\rho b\varepsilon_0 \left.\frac{\partial^2 V(x,z,t)}{\partial z \partial t}\right|_{z=0} \tag{3.14}$$

Substituting $V(x,z,t)$ from equation (3.5) into the above equation, one obtains:

$$\frac{\partial^2 V_0(x,t)}{\partial x^2} = -\rho b\varepsilon_0 \left(-\frac{1}{ld}\int_0^l \frac{\partial}{\partial t} V_0(x,t)dx + \frac{2\pi}{l^2}\sum_{n=1}^{N} n \left(\begin{array}{l} \dfrac{\exp\left(2\frac{n\pi d}{l}\right) - \exp\left(-2\frac{n\pi d}{l}\right)}{\left(1-\exp\left(2\frac{n\pi d}{l}\right)\right)\left(1-\exp\left(-2\frac{n\pi d}{l}\right)\right)} \\ \times \int_0^l \frac{\partial}{\partial t} V_0(x,t)\cos\left(\frac{n\pi x}{l}\right)dx \end{array} \right) \cos\left(\frac{n\pi x}{l}\right) \right) \tag{3.15}$$

Multiplying both sides of equation (3.15) by $\cos\left(\frac{n\pi x}{l}\right)$ when n varies from 0 to N, then integrating with respect to x from 0 to l, one obtains:

$$\left(\frac{\partial V_0(x,t)}{\partial x}\right)\Big|_{x=0}^{l} = -\rho b\varepsilon_0\left(-\frac{1}{d}\int_0^l \frac{\partial}{\partial t}V_0(x,t)dx\right) \ (a)$$

$$\int_0^l \frac{\partial^2 V_0(x,t)}{\partial x^2}\cos\left(\frac{n\pi x}{l}\right)dx \tag{3.16}$$

$$= -\rho b\varepsilon_0\frac{n\pi}{l}\left(\frac{\exp\left(2\frac{n\pi d}{l}\right)-\exp\left(-2\frac{n\pi d}{l}\right)}{\left(1-\exp\left(2\frac{n\pi d}{l}\right)\right)\left(1-\exp\left(-2\frac{n\pi d}{l}\right)\right)}\times\int_0^l \frac{\partial}{\partial t}V_0(x,t)\cos\left(\frac{n\pi x}{l}\right)dx\right) \ (b)$$

Applying the integration by parts method to the left-hand side of equation (3.16-b), one obtains:

$$\int_0^l \frac{\partial^2 V_0(x,t)}{\partial x^2}\cos\left(\frac{n\pi x}{l}\right)dx = \left(\frac{\partial V_0(x,t)}{\partial x}\cos(n\pi)\right)\Big|_0^l - \left(\frac{n\pi}{l}\right)^2 V_{0n}(t) \tag{3.17}$$

where:

$$V_{0n}(t) = \int_0^l V_0(x,t)\cos\left(\frac{n\pi x}{l}\right)dx \tag{3.18}$$

Denoting currents passing through the substrate at $x = 0$ and l, by I_0 and I_l, respectively, according to equation (3.13) one has:

$$I_0 = \frac{1}{\rho}\left(\frac{\partial V_0(x,t)}{\partial x}\right)\Big|_{x=0}, I_l = \frac{1}{\rho}\left(\frac{\partial V_0(x,t)}{\partial x}\right)\Big|_{x=l} \tag{3.19}$$

Substituting equations (3.17), (3.18) and (3.19) into (3.16), results in:

$$I_l - I_0 = \frac{b\varepsilon_0}{d}\dot{V}_{00} \ (a)$$

$$\rho(I_l(-1)^n - I_0) - \left(\frac{n\pi}{l}\right)^2 V_{0n}(t) = -\rho b\varepsilon_0\frac{n\pi}{l}\left(\frac{\exp\left(2\frac{n\pi d}{l}\right)-\exp\left(-2\frac{n\pi d}{l}\right)}{\left(1-\exp\left(2\frac{n\pi d}{l}\right)\right)\left(1-\exp\left(-2\frac{n\pi d}{l}\right)\right)}\right)\dot{V}_{0n} \ (b) \tag{3.20}$$

In the case that the LCR meter applies a sinusoidal voltage of frequency ω to the electrodes, the above equation should be solved with respect to the following boundary conditions:

$$x = 0,\ V_0 = V_{exc}\cos(\omega t)$$
$$x = l,\ V_0 = 0 \tag{3.21}$$

Considering the steady state solutions for of V_0, I_0, and I_l as:

$$\tilde{V}_{0n}(t) = \tilde{v}_{0n}e^{i\omega t}$$
$$I_0(t) = i_0 e^{i\omega t} \tag{3.22}$$
$$I_l(t) = i_l e^{i\omega t}$$

then substituting into equation (20), results in:

$$v_{0n} = \alpha_n i_0 + \beta_n i_l x = l,\ V_0 = 0 \tag{3.23}$$

where:

$$\beta_0 = -\alpha_0 = \frac{d}{b\varepsilon_0 i\omega}, \alpha_n = -g(n), \beta_n = (-1)^n g(n)$$

$$g(n) = \frac{\rho}{\left[\left(\frac{n\pi}{l}\right)^2 - \rho b\varepsilon_0 \frac{n\pi}{l}\left(\frac{\exp\left(2\frac{n\pi d}{l}\right) - \exp\left(-2\frac{n\pi d}{l}\right)}{\left(1-\exp\left(2\frac{n\pi d}{l}\right)\right)\left(1-\exp\left(-2\frac{n\pi d}{l}\right)\right)}\right) i\omega\right]} \tag{3.24}$$

$V_0(x,t)$ may be represented using a Fourier series as:

$$V_0(x,t) = \frac{2}{l}\sum_{n=0}^{N} V_{0n}(t)\cos\left(\frac{n\pi x}{l}\right) \tag{3.25}$$

Substituting equation (3.25) into (3.21) results in:

$$\frac{2}{l}\sum_{n=0}^{N} v_{0n} = V_{exc}, \quad \sum_{n=0}^{N} v_{0n}(-1)^n = 0 \tag{3.26}$$

Using the representation given in equation (3.23), one has:

$$\begin{gathered}\left(\sum_{n=0}^{N}\alpha_n\right) i_0 + \left(\sum_{n=0}^{N}\beta_n\right) i_l = \frac{l}{2}V_{exc} \\ \left(\sum_{n=0}^{N}(-1)^n\alpha_n\right) i_0 + \left(\sum_{n=0}^{N}(-1)^n\beta_n\right) i_l = 0\end{gathered} \tag{3.27}$$

Solving the above equation for i_l, the following expression is found for the input current to the right-hand electrode:

$$i_l = \frac{\frac{l}{2}\left(\sum_{n=0}^{N}(-1)^n\alpha_n\right)V_{exc}}{\left(\sum_{n=0}^{N}(-1)^n\alpha_n\right)\left(\sum_{n=0}^{N}\beta_n\right) - \left(\sum_{n=0}^{N}\alpha_n\right)\left(\sum_{n=0}^{N}(-1)^n\beta_n\right)} \tag{3.28}$$

The total impedance seen by the LCR meter may be calculated through dividing the applied voltage V_{exc} to the input current of the right hand electrode i_l. The real part of derived impedance represents the equivalent resistance due to the finite resistivity of the nanocomposite substrate while its imaginary part represents the equivalent capacitance between the electrodes and the object. Therefore, the following expression may be used for calculation of the equivalent capacitance of the system:

$$C_{eq} = -\frac{\mathrm{Im}(i_l)}{\omega V_{exc}}, R_{eq} = -\frac{V_{exc}}{\mathrm{Re}(i_l)} \tag{3.29}$$

3.4 Results and Discussions

In this section, analytical closed-form results are discussed and validated by experimental measurements. From the expression model of sensor, equation (29) shows cleraly that the fring capacitance C_{eq} is determined by the geometrical parameters, the proximity distance, relative permittivity, and the resistivity of the sensor design. However, here the geometrical parameters are not of interest to be investigated. Based on the CNT contents inside the film sensor, the resistivity changes from relatively high-resistant sample (the sensor with low volume of CNTs) to very conductive sample containing a great volume of CNTs. From the experimental measurement tests, the value of resistivity for samples varies from 0.1 to 10^5 Ω.m; yet, by increasing CNTs content, after percolation threshold which takes place in the lower percentage of CNT contents, the resistivity becomes extremely low. So, the TPU with more than 2 wt % CNTs exhibits low resistivity and draws a very high current from LCR meter. Accordingly, in this numerical study the CNT contents are adjusted so that the resistivity falls between 10^2 Ω.m to 10^6 Ω.m. Frequency 500kHz was earlier experimentally optimized with the purpose of maximize signal to noise ratio (SNR) of measured signals. Fig. 4a. shows the proximity results of the capacitance change for different resistivities of film sensor through the proximity distance of 24cm. The sensor with resistivity of 10^2 Ω.m presents the initial capacitance about 0.045pF at the farthest distance and the capacitance reaches to 0.022pF at the distance of 4cm. As expected by the fringe effect, the capacitance becomes lower in magnitude when the object approaches to the nanocomposite sensor. Furthermore, the analytical model shows that by increasing the resistivity beyond 10^5 Ω.m, the capacitance is not being affected anymore. While the impedance increases drastically, it demands infinite amount of current which is not feasible. Thus, there is no significant effect on the capacitance behavior for the higher resistivity.

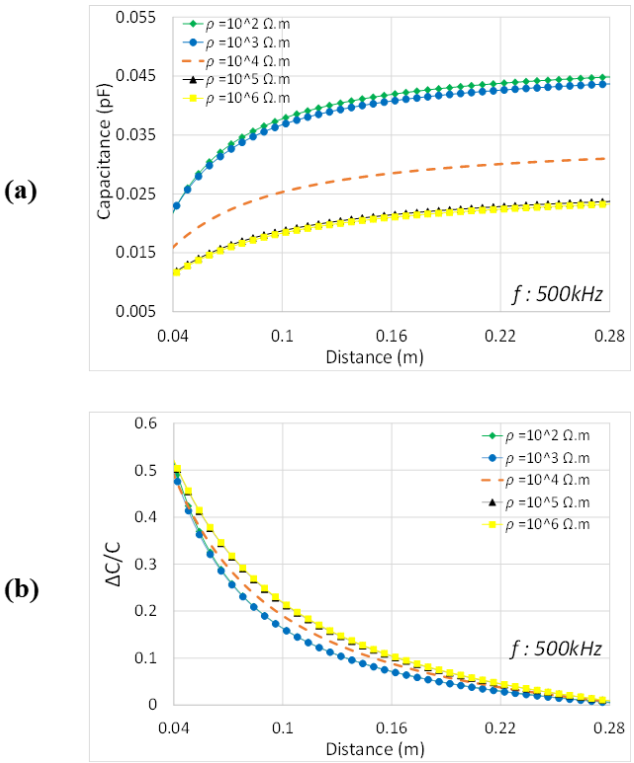

Figure 3.4. Analytically calculated capacitance versus object proximity for different value of TPU-CNT resistivities at the ecitation frequency of 500kHz a) absolute value b) relative changes.

To capture the highest sensitivity among different values of resistivity, the absolute change of capacitance to the initial capacitance recorded at the farthest distance (d=28cm) is plotted in Figure 3.4 (b). Here, the remarkable trend is that the proximity sensitivity of the TPU-CNT sensors rises by increasing the resistivity (lower volume of CNTs). Technically, TPU has been known as a high polar polymer which can be used as a perfect insulator. Addition of CNTs inside the TPU structure, makes the film semi-conductive and increases the effective area of electrodes and consequently the capacitance. Therefore, as evidently expected in fig. 4a, the initial capacitance of the TPU/CNT film has been increased by adding CNTs content. Nevertheless, from fig. 4b, the maximum sensitivity (ΔC/C) is being observed at the lower content of CNTs (ρ =105,106 Ω.m).

Figs. 5 and 6 show the analytically calculated voltage distribution within the neighboring area between the sensor and object at different values of resistivity. Where, the graph's horizontal axis shows the size of sensor length where electrodes are placed and, the vertical axis indicates the distance with the moving object. Furthermore, contour lines corresponding to certain values of the voltage are plotted together with vectors (in red) indicating the magnitude and direction of the

electric field at different points. As a consequence of the nonzero electrical resistivity of the sensor both voltage and electric field have some phase difference with respect to the excitation voltage. Therefore, to fully illustrate how these two variables change as functions of time one needs to have both in-phase and out of phase components. These two components are schematically shown in Figure 3.5, Figure 3.6, respectfully. As seen, when a target object comes closer to the sensor, it interferes with the field lines between the electrodes. As a consequence, the fringing field lines are reconfigured due to presence of the object which in turn reduces the equivalent capacitance (self-capacitance). Additionally, a comparison of the graphs corresponding to different resistivities shows that the electric field at the vicinity of the electrodes is intensified as resistivity decreases. That emerges because at higher conductivities some portion of the stored charge is distributed on the TPU/CNT film leading to enhancement of the effective area of the electrodes, increasing the capacitance, and generating a more intense electric field.

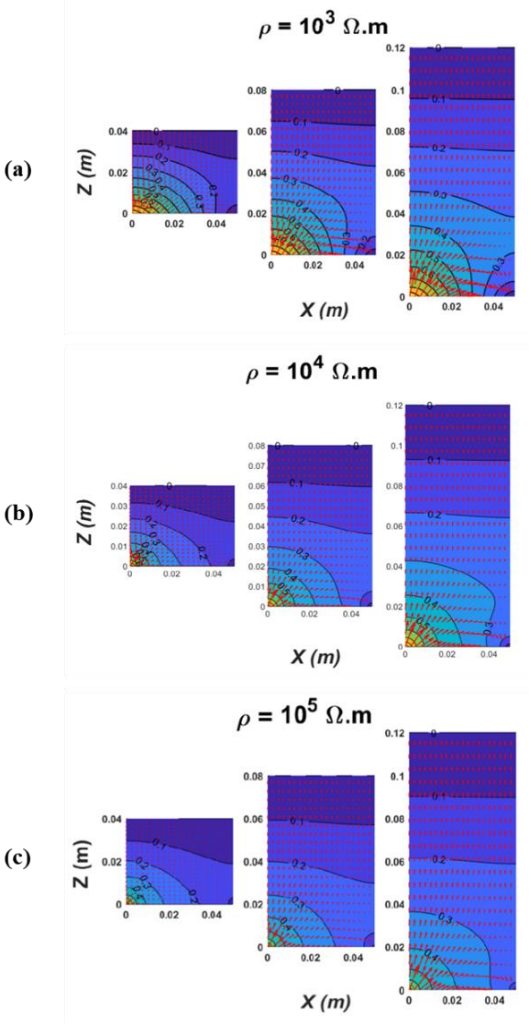

Figure 3.5. Potential contour for the in phase voltages between probes and object for three different location of the object a) ρ =10^3 Ω.m b) ρ =10^4 Ω.m c) ρ =10^5 Ω.m

As earlier mentioned, the sensing mechanism is based on the object interference with the electrical field between two probes. The interference disturbed and reduced the number of electric field lines (i.e., C_{eq} self-capacitance) and consequently, stored charges decreased radically over the polymer. To validate that the change of capacitance comes from the fringe phenomenon and also to capture the effect of resistivity, experimental tests are being carried out for three different CNT volumes. Figure 3.7 (a) demonstrates that the sensitivity goes up when the film resistivity increases. It closely confirms what the analytical model earlier proved. The experiments also reveal that TPU film containing 1wt% CNTs presents the maximum sensitivity to the proximity sensing. Resistivity of 1wt.% TPU/CNT was earlier measured 10^5 Ω.m. From both analytical and

experimental results, it can be deemed that either this CNT volume or a very close volume would be the optimal nanocomposite sensor out of TPU/CNT, taking into account the sensitivity and impedance.

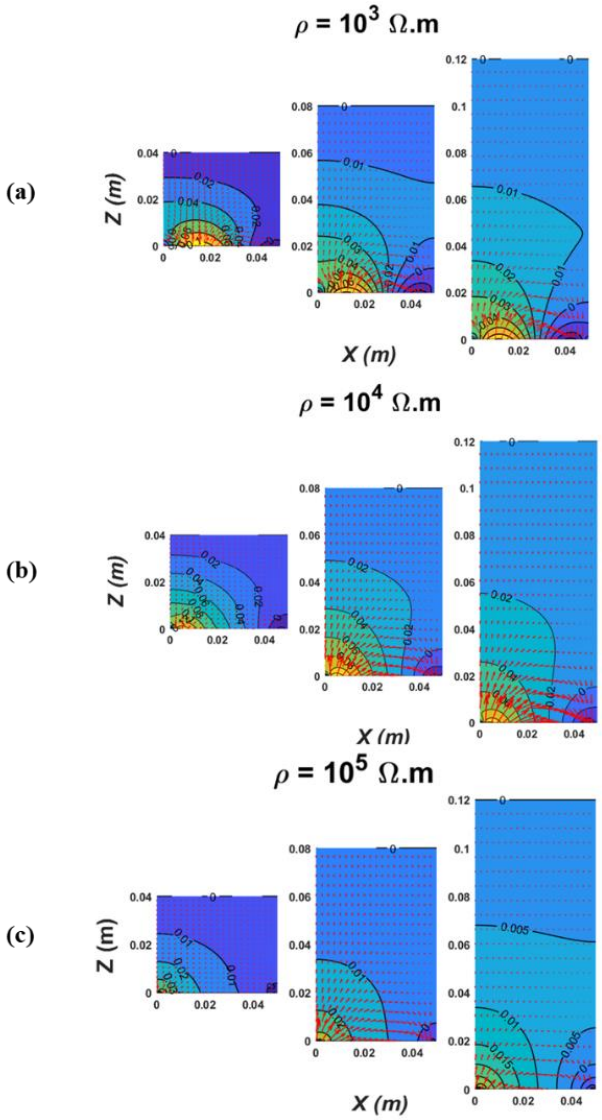

Figure 3.6. Potential contour for the out of phase voltages between probes and object for three different location of the object a) ρ =10^3 Ω.m b) ρ =10^4 Ω.m c) ρ =10^5 Ω.m

On the other hand, a comparison of analytical and experimental models is plotted in Figure 3.7 (b) over a distance of 0.14m (capacitance variation is being normalized with respect to the initial capacitance). Both plots have shown relatively similar sensitivity behavior and reached to the peak of 0.5-0.6 at the distance of 0.02 m. Apparently, the analytical model results are larger than the measured ones. This discrepancy is primarily introduced by the object used in the

measurement. The object dimension was assumed infinite in the analytical model, but finite in the experiment. The body section of the probes is relatively large compared with the size of polymer, which can be other possible sources of error. The difference between the mathematical model and the fabricated nanocomposite sensor is within 10% if the CNT content of polymeric insulator is limited to 1 wt %.

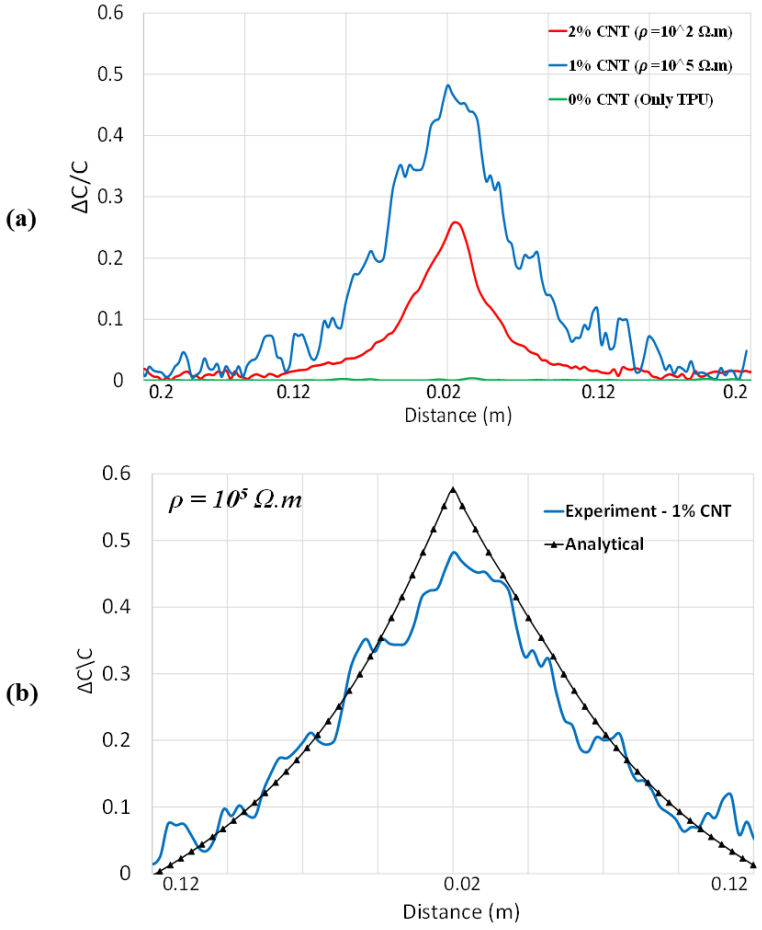

Figure 3.7. Sensitivity (change of capacitance to the initial) comparison (a) empirical sensitivity of different wt %. CNTs through a distance of 0.2 m (b) Simulation result versus experimental one at $\rho = 10^5$ Ω.m

3.5 Conclusion

To summarize, according to the physical cartesian model of fringe capacitances, this paper established a 2-D analytical model of the potential, which was based on changing the measured capacitance of rectangular nanocomposite film sensor while an object approached in and moved away. In this work, the modeling of capacitive proximity sensors using the Laplace's equation has

proven to be a fast and reliable technique to obtain the capacitance of a capacitive proximity sensor. The resistivity of sensor film demonstrated a significant effect on the sensitivity while it is in the range of 10^3-10^5 Ω.m. Accordingly, the fabricated proximity sensor with different volume of CNTs not only clearly confirmed the decreasing trend of the analytical capacitance but it was also compatible with the sensitivity results of the analytical model. As a comparison, 1wt% CNT which its resistivity was measured around 10^5 Ω.m was plotted over the analytical results with a good agreement. The potential contour of our model has been compared for the different distances from the object, from the probes and for different resistivities.

The calculated capacitance values from the designed tool have been compared to the experimental values and a close agreement between them was observed. This agreement confirmed that the polymeric nano-based sensor as a designed tool can generate optimal capacitive proximity sensitivity in the wide range of detection and accuracy while it has solid-state manufacturing technology.

4 3D-PRINTED FLEXIBLE STRUCTURES WITH EMBEDDED DEFORMATION/DISPLACEMENT SENSING FOR THE CREATIVE INDUSTRIES

Acknowledgment: This is a post-peer-review, pre-copyedit version of an article published in AIAA. The final authenticated version is available online at:
https://arc.aiaa.org/doi/abs/10.2514/6.2021-0534

Author contributions
R.M. developed and executed the research study, simulations, material preparation, mechanical characterization, and wrote the manuscript. M.A. and H.D. supervised the findings and coordinated various aspects of the project.

4.1 Introduction

Electronic technologies including sensors are one of the key components in smart devices. Flexible sensors have been highly explored recently for incorporation into textiles or for direct connection to the body of a human/robot for wearable smart devices and robotic systems. Multiple flexible or stretchable sensors have been developed by Micro-electro-mechanical system (MEMS) micromachining techniques for different purposes. For instance, strain sensors can detect body motion[75, 76, 122], tactile sensors [80-82] enable to monitor three-axis handling/manipulation of objects, while proximity sensors [61, 82, 83] avoid any possible accident of humans and robots to unknown obstacles. Additive Manufacturing has been leveraged to fabricate form-and-fit prototypes in arbitrary geometries for decades. The integration of electronic components within these shapes has been pursued since the 1990s providing advances in antennas, biomedical devices, smart wearables, prosthetics, electromechanical devices, and satellites [123, 124]. In 3D printed electronics, conductors serve as interconnect between embedded electronic components with a variety of methods including micro-dispensing, ink jetting and aerosol jetting of conductive inks [124, 125] as well as by the structural embedding of bulk conductors inserted directly into additively-manufactured dielectric substrates [126, 127]. The integration of these 3D-printed structures with electronic needs a few manufacturing strategies: (a) during fabrication with process interruptions, (b) after the fabrication with insertion of components into layers. Generally, 3D printed electronics have included process interruptions of the additive manufacturing for both the component placement and interconnect printing. Within the context of additive manufacturing, lattices are the focus of significant research as the structures since they (a) provide a tailored weight

versus-strength balance and (b) can be fabricated to include strut-size variation – gracefully modulating the density and mechanical response from one side to the other within the structure [128, 129]. Additionally, 3D printing of haptic gloves out of TPU/CNT is addressed to be challenging due to manufacturing limitations [130]. Mostly, these gloves are made of flexible substrates without any conductive nanoparticles and its sensing mechanisms are embedded through printed circuit board (PCB). Introducing wires into these structures for the embedding of electronics seems to fit into aerospace applications in which light weighting is paramount. Other potential applications include wearable electronics, in which soft and resilient elastomers provide dampening for comfort and safety. In both applications, sensing in these structures provides unprecedented internet-of-things data acquisition for structural health monitoring in automotive or health and proximity activity monitoring for the general public. In the first section we look over how the film sensor works as a complex capacitor and in the next section, investigations on 3D printing strategies are being studied and in the final section we come up with the design modeling of the lattice and glove and how consequently wiring could be implemented in them with minimizing the overall weight of the structures and high range of proximity measurement.

4.2 Materials and Methods

4.2.1 Materials Preparation

TPU (Elastollan 1185A polyurethane, with a density of 1.12g/cm3) and TPU/MWCNT masterbatch (A 5wt% of TPU/MWCNT containing NC7000 MWCNT with 90% purity with an average diameter and length of 9.5nm and 1.5μm, respectively) were purchased and diluted. TPU filaments containing 1,2,3,4 and 5 wt % MWCNT were produced by diluting a 5wt % masterbatch of TPU/MWCNT with pure TPU through a 16 mm twin-screw extruder with L/D ratio of 16/40 (LabTech Engineering Company LTD., Thailand). To make TPU-CNT films, pellets of TPU-CNT were then cut from filaments and later compressed in a hot press machine (Carver Inc., Wabash, Indiana) at 2.25 metric tons at 185 °C for 60 seconds. The films were cooled down to the room temperature and utilized to fabricate the sensors and for characterizations. Samples were cut from the films in 60×20 mm squares with 0.5 mm thickness. Figure 4.1 showed the final product and the flexibility of the film sensor.

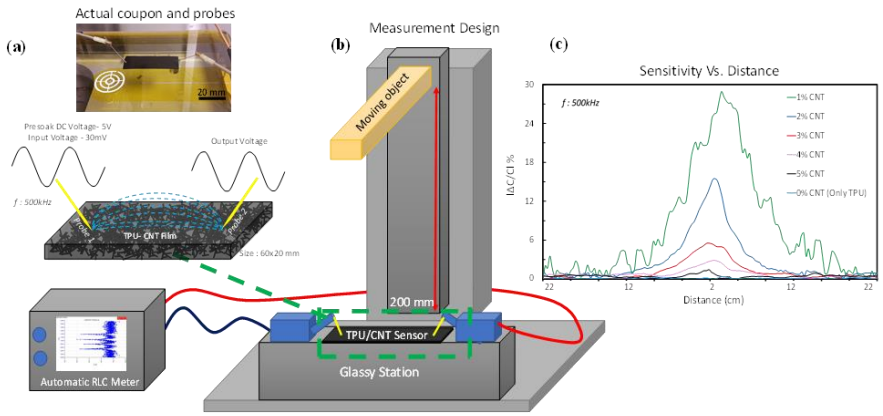

Figure 4.1. Schematic illustration of a TPU/CNT proximity sensor setup and sensitivity. **a)** Actual coupon and semi-planar probes. **b)** Measurement setup vs. distances ranging from 20 to 220 mm were applied by using a probing station (Keithley 4200-SCS, Tektronix, USA). To detect the maximum change in the capacitance, the samples were pre-soaked with 5V direct current (DC) to saturate and reduce the tunneling effect. Furthermore, a 30mv alternate current (AC) swiping signal was applied to measure the capacitance of the film with varying frequencies. Negative change plot in capacitance showing sensitivity on RLC meter screen. **c)** Maximum sensitivity comparison of different wt %. CNTs. Absolute percentage change of capacitance to the initial capacitance is plotted against distance.

Proximity measurements and sensor readout: Distances ranging from 20 to 220 mm were applied by using a probing station (Keithley 4200-SCS, Tektronix, USA). The TPU-CNT film was fixed over a glass substrate to eliminate noise and the conductive sensing object (brass bar- 10 mm (height)×20 mm (width)×200 mm (length)) approached the sample with a speed of 6.6 mm/s. To detect the maximum change in the capacitance, the samples were pre-soaked with 5V direct current (DC) to saturate and reduce the tunneling effect. Furthermore, a 30mv alternate current (AC) swiping signal was applied to measure the capacitance of the film with varying frequencies to achieve maximum stability of the working window for the fabricated sensors. As demonstrated in Figure 1(a-c), the experimental setup and how change of capacitance to the initial capacitance ($\Delta C/C_0\% - \text{sensitivity}$)) were analyzed. The entire three set of tests were done for each CNT content.

4.2.2 3D Printing parameters

To investigate the additive manufacturing effect in the sensitivity of TPU/CNT sensor, samples are printed out by Ultimaker 3 with similar thickness and size but different orientations in order to be compared with hot-press samples. Printing parameters and the sensitivity for the two

most sensitive samples (2 & 3% wt.) are displayed in Figure 4.2. As it has shown, 3D printing of materials exhibits quite higher sensitivity respect to the hot-press ones, particularly for 2% wt. Among the different 3D printed patterns, [0,0] direction provides us the most sensitivity which can be selected as an optimized strategy to get higher sensitivity. Unlike the hot-press samples, 3D-printed TPU/CNT film contains a crystalline network which can help to flow surface charges better and subsequently the capacitance changes more.

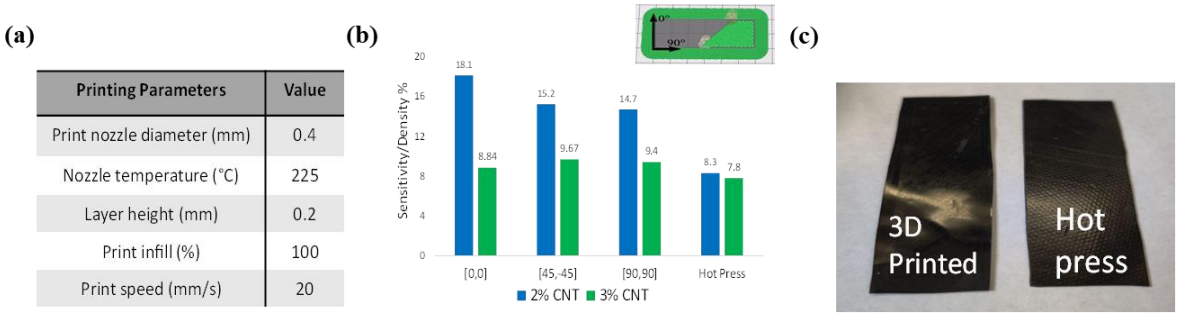

Figure 4.2. 3D-printing parameters with different printing orientations versus hot press for two different CNT content.

4.3 Design of 3D printed structures

4.3.1 Haptic Glove

Wearable sensors are of great importance in healthcare studies to help people to perceive, touch and hold objects. Specifically, proximity sensor is nowadays very demanded for the visually impaired people. Although a quite number of studies have been carried out to employ proximity sensors in a wearable gadget like glove, flexibility, sensitivity, and manufacturing of them are still challenging. Here, TPU as a substrate addressed a very flexible material reinforced with CNTs as conductive particles will be mixed and fed into the Ultimaker 3D printer. The purpose of this glove is to provide proximity guidance feedback to the user and allow destination selection through the use of pushbuttons. The system helps users navigate by understanding objects position with the use of capacitive based sensor and routing a path selected by the vision impaired individual, dependent on the number of obstacles. Glove-based technologies capture real-time finger movements and gestures with high degrees of freedom. To do a very preliminary result, we have come up with a detailed-sketch and a prototype is 3D printed with PVA (Polyvinyl acetate) and TPU/CNTs and demonstrated in Figure 4.3. The 3D printable plastic, which is often used as a support material with dual extrusion 3D printers and which dissolves in water is PVA. TPU easily

is being left once glove is washed with water and then TPU/CNT filament used to make a sensitive shell to be used as the film sensor. The glove was required to complete manufacturing tasks, with three steps: 1) preparing filaments of TPU/CNTs with extruder, 2) choosing the best support and strategy to 3D print TPU/CNT/PVA 3) embedding the wiring system internally to prevent any dilution in data acquisition. We measured the time to complete step 1 as material preparation, and step 2 as design and 3Dprinting time, and the total wiring time to complete the tasks.

4.3.2 Lattice cube

Lattices have attracted substantial attention in recent research as additive manufacturing can fabricate these structures more easily than traditional methods. Modulating the density of the structures by varying strut or beam size throughout the lattice has been achievable by the combination of AM and advances in CAD software, both of which have dramatically improved particularly for generating complex geometries. Many lattice unit cells have been explored for optimizing stiffness or compression performance while minimizing the overall weight of the structure [131-134] and the exploration has included functionally graded lattices that can modulate the effective density for tailoring the mechanical and electromagnetic response. In this study, a simple uniform hexagonal lattice was used (51mm × 51mm × 25mm) to investigate the functionality of sensor under proximity detection and impact by human or any other object. Figure 4.4 (a). shows the lattice that was designed primarily, printed with 3% wt CNTs, and tested. Sensitivity also was measured at three various frequencies in Figure 4.4 (b) & Figure 4.4 (c). Lattice structure does not reveal any different in sensitivity while frequency changed while in the film sensor, we captured quite greater value of sensitivity at higher frequencies. Furthermore, to evaluate the proximity and impact of properties of the lattice, human hand approaches and human fist hits the lattice (with speed of 6.6 mm/s), respectively. As seen in Figure 4.5, proximity and impact sensing values of the lattice are captured in the different range. This capability gives the consumer such advantages to not only perceive the moving object, but it can also absorb the impact by the external object, no matter that it is conductive or non-conductive. We also have a plan to optimize the weigh to strength property of the lattice with similar sensitivity.

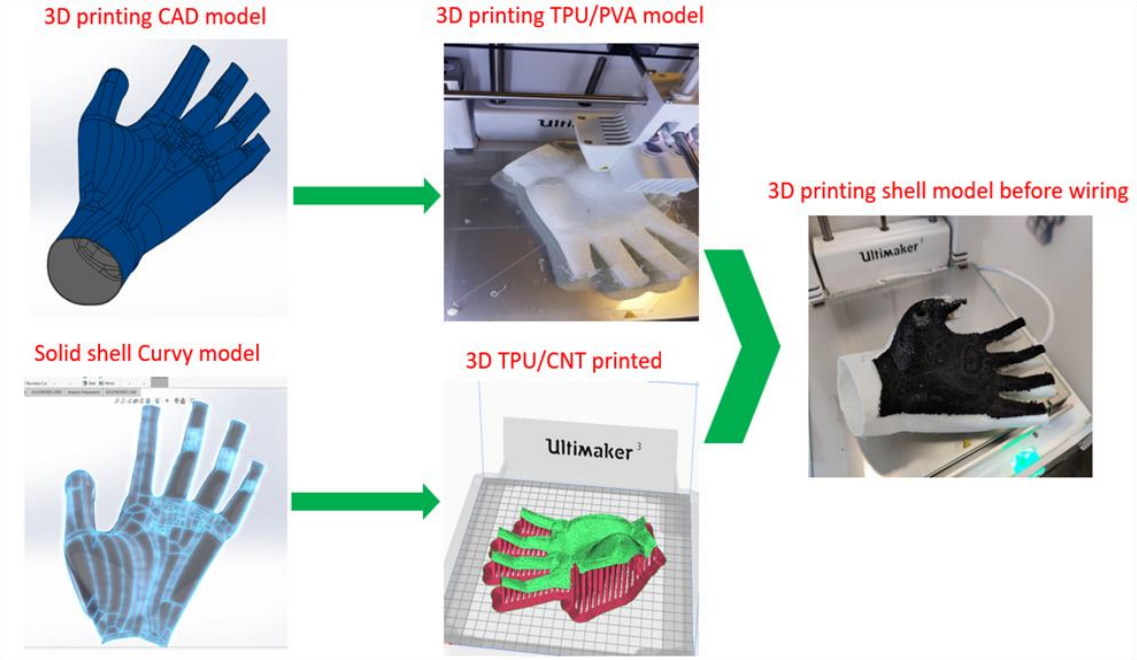

Figure 4.3. Design strategy to make the main skeleton of haptic glove before wiring implementation.

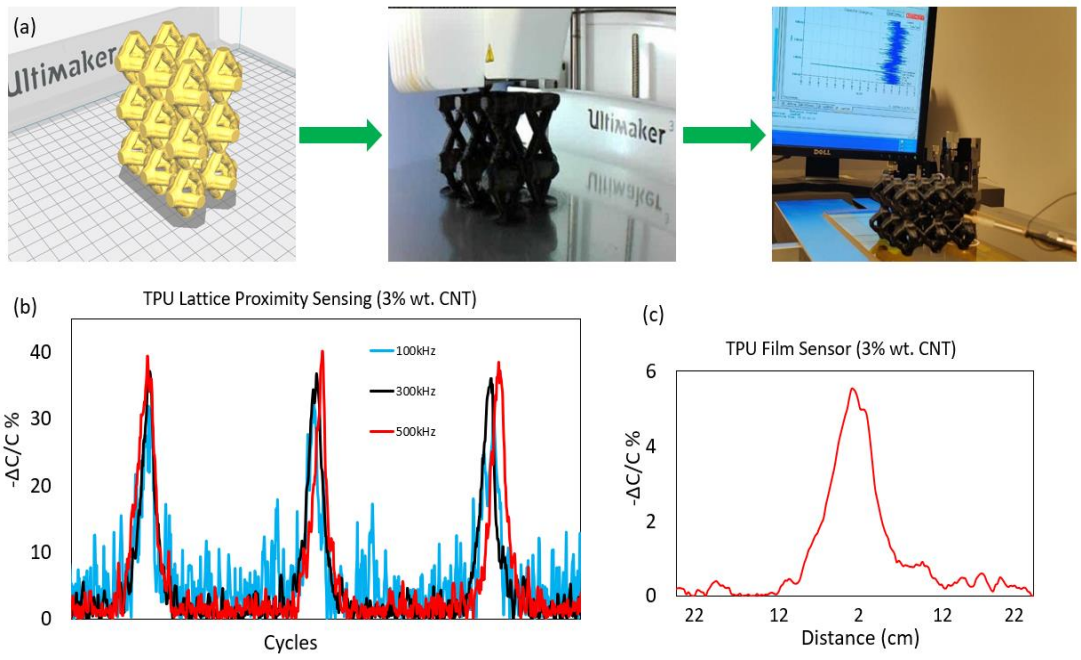

Figure 4.4. (a) Sensitized lattice cube design and 3D printing (b) Sensitivity of TPU/CNT Lattice under proximity measurement in the range of 20 cm. for different frequencies. (c) Sensitivity of TPU/CNT film sensor.

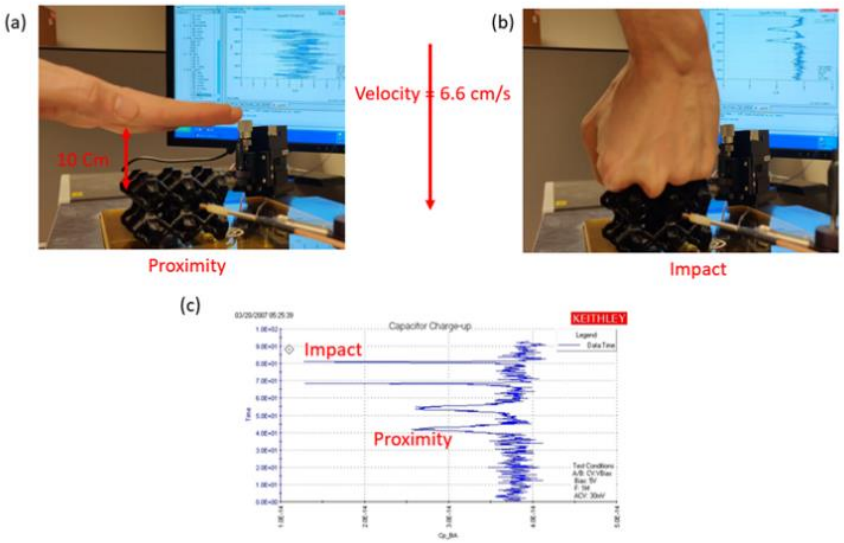

Figure 4.5. (a) proximity sensing of human hand (b) Impact sensing of human fist hit (c) Capacitance changes for two similar cycles of proximity and impact, respectively.

4.4 Conclusion

A sensorized elastomer lattice and haptic glove were printed by Ultimkaer 3 out of flexible polymer reinforced with CNTs; it was shown that the sensor measures both high-performance mechanical response while exhibiting accurate proximity measurement of moving object and reasonable low-velocity impact sensing. By combining both the mechanical benefits of structures coupled with embedded intelligence and sensing, new anatomy-specific smart wearables are now achievable. The elastomer material used in this work is durable and flexible, and consequently, the resulting structures need sensors and electronics fabricated and integrated in novel manners to survive in harsh environments. The capacitance changes which come from the fringe and tunneling effect in the system helps to be used as a sensitivity of these sensorized structure. CNTs made these insulating structures conductive and ready to transfer stored charges and consequently changes in the capacitance. These structure needs to be tested in place with embedded pair of wiring acting as a sensor. a small board-a chip includes an additional battery, and the two sensor wires needs to be alongside with the structures because the wires and needles outside of the lattice dilute the measurement and decrees the sensitivity and it would be more convenient to be presented in market (Miniaturization).

5 AN INTEGRATED NANOCOMPOSITE PROXIMITY SENSOR: MACHINE LEARNING-BASED OPTIMIZATION, SIMULATION, AND EXPERIMENT

Acknowledgment: This is a post-peer-review, pre-copyedit version of an article published in Nanomaterials. The final authenticated version is available online at:
https://www.mdpi.com/2079-4991/12/8/1269

Author contributions
R.M. developed and executed the research study, simulations, software, material preparation, mechanical characterization, and wrote the manuscript. M.G. and H.D. supervised the findings and coordinated various aspects of the project.

5.1 Introduction

Thanks to the fascinating and broad applications, wearable electronics grow swiftly and require mainly a very efficient sensing system [60, 68, 73, 87, 104, 135, 136]. Fabrication and design of these systems require a balance between system functionality and cost/energy reduction [52, 136-139]. The recent employment optimization methods in the energy consumption of sensory designs are highlighted, which also has motivated researchers to identify more efficient sensors. However, not many optimization strategies are available in the sensor literature nowadays [53, 140-144]. Among commercial sensors used in wearable smart devices, flexible nano-based sensors whose sensing materials are nanoparticles such as carbon nanotubes (CNTs), graphene, and metal nanowires become appealing and valuable because they are skin-friendly and durable to withstand mechanical damage [10, 33, 40, 44, 98, 99].

Proximity sensors are especially demanding candidates for nondestructive measurement of collision prevention in biomedical industries [22–29]. Consequently, it is essential to detect the presence of an object without making contact. Although some optical, ultrasonic, and inductive-based models for proximity sensing have been developed, capacitive-based sensors have a simpler design, easier readout, and a wider range of functionality for metallic and non-metallic targets [30–32]. The design of a capacitive proximity sensor should be informed by fundamental electrostatic theories and the tradeoff of sensitivity, resolution, and energy consumption. Although theoretical analyses are somewhat simplified, with some idealized assumptions and strict boundary conditions, and all sensor responses cannot be completely stated, such models still contribute to

optimizing sensor parameters to obtain the highest design priority for a practical application. Similarly, studies on wireless sensor networks have proposed an optimization formulation based on experiments and achieved a tradeoff between sensing coverage and energy consumption [145, 146]. Recently, optimization of motion sensors was carried out by developing an integrated electromechanical model to predict and simulate the operation of a prototype [140]. For the first time, they directly addressed all device parameters, regardless of their importance. However, a comparative study of capacitive sensors, which benefits of machine learning as a powerful tool, is of great need in wearable electronics.

This paper presents a novel procedure for finding nanocomposite proximity sensors' optimal size and properties. The nanocomposite sensor has a nanostructure simpler than that of previous studies [34, 37, 40, 70, 147, 148], but in our previous studies [43], there was an intricate microstructure in which CNTs were utilized as a reinforcement in the mold substrate thermoplastic polyurethane (TPU). Our primary results captured the initial testing validation of a capacitive-based sensor (experiment), and later this sensor was simulated by solving the partial differential Laplace equation [149]. Specifically, it was shown that the behavior becomes very sensitive in the specific range of the active materials (CNTs) used as reinforcements in the TPU matrix. Furthermore, other parameters, including geometry, resistivity, dielectric, energy consumption, and frequency, also impact the sensor's sensitivity.

Our proposed geometrical sensing system was modeled in MATLAB as a Fourier series that uses the key parameters as inputs [149]. One of the main requirements for optimization process is a low runtime. However, this analytical model results in extremely time-consuming simulations, making the optimization process impossible. An Artificial Neural Network can instead provide a black-box model (or function) that works similar to the original MATLAB model and can solve the problem in milliseconds.

Hence, this work represents a Genetic Algorithm (GA) dual-objective optimization process to simultaneously achieve the maximum sensitivity and the minimum cost of nanocomposite materials. The proposed approach builds a black-box model by training an artificial neural network (ANN) with 1000 samples with arbitrary inputs and outputs. Then, the black-box model is employed as the fitness function of a genetic algorithm for a dual-objective optimization of the sensor sensitivity and cost of active materials (CNTs). Consequently, a two-dimensional Pareto Frontier and the scatter distribution of decision variables are employed to find the optimum value

or range of decision variables that lead to maximum sensitivity and minimum cost. The primary objectives and novelties of this study are as follows:

- To propose an integrated proximity sensing system that is capable of detecting objects in a wide range by means of active materials.
- To train an ANN black-box model that substitutes the original analytical model and thus makes the GA optimization feasible.
- To implement a dual-objective optimization of sensitivity and cost and later present a two-dimensional Pareto Frontier of the optimum solutions.
- To compare the best solutions for different CNT percentages and illustrate the effect of CNT on the optimum sensitivity and cost.
- To find the effect of different decision variables on each other and on the objective functions using two-by-two scatter distributions.
- To simulate the optimum film sensor using the closed-form analytical model and validate the GA optimization process.

5.2 Model and experiment validation

5.2.1 Background

Figure 5.1 shows a schematic illustration of the proposed nanocomposite to be used as a nano-based proximity sensor. The device consists of a flexible rectangular-shaped nanocomposite film with two probes (needles) of tungsten mounted across its ends. Th narrow strip of two ends were then coated with conductive silver paste. A dielectric (Thermoplastic polyurethane) acts as a substrate to restore charges and it is reinforced with Carbon Nano Tubes (CNTs) to make the dielectric conductive. The two electrodes are then connected through an external circuit to an impedance measurement setup. When the film sensor is subjected to vertical movement of an object, electric field among the probes is stolen from its surface and its surfaces charges migrate to the surface of the object.

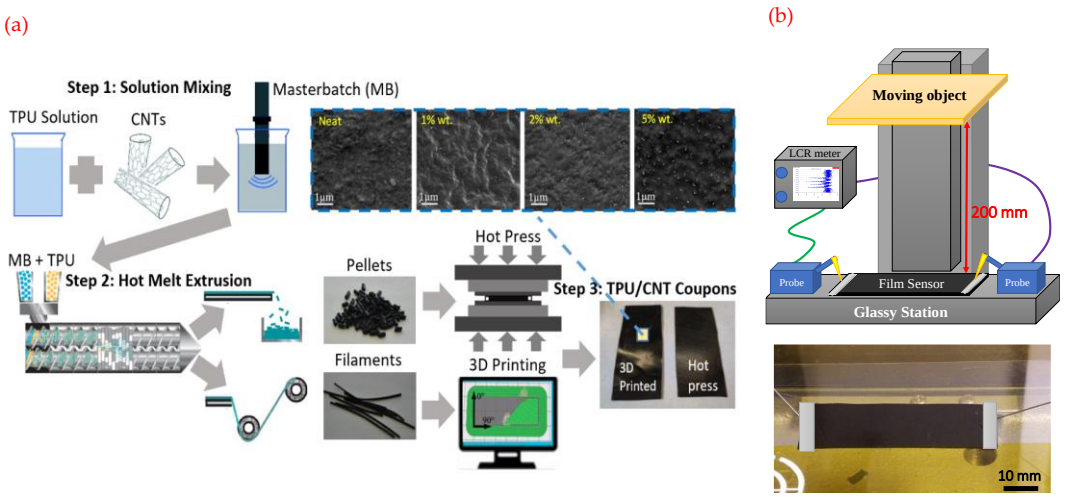

Figure 5.1. a) Proposed method to process-manufacture TPU with CNT nanocomposites. Step 1: Solution mixing of TPU and CNTs using probe sonication to prepare 10 wt% TPU/CNT masterbatch. Step 2: Melt extrusion to synthesize 1- 5 wt% TPU/CNT Pellets and Filaments. Step 3: Hot press of TPU/CNT coupons. SEM images of neat TPU, 1, 2, and 5 wt% TPU/CNT coupons. b) Schematic illustration of a TPU/CNT proximity sensor setup[43].

To recognize physics of the probing sensation, this sensing film (TPU-CNTs) constitutes two types of capacitors including a capacitor between neighboring probes (self-capacitance -C_s) and fringe capacitance (mutual capacitance-C_m), caused by the overlapping fringing field [43]. As shown in Figure 5.1 (a), when an object is quite far with respect to the film, the fringe capacitance between each probe with object is small. Approaching to the probes, the fringe field between film and the sensing object turn out to be significant, (Figure 5.2). In theory, shunting of the electric field changes the overall capacitance of the film. Hence, strength of electric field arising from film capacitor is shifted and weakened by the object, thus reducing the stored charges in the film capacitor. Moreover, the mutual capacitance of sensor enhances due to the reduced distance between probes and object while the capacitance of the actual film (self-capacitance) decreases owing to the change in the charge balance. Finding out an optimal nanocomposite sensor, different CNT contents were earlier investigated [43]. Absolute percentage change of capacitance to the initial capacitance at the different distance to the object was calculated and addressed as sensitivity. we earlier demonstrated that resistivity of the film sensor originated from CNTs amount can affect the sensitivity.

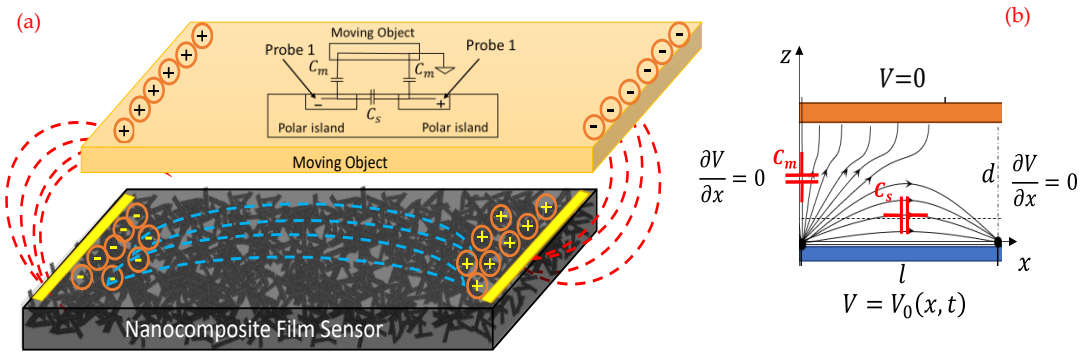

Figure 5.2. Schematic illustration of sensor mechanism for fringe-based TPU-CNT proximity sensor a) 3D model, charge distribution and fringe fields while object is in vicinity of the film sensor (b) Symmetric cross section of the rectangular-shaped sensor model with cartesian coordinate system demonstrates boundary conditions[149].

5.3 Experimental work

5.3.1 Material preparation

TPU and MWCNT were used as the constituents of the nanocomposite sensors. A set of prototypes of film sensors were fabricated for different dilution of CNTs. To obtain TPU-CNT films with 0.5-0.6 mm thickness, TPU/CNT 10 wt% masterbatch nanocomposites; TPU/CNT 1-5 wt% pellets and filaments (twin-screw extruder) as well as TPU/CNT hot press were prepared. Samples were cut out from the films in 60×20 mm squares. Figure 1 shows major steps of the proposed method to process and manufacture the final product. Need to say, preparing of sensor samples can be done also with 3D printing method.

5.3.2 Sensor Read-out characterization

While distances are ranging from 20 to 220 mm, the impedance analysis was performed by utilizing a probing station (Keithley 4200-SCS, Tektronix, USA). 60×20 mm nanocomposite coupons were either compression molded (Carver 3946, Carver Inc., Indiana, US) into films of 0.5-0.6 mm in thickness from pellets. A brass bar (sensing object -10 mm height×20 mm width×200 mm length) approached the TPU/CNT sensor with a speed of 6.6 mm/s. To detect the maximum change in capacitance, the samples were pre-soaked with 5V direct current to saturate and reduce the tunneling effect. Additionally, a 30-mV alternate current swiping signal was applied to measure the capacitance of the film with variable frequencies to achieve maximum stability of

the working window for the fabricated sensors considering the energy consumption. Figure 5.1 (a) and Figure 5.1 (b) represent the experimental setup and how change of capacitance to the initial capacitance ($\Delta C/C_0$) were analyzed. The full three set of experiments were completed for each CNT content. Other conditions, including temperature and humidity, were strictly controlled to obtain a accurate measurement. The thin strip of both ends of samples were then coated with conductive silver adhesive to erase the influence of contact resistance. The model parameters used for the tests are listed in Table 5.1.

Table 5.1. Experiment testing parameters and setup

Property (symbol)	**value**
TPU Density	1.12 (g/cm3)
MWCNT Density	1.75 (g/cm3)
Cost MWCNTs	20 $/grm
Dielectric Thickness	0.5 (mm)
Vacuum Permittivity	8.8542 (pF/m)
Film Sensor Resistivity	$1\text{-}10^5$ (Ω.m)
Frequency	100-1000 (kHz)
AC Voltage	30 mV
DC Voltage	5 V
Object's speed	6.6 mm/s

5.4 Methodology

5.4.1 Governing equation and numerical simulation

Schematic view of our proposed sensor along with a moving object and the fringe effect concept were shown in Figure 5.2. As observed, two-line electrodes are positioned at both side of the nanocomposite substrate. When a voltage is applied between the electrodes some amount of current flow inside the substrate resulting in charge distribution on the substrate. Furthermore, some fringing fields are being developed outside the substrate which contribute on the stored charge on the nanocomposite surface. The current passing on the electrodes is monitored and by dividing the current by the exciting voltage the effective capacitance can be measured. While the object gets closer to the nanocomposite sensor it distorts the fringing fields and consequently changes equivalent(self-capacitance). This characteristic of the system may be used to recognize the external object which is approaching the sensor. As Gauss's law indicates the amount of the stored charge on the right-hand side electrode decreases and therefore the measured capacitance declines too. Experimental measurements show this behavior of the system clearly [43]. In addition to experimental observations, an analytical analysis was accomplished with a couple of goals by the authors [149]. Firstly, an analytical solution (simulation) helps to higher level of understanding of what happens in the system and secondly quantization of the changes of capacitance with respect to the distance of the object not only helps in calibration of the sensor but also is beneficial in design of different sensors for various applications. Finally, this closed-form model (analytical simulation) will be employed to optimize the sensing system.

Since there is no free stored charge in the part of space enveloped between the polymer substrate and the surface of object, the following equation governs the distribution of voltage in this region:

$$\nabla^2 V(x, y, z, t) = 0 \tag{4.1}$$

This solution was obtained by application of Gauss, conservation of charge and Ohm laws into Laplace equation. The total impedance seen by the LCR meter was calculated through dividing the applied voltage (V_{exc}) to the input current (i). The real part of derived impedance signified the equivalent resistance owing to the finite resistivity of the nanocomposite substrate while its imaginary part characterized the equivalent capacitance between the electrodes and object. Therefore, the following expression was used for calculation of the equivalent capacitance of the system [149]:

$$C_{eq} = -\frac{\mathrm{Im}(i)}{\omega V_{exc}}, R_{eq} = -\frac{V_{exc}}{\mathrm{Re}(i)} \tag{4.2}$$

A comparison of analytical and experimental models is plotted in Figure 5.3a over 9cm (capacitance variation was normalized with respect to the initial capacitance). Both plots have displayed quite similar sensitivity behavior and reached to the peak of 0.5-0.6 at the distance of 3cm. Apparently, the analytical model results are a bit larger than the measured ones. This discrepancy is primarily originated by the object used in the measurement. In the analytical model, the object dimension ought to be assumed infinite, contrary to that of the *in-situ* object. Figure 5.3 (b) illustrates the analytically calculated voltage distribution within the neighboring area between the sensor and object at the certain values of resistivity (CNTs Content). The graph's horizontal axis shows the size of sensor length and, the vertical axis indicates the distance with the moving object. Furthermore, contour lines associated to certain values of the voltage are plotted together with vectors (in red) suggesting the magnitude and direction of the electric field at different points.

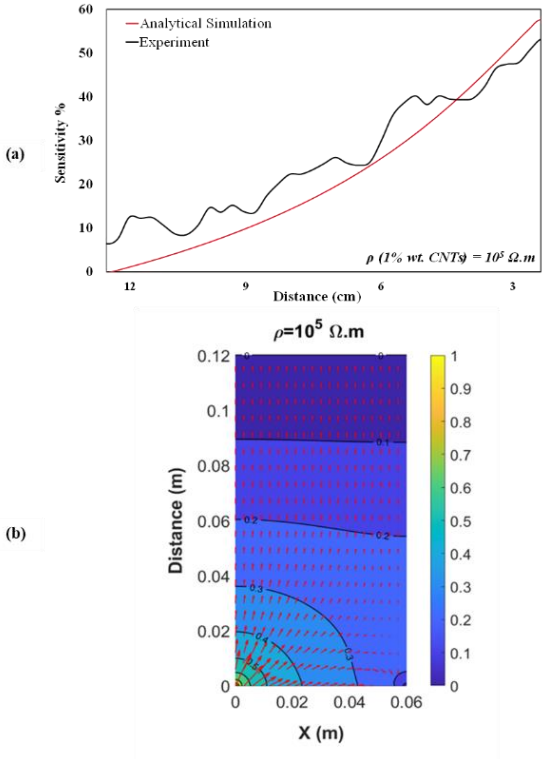

Figure 5.3. Sensing performance of the film sensor with 1% CNTs, ρ =10^5 Ω.m a) Sensitivity (change of capacitance to the initial) comparison simulation result versus experimental one b) Potential contour for the in-phase voltages between probes and object at the distance of 12 cm.

5.5 Artificial neural network (ANN)

ANN is among the best methods employed in machine learning (ML). It is created according to biological nervous systems and works based on the training-testing method. ANN is comprised of several components namely, input, hidden, and output layers, neurons, and connections. In ANN, the network gathers data from previously solved problems to establish an arrangement of neurons that comprehend solving a new investigated problem. This method is extensively used to predict complicated functions with several inputs and outputs which causes a considerable reduction in solving time.

The optimization process seeks the feasible domain of variables and then finds the objective functions in each iteration so as to find the optimum design variables. Considering multiple design variables, two objective functions as well as employing the closed-form simulation (analytical model) makes the process time-consuming. Using an accurate and fast approximation method raises the efficiency of the process and considerably reduces the optimization time. In the current work, Artificial Neural Network (ANN) is employed as a tool to achieve sensitivity of sensor based on previously obtained results.

In this study, a Multi-Layers Perceptron (MLP) network with layers, two hidden and one output layers, are defined. The training is accomplished by the Levenberg-Marquardt backpropagation training function. In the training procedure, minimization of Root Mean Square Error (RMSE) between the outputs and targets of the training set is considered as the criterion to evaluate the network performance. Figure 5.4 describes the design of neural network. x_1 to x_6 represent the defined design variables and O_1 to O_2 are the network's outputs namely sensitivity and cost. Table 5.2 shows the domain (the lower and upper limits) of all design variables. For (L) and (b) the limits were chosen so that they could be easily cut from the fabricated film sheets while still maintaining the assumption that the length to width ratio does not pass five. Excessive upper bounds that would lead to very big devices were also avoided. For (R) the lower bound is to ensure there is sufficient reinforced CNTs to make the dielectric semi-conductive while the upper bound is to avoid an excessively amount of current which is not feasible and consuming energy. For (h) the lower bound is the least possible thickness of a easily available dielectric sheet while the upper bound is to ensure that the thickness can be altered to match the other parameters as much as possible because it is unlikely to ever pass this value for the chosen resistance value. A 1000 samples dataset is provided by the MATLAB analytical script. The inputs of these samples are

generated randomly in the explained range in Table 5.2. This data set is entered into the ANN as the training data in order to comprehend the relationship between the inputs and the output. The architecture of the utilized ANN including the number of neurons and transfer functions of each layer are selected based on the latest studies [150, 151] and are described in Table 5.3.

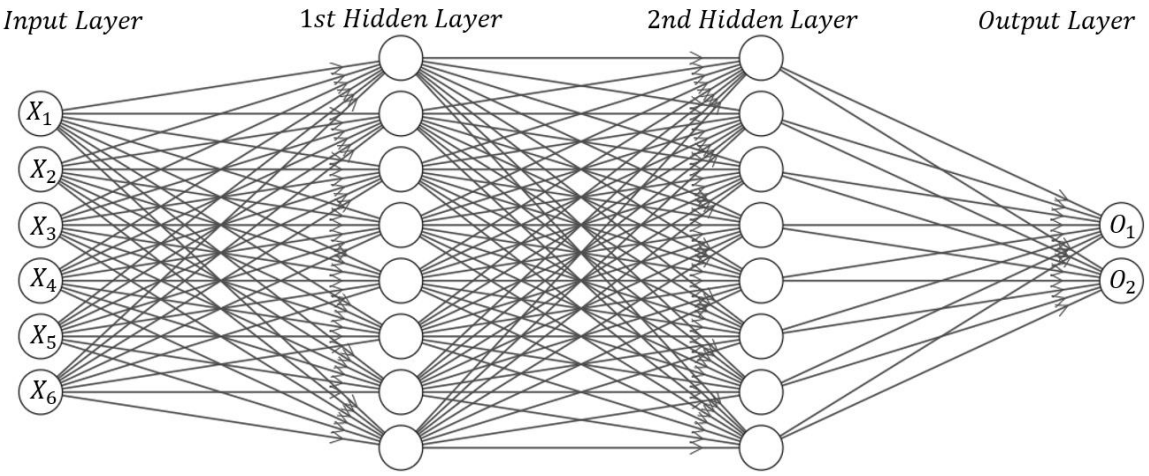

Figure 5.4. Schematic of implemented Neural Network for black-box modeling (with 1000 samples).

Table 5.2. Domains and characteristics of the variables

Variable		**Design Parameters**	**(Symbol)**	**Lower bound Min.**	**Upper bound Max.**
X_1		Device Thickness	h (mm)	0.5	1
X_2		Device Length	*L* (mm)	50	100
X_3		Device Width	*b* (mm)	20	50
X_4		Frequency	f (Hz)	10^3	10^7
X_5		Dielectric Relative Permittivity	ε_r	1	8
X_6		Impedance (resistivity)	ρ (Ohm.m)	10^2	10^5

Table 5.3. The architecture of ANN

1st Hidden Layer		**2nd Hidden Layer**		**Output Layer**		**Training samples**	**Testing samples**	**Validating samples**
neurons	Transfer fn.	neurons	Transfer fn.	neurons	Transfer fn.	80%	10%	10%
8	Tangent sigmoid	8	Tangent sigmoid	2	Linear			

5.6 Genetic Algorithm Optimization

The purpose of optimization process is finding the optimum range or value for objective functions and also determining the corresponding value of decision variable in which the optimum points are attained. Since, the fitness function of this study is highly non-linear the heuristic optimization methods have priority to be utilized for the optimization process[151]. Genetic Algorithm as one of evolutionary optimization methods is one of the most popular methods for optimizing complicated models. In this research non-dominated Genetic Algorithm (NSGA2) toolbox of MATLAB is used to optimize the proposed model. As it is mentioned in the previous section, the fitness function of optimization is the output network of ANN which has an acceptable runtime. The runtime of analytical model is around 10 minutes; however, the runtime of ANN black box model is around 13ms.

Figure 5.5 exhibits the flowchart of optimization and machine learning procedures. Accordingly, firstly the machine learning process is accomplished to train a black box model using one-thousands samples of inputs and outputs, and then the black-box model is considered the fitness function of the genetic algorithm to find the optimum solutions for sensitivity and cost of the proposed system.

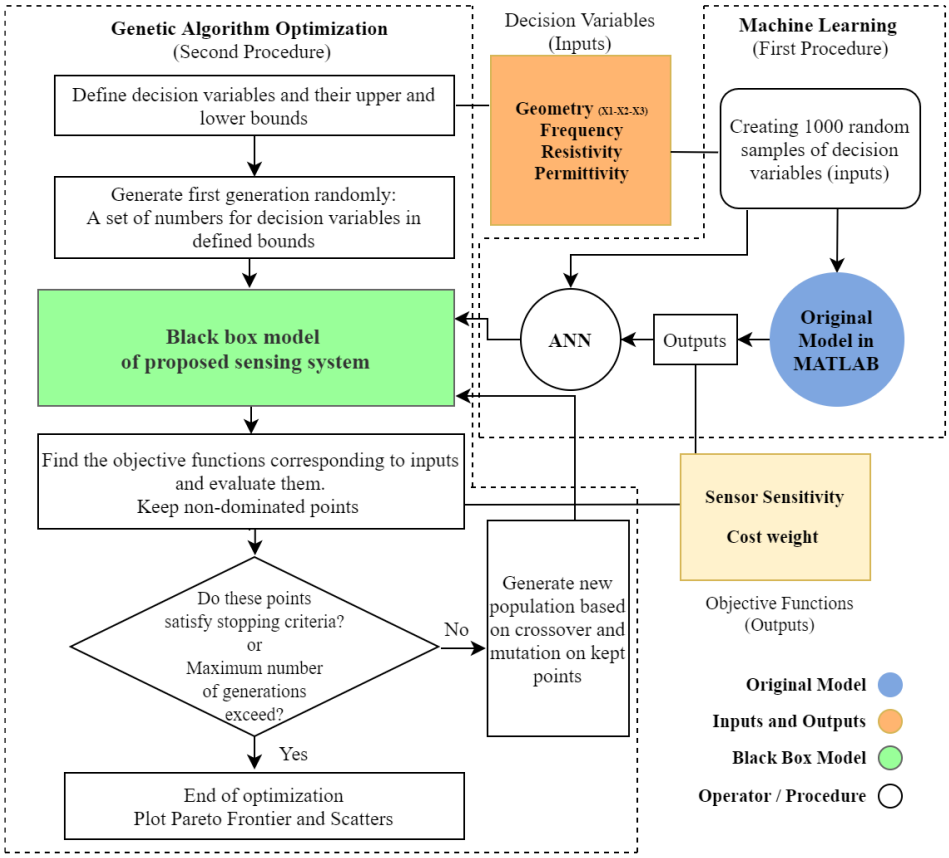

Figure 5.5. The flowchart of ANN and Genetic algorithm process and connections

5.7 Results and Discussion

5.7.1 ANN results

The Artificial Neural Network (ANN) has shown a perfect match with the original model. The root mean square error (RMSE) of sensitivity for different number of samples are calculated in order to show that the 1000 samples are enough for training an accurate network. Figure 5.6 illustrates the training, validation and testing errors of sensitivity for different number of samples from 100 to 1000. This figure which is also known as error elbow figure indicates that a higher number of samples than 600 is sufficient for training a neural network for the present dataset. It should be noted that Figure 5.6 shows the ANN results for CNT of 1.25% wt. and in this study all the 1000 samples are used to attain the most accuracy. Earlier in Table 5.3, the characteristics of ANN was presented. Accordingly, a network with two hidden layers containing 8 neurons shows a sufficient accuracy. The maximum relative network error that observed in the training were 0.56% and 2.89% for sensitivity and cost respectively.

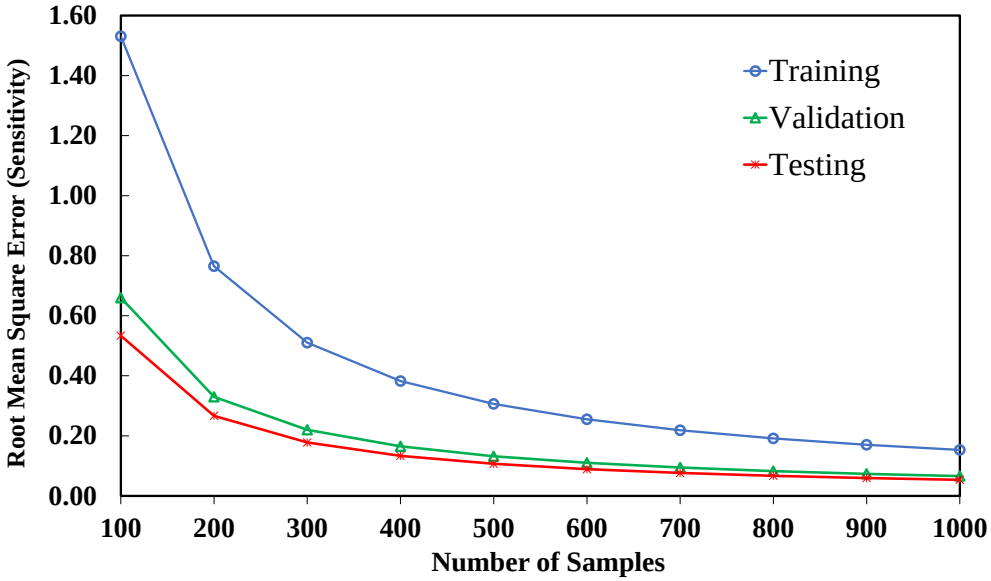

Figure 5.6. The effect of the number of samples on the RMSE of training, validation, and test sets.

5.7.2 Optimization results for 1.25% CNT

The result of sensitivity and cost dual-objective optimization of film sensors reinforced with 1.25% wt. CNT is presented in Figure 5.7. As it can be viewed, every point has a special input vector and two objective values, cost, and sensitivity. The blue points show all the generated points by Genetic Algorithm which are called as dominated points. The red points are the non-dominated optimum solutions which are also known as Pareto Frontier. The purple point is the ideal point which has the maximum sensitivity and minimum cost. The ideal point is not a feasible solution; however, it can be used for finding the best point of Pareto Frontier. The best point of Pareto Frontier is the closest point to the ideal point in a dimensionless environment which is presented in Figure 5.8. Genetic Algorithm searches the area inside the bounds which are presented in Table 5.2 to find the prominent members of the input vectors to have the maximum sensitivity at the minimum given cost. Among all solutions, Pareto-frontier curve illustrates the optimal solutions for the optimization problem. Each point of this curve defines a design variables vector, ($x_1 \ldots x_6$), which in turn has the maximum sensitivity for a corresponding cost. According to Figure 5.7, the ideal point has a sensitivity of 91%, and a cost of $4.7. The best point has a sensitivity of 87.02 % and a cost rate of 18.14 $.

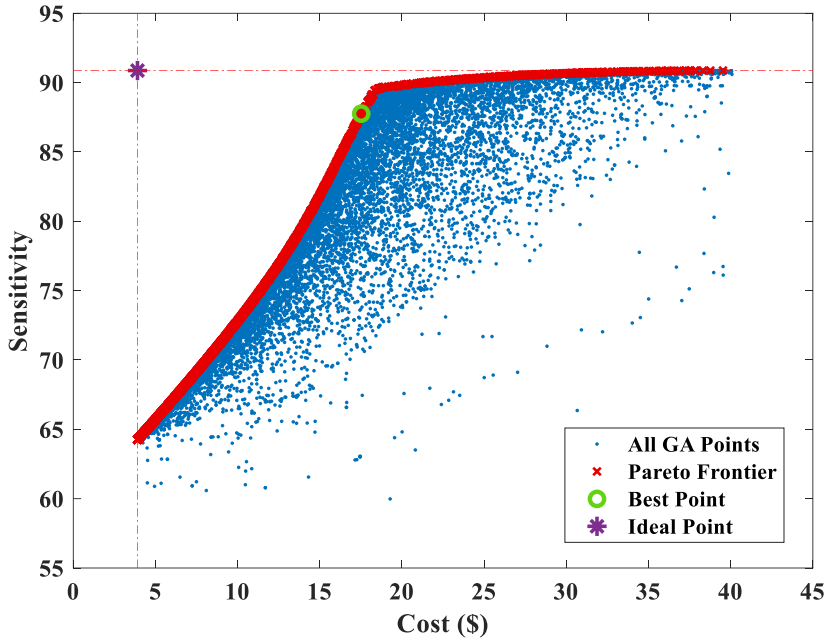

Figure 5.7. Pareto Frontier of cost and sensitivity as a result of optimization for nanocomposite sensor with 1.25 %wt.

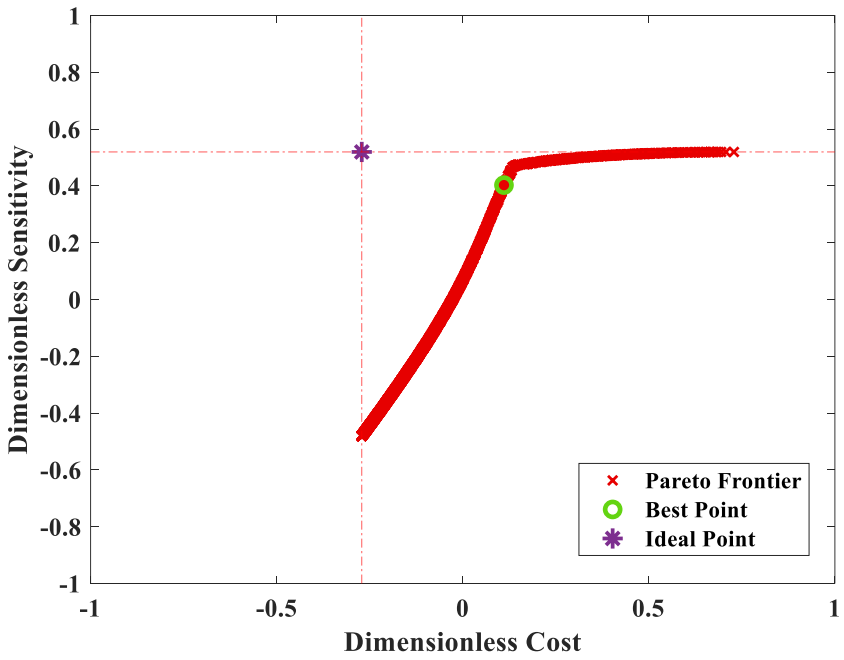

Figure 5.8. Dimensionless Pareto Frontier of cost and sensitivity as a result of optimization for nanocomposite sensor with 1.25 %wt.

5.7.3 Optimization results for all CNTs

Regarding the CNTs' functionality as the building blocks of the sensor, behavior of other film proximity sensors with different CNTs weight through a distance of 24 cm has been depicted in Figure 5.9. Earlier, it was shown that changing the percent of active materials (CNTs) used in the film sensor can significantly affect the sensitivity of the sensor[43]. So, a comprehensive study on the other CNTs percentage (resistivity) was needed.

As expected, Figure 5.9 demonstrates that highest sensitivity occurs where between 1-2% CNTs and it entirely follows our previous studies[43, 149]. They showed that the highest sensitivity at the certain distance happens occurs around the percolation threshold where the conductive pathways are fully constructed. Pareto-Frontier of 1.25% and 1.5 % CNTs exhibits a big shift from others. However, a film sensor with 1.5% CNTs illustrates a sharp slop at the beginning and the cost range is more limited in respect to other plots.

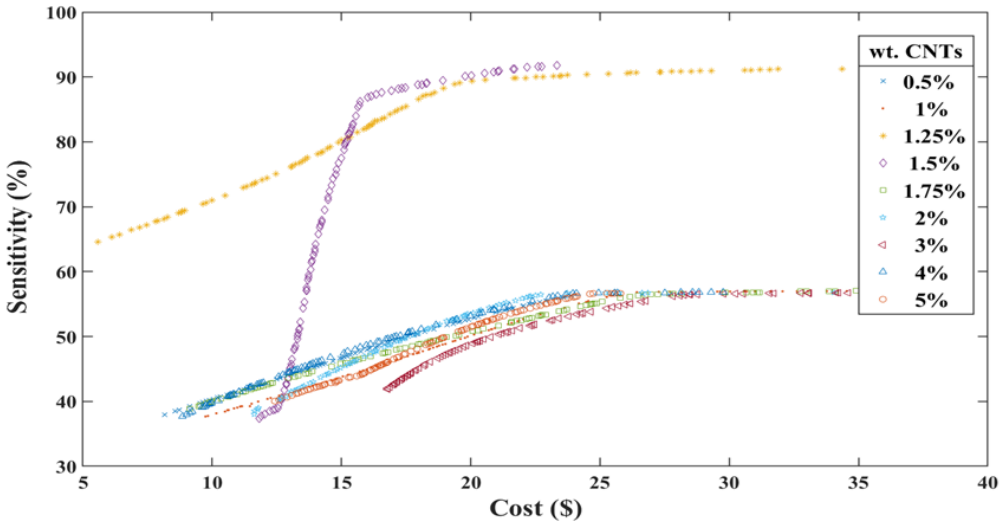

Figure 5.9. 2D Pareto Frontier of Sensitivity and cost of active materials, for different CNTs %wt.

With this in mind, the detailed values for decision variables and objective functions of best points are specified and depicted on table 8. On the right hand of the table, cost, ANN and analytical(simulation) sensitivity are listed. As

Table 5.4 shows, approximate (ANN) results are in acceptable agreement with analytical results. Geometry-related design variables (X_1, X_2, X_3) of the best points for different CNTs percentage

are almost in the same range. However, a wider range of change can be seen for property-related design variables (X_4, X_5, X_6). Hence, there is an agreeable certainty on the optimized geometry for all the film sensors. As the result of that, thickness, length, and width can be selected about 0.5 mm, 90mm, and 20 mm, respectively. On the other side, the value of property-based design variables such as frequency and system impedance does not have a significant pattern. For instances, a film sensor with 1.25% and 1.5 % CNTs, frequency and impedance show quite low magnitudes in respect with other weight of CNTs. It should be mentioned that a lower value of frequencies also results in energy usage reduction (about one hundreds of other CNTs weight).

Table 5.4. Detailed value for decision variables and objective functions of Pareto Frontier best points for different CNTs %wt.

	Inputs						**Outputs**			
CNTs %wt.	X_1 (10^{-4})	X_2	X_3	X_4 (10^{6})	X_5 (10^{-12})	X_6 (10^{4})	**Predicted by AAN**		**Calculated by Simulation**	
							Sensitivity %	**Cost $**	**Sensitivity %**	**Cost$**
0.5	5.012	0.0926	0.0201	1.2953	9.991	1.4463	54.05	21.014	54.53	20.94
1	5.0955	0.0857	0.0201	8.82	9.8964	6.0655	52.65	22.026	52.64	22.75
1.25	5.0658	0.0935	0.0202	0.096978	9.567	0.03092	87.02	18.14	84.70	21.49
1.5	5.2305	0.0503	0.0201	0.091565	9.2711	0.2268	85.35	15.64	83.12	16.89
1.75	5.0181	0.09199	0.02005	1.34906	9.99127	1.73746	54.00	20.96	54.39	20.85
2	5.0218	0.0944	0.02101	5.8707	9.1241	5.8509	55.24	21.37	55.18	21.51
3	5.2225	0.0956	0.0212	4.8568	9.1334	6.3342	56.35	23.06	56.45	22.71
4	5.2519	0.0977	0.0200	6.9567	9.8529	4.1619	56.07	23.07	56.07	23.38
5	5.1270	0.0782	0.02004	4.04022	9.7919	5.3694	50.12	19.108	50.14	18.34

5.7.4 Scatters of distribution for 1.25% CNT

Figure 5.10 illustrates the scatters of distribution for the different optimum design parameters with corresponding value for the objective functions. In this figure, the optimum value of design parameters for Pareto Frontier are presented in order of the population they are found in.

Using this figure, researchers can obtain what is the best range for decision variables in order to have a robust sensor in terms of sensitivity and cost. Evaluating Figure 5.10Figure 5.10 (a) and Figure 5.10 (d) demonstrate that all cases nearly take the minimum feasible value in the domain. However, regarding Figure 5.10 (b), length captures mostly the maximum possible value in the domain and the sensor performance is thought to be most affected by the length. The longer the sensor is being made the better sensitivity would be achieved. Therefore, this is mainly to increase the volume and subsequently the cost which is also raising up with the smaller slop and it finally reaches to maximum cost. Hence, an optimized proximity sensor can be achieved with fabrication of a thin strip film with a narrow width. This scatter plot also gives a solid perception on the properties effect. Figure 5.10 (d) shows that the operating frequency does not need to exceed 100 kHz to reach the optimum point. The smaller frequency the sensing system needs the lower energy it consumes. Regarding the permittivity and resistivity, the optimum point is obtained in the mid-range.

5.7.5 Parametric studies of different parameters on sensitivity

To illustrate the complexity of accurately assessing the direct impact of two input parameters at their bound, a 3D surface can be utilized to denote the objective function while the other parameters are varied. The sensitivity results and the most important parameters which influence more on the performance of the sensing device are illustrated in Figure 5.11. This section mostly focuses on two best Pareto-Frontier which noticeably show higher range of sensitivity. It is obvious that the objective function does not form a clearly convex shape for a film sensor with 1.25% wt. CNTs, however, there is a complete dome for one with 1.5% wt. CNTs (Figure 5.11 (b)). Furthermore, higher applied frequencies do not provide necessarily a better sensitivity. For both CNTs percentage, the maximum point could occur at the lower frequencies and similarly resistivities. No need to say, higher frequency and resistivity demand infinite amount of current which is very costly. Having lower amount of these parameters gives the manufacturer this certainty that energy consumption is seriously addressed in fabrication process. In addition, the effect of frequency and length can be observed simultaneously on the sensitivity for both CNTs weight in the photo. The sensitivity grows quite linear while these two changes over their domain. As expected, frequency becomes noticeable in those film sensors which are fabricated longer. . Lastly, we manufactured 1.25% wt. CNTs and did the experiment for the optimum value to have

further confirmation with the data obtained from the simulation. The cut-out film sensor showed a sensitivity of 85.92% with around 1% difference with ML.

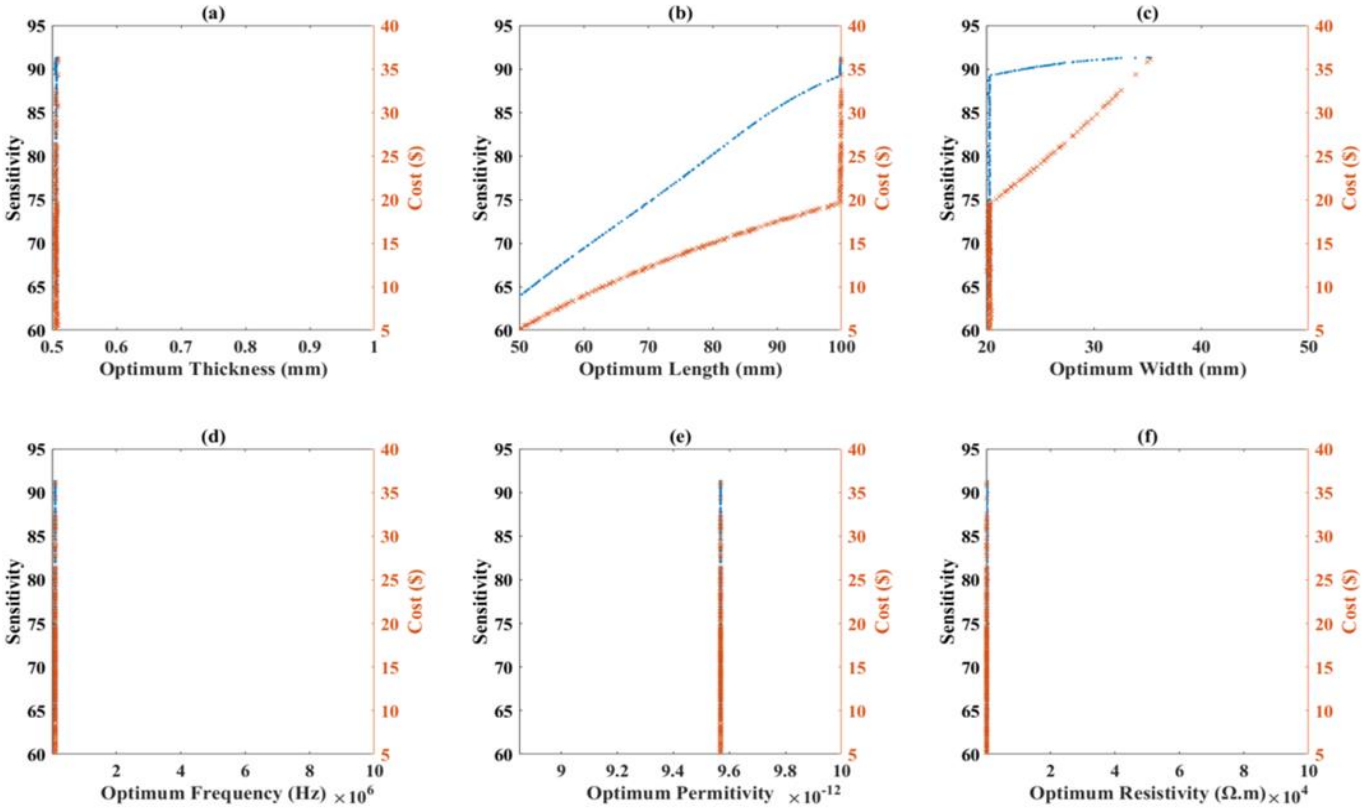

Figure 5.10. Scatter of distribution for different design parameters versus objective functions as a result of optimization for a sensor with 1.25% wt. CNTs.

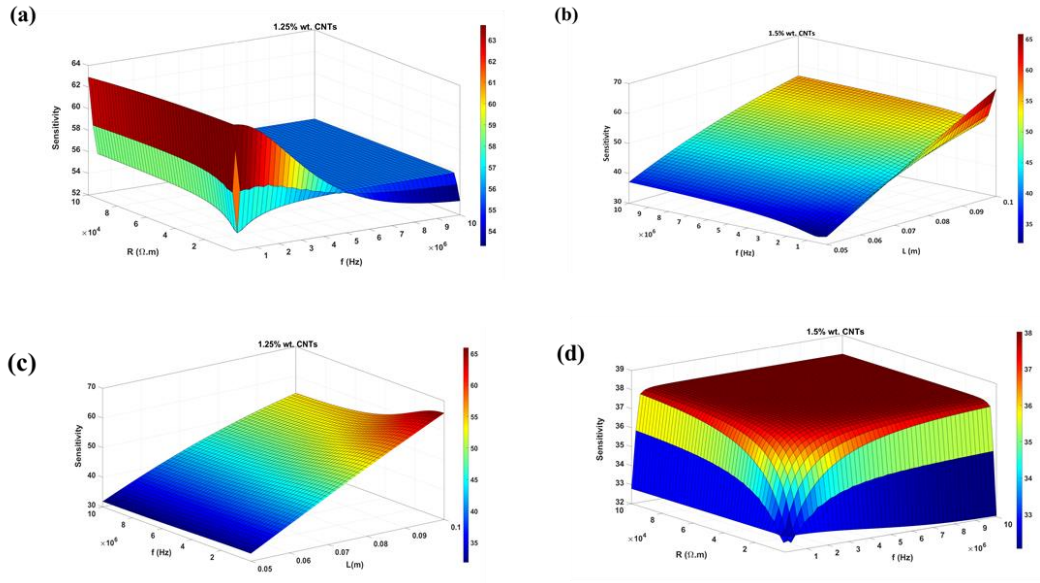

Figure 5.11. 3D effect of different input parameters on shape of objective function (sensitivity): a) Frequency & Resistivity for 1.25% wt. CNTs b) Frequency & Resistivity for 1.5% wt. CNTs c) Frequency & length for 1.25% wt. CNTs d) Frequency & length for 1.25% wt. CNTs

5.8 Conclusion

In this chapter, the multi-objective optimization of a nanocomposite proximity sensor was conducted considering two objective functions, namely, sensitivity, and cost. Six design variables including thickness, width, length, frequency, permittivity, and impedance of the film sensor were taken into account. The sensory system was manufactured, tested, and later analytically modeled in MATLAB. Running the analytical model is a time-consuming procedure since every run of Fourier series should be solved for at least 100 nodes which takes 10 min. The optimization process requires thousands of runs, and using the original model was impossible. An artificial neural network was used to simulate the sensing process and reduce the solution time. Utilizing the GA method, the maximum sensitivity load for each given CNTs percentage was obtained and the Pareto-frontier curve was generated. Results demonstrate that the thickness of the film sensor and its width tend to reach determined low values during the optimization process. In contrary, the sensor length follows the linear trend in which takes maximum values among optimum solutions. As expected, the nanocomposite sensor reaches the maximum sensitivity at the specific range of nanoparticle contents (1.0-1.5% CNTs). Moreover, the results shows that almost all of the optimum points on the Pareto-frontier curve have minimum thickness and frequency which depicts the importance of the thickness related to the other design variables.

6 SUMMARY AND FUTURE WORK

6.1 Summary and Conclusion

In chapter one, the topic of nanocomposite sensor was introduced with brief discussions of historical background, and outline of this study. Sensing mechanism and performance characteristics of different proximity sensor were also discussed. Capacitive based proximity sensor was focused, subsequently, theoretical analysis of this type of sensor.

Accordingly, in chapter two, a flexible ultrasensitive polymer-based proximity sensor was proposed. The TPU was reinforced by adding CNTs delivering the potential to adjust the sensitivity based on the electrical behavior of CNTs. The developed sensor was sensing based on the change of the capacitance that was mainly quantified by fringe effects. Although 1wt % CNTs showed higher sensitivity, 2wt % CNTs which was implied as percolation threshold exhibited lowest noise along with significant sensitivity. Fringing field and tunneling effects were addressed as two main explanations of observing the changes trend of the capacitance. Lastly, the numerical simulation results were capable of accurately following the fringe effect and showed decreasing trend of capacitance as previously shown in the experiments.

According to the physical cartesian model of fringe capacitances, chapter three established a 2-D analytical model of the potential, which was based on changing the measured capacitance of rectangular nanocomposite film sensor while an object approached in and moved away. In this work, the modeling of capacitive proximity sensors using the Laplace's equation has proven to be a fast and reliable technique to obtain the capacitance of a capacitive proximity sensor. The resistivity of sensor film demonstrated a significant effect on the sensitivity while it is in the range of 10^3-10^5 Ω.m. As a comparison, 1wt% CNT which its resistivity was measured around 10^5 Ω.m was plotted over the analytical results with a good agreement. The potential contour of our model has been compared for the different distances from the object, from the probes and for different resistivities.

In chapter four, additive manufacturing has been leveraged to fabricate form-and-fit prototypes in arbitrary geometries. To investigate whether control of filament orientation could affect CNT alignment and thereby enhance sensitivity of TPU/CNT sensors, 2 wt% TPU/CNT filaments were 3D printed from the extruded filaments to the same dimensions of those made by

hot press. The samples were manufactured for different filament orientations and their specific sensitivity ($|\Delta C/\rho C|$, where ρ is the sensor density) was compared with hot-press samples. Unlike the hot-press samples where CNT networks are random, 3D-printing of the TPU/CNT films allowed a custom design of these networks enabling manufacturing of proximity sensors with adjustable resistivity and capacitance.

In the chapter five, to have a better understanding which feature, and parameter can give us the most sensitivity we needed to do an optimization. This was accomplished by collecting experimental and computational results and using them as a basis for establishing a computationally and experimentally supported Genetic Algorithm Assisted Machine Learning (GAML) framework combined with artificial neural network (ANN) to develop TPU/CNT nanocomposite flexible sensors in which material characterizations were coupled to strain, tactile, electronic and proximity characteristics to probe intermolecular interactions between CNTs and polymers. The proposed framework provided enhanced predictive capabilities by managing multiple sets of data gathered from physical testing (material characterization and sensor testing) and multi-fidelity numerical models spanning all lengths scales. The GAML-ANN framework allowed the concurrent optimization of processing parameters and structural features of TPU/CNT nanocomposites, enabling fabrication of high-performance, lightweight flexible sensor systems.

6.2 Recommendation for Future Study

This section suggests further research efforts for continued investigations of proximity sensing phenomenon. Considering the current state of understanding of proximity sensing, there are several promising directions in which more research can be conducted. The mathematical model described in the previous chapters can be extended to include effects that are more comparable to experiments or in actual operation. We did some simplifications and also only considered a few numbers of nodes for Fourier series. The future work avenues are a result of initial project goals as well as investigations conducted during this study.

Furthermore, the additive manufacturing can help to optimize the navigation of the surface charges more efficiently and subsequently design of sensors with higher sensitivity and lower noise. These unprecedented observations open up new opportunities in the field of flexible proximity sensors which require further investigation. If one can run a molecular dynamic simulation on the process of printing of TPU-CNTs, it allows to understand how the 3D printing

can play a giant role in the realm of proximity sensors. Materialistically speaking, other active materials like nanowires and Graphene can be a fit alternative to CNTs since they are on the center of attention nowadays.

Optimization also can be done via different method and with a greater number of samples. Researcher would be capable of implementing optimization on the additive manufacturing of 3D printed samples. Samples can be printed with a couple of different printing parameters (design variable) and optimized based on those to get the film sensor printed with optimum functionality.

REFERENCES

[1] Y.-L. Chen *et al.*, "A Dual Sensing Modes Capacitive Tactile Sensor For Proximity and Tri-Axial Forces Detection," 2022: IEEE, pp. 710-713 %@ 1665409118.

[2] I. Mondal, M. K. Ganesha, A. K. Singh, and G. U. Kulkarni, "Inkjet Printing Aided Patterning of Transparent Metal Mesh for Wearable Tactile and Proximity Sensors," *Materials Letters*, pp. 131724 %@ 0167-577X, 2022.

[3] H. Lee, J. K. Mandivarapu, N. Ogbazghi, and Y. Li, "Real-time Interface Control with Motion Gesture Recognition based on Non-contact Capacitive Sensing," *arXiv preprint arXiv:2201.01755*, 2022.

[4] C. Ge *et al.*, "Capacitive Sensor Combining Proximity and Pressure Sensing for Accurate Grasping of a Prosthetic Hand," *ACS Applied Electronic Materials*, vol. 4, no. 2, pp. 869-877 %@ 2637-6113, 2022.

[5] Z. Zhang, J. Li, B. Yu, D. Huang, Q. Wang, and Z. Li, "Low-Cost, Flexible Annular Interdigital Capacitive Sensor (Faics) with Carbon Black-Pdms Sensitive Layer For Proximity and Pressure Sensing," 2022: IEEE, pp. 35-38 %@ 1665409118.

[6] A. J. Fleming, "A review of nanometer resolution position sensors: Operation and performance," *Sensors and Actuators A: Physical*, vol. 190, pp. 106-126 %@ 0924-4247, 2013.

[7] B. George, Z. Tan, and S. Nihtianov, "Advances in capacitive, eddy current, and magnetic displacement sensors and corresponding interfaces," *IEEE Transactions on Industrial Electronics*, vol. 64, no. 12, pp. 9595-9607 %@ 0278-0046, 2017.

[8] T. Grosse-Puppendahl *et al.*, "Finding common ground: A survey of capacitive sensing in human-computer interaction," 2017, pp. 3293-3315.

[9] T. Sivayogan, "Design and development of a contactless planar capacitive sensor," University of Toronto, 2013.

[10] M. R. Kulkarni *et al.*, "Transparent flexible multifunctional nanostructured architectures for non-optical readout, proximity, and pressure sensing," *ACS applied materials & interfaces*, vol. 9, no. 17, pp. 15015-15021, 2017.

[11] C. Tholin-Chittenden, J. F. P.-J. Abascal, and M. Soleimani, "Automatic parameter selection of image reconstruction algorithms for planar array capacitive imaging," *IEEE Sensors Journal,* vol. 18, no. 15, pp. 6263-6272 %@ 1530-437X, 2018.

[12] R. Moheimani, M. Agarwal, and H. Dalir, "3D-Printed Flexible Structures with Embedded Deformation/Displacement Sensing for the Creative Industries," 2021, p. 0534.

[13] S. Zeinali, S. Homayoonnia, and G. Homayoonnia, "Comparative investigation of interdigitated and parallel-plate capacitive gas sensors based on Cu-BTC nanoparticles for selective detection of polar and apolar VOCs indoors," *Sensors and Actuators B: Chemical,* vol. 278, pp. 153-164 %@ 0925-4005, 2019.

[14] W.-P. Chen, Z.-G. Zhao, X.-W. Liu, Z.-X. Zhang, and C.-G. Suo, "A capacitive humidity sensor based on multi-wall carbon nanotubes (MWCNTs)," *Sensors,* vol. 9, no. 9, pp. 7431-7444, 2009.

[15] K. Zhu, W. K. Lee, and P. W. T. Pong, "Non-contact capacitive-coupling-based and magnetic-field-sensing-assisted technique for monitoring voltage of overhead power transmission lines," *IEEE Sensors Journal,* vol. 17, no. 4, pp. 1069-1083 %@ 1530-437X, 2016.

[16] K. K. Sadasivuni, A. Kafy, L. Zhai, H. U. Ko, S. Mun, and J. Kim, "Transparent and flexible cellulose nanocrystal/reduced graphene oxide film for proximity sensing," *small,* vol. 11, no. 8, pp. 994-1002 %@ 1613-6810, 2015.

[17] D. Watzenig and C. Fox, "A review of statistical modelling and inference for electrical capacitance tomography," *Measurement Science and Technology,* vol. 20, no. 5, pp. 052002 %@ 0957-0233, 2009.

[18] H. Kim *et al.*, "Transparent, flexible, conformal capacitive pressure sensors with nanoparticles," *Small,* vol. 14, no. 8, pp. 1703432 %@ 1613-6810, 2018.

[19] N. Luo *et al.*, "Flexible piezoresistive sensor patch enabling ultralow power cuffless blood pressure measurement," *Advanced Functional Materials,* vol. 26, no. 8, pp. 1178-1187 %@ 1616-301X, 2016.

[20] M. Zhu *et al.*, "Self-powered and self-functional cotton sock using piezoelectric and triboelectric hybrid mechanism for healthcare and sports monitoring," *ACS nano,* vol. 13, no. 2, pp. 1940-1952 %@ 1936-0851, 2019.

[21] V. Kumar, A. Kumar, S. S. Han, and S.-S. Park, "RTV silicone rubber composites reinforced with carbon nanotubes, titanium-di-oxide and their hybrid: Mechanical and piezoelectric actuation performance," *Nano Materials Science*, vol. 3, no. 3, pp. 233-240 %@ 2589-9651, 2021.

[22] S. D. Min, C. Wang, D.-S. Park, and J. H. Park, "Development of a textile capacitive proximity sensor and gait monitoring system for smart healthcare," *Journal of Medical Systems*, vol. 42, no. 4, pp. 1-12 %@ 1573-689X, 2018.

[23] M. S. Sarwar, Y. Dobashi, C. Preston, J. K. M. Wyss, S. Mirabbasi, and J. D. W. Madden, "Bend, stretch, and touch: Locating a finger on an actively deformed transparent sensor array," *Sci. Adv.*, vol. 3, no. 3, p. e1602200, 2017, doi: 10.1126/sciadv.1602200.

[24] T. Addabbo, A. Fort, M. Mugnaini, S. Rocchi, and V. Vignoli, "A heuristic reliable model for guarded capacitive sensors to measure displacements," 2015: IEEE, pp. 1488-1491 %@ 1479961140.

[25] A. Arshad, S. Khan, A. H. M. Z. Alam, K. A. Kadir, R. Tasnim, and A. F. Ismail, "A capacitive proximity sensing scheme for human motion detection," 2017: IEEE, pp. 1-5 %@ 1509035966.

[26] M. Hosseini, G. Zhu, and Y.-A. Peter, "A new formulation of fringing capacitance and its application to the control of parallel-plate electrostatic micro actuators," *Analog Integrated Circuits and Signal Processing*, vol. 53, no. 2, pp. 119-128 %@ 1573-1979, 2007.

[27] B. Wang, J. Long, and K. H. Teo, "Multi-channel capacitive sensor arrays," *Sensors*, vol. 16, no. 2, p. 150, 2016.

[28] S. M[illegible]hlbacher-Karrer *et al.*, "A driver state detection system[illegible] Combining a capacitive hand detection sensor with physiological sensors," *IEEE transactions on instrumentation and measurement*, vol. 66, no. 4, pp. 624-636 %@ 0018-9456, 2017.

[29] Y. Ye, C. Zhang, C. He, X. Wang, J. Huang, and J. Deng, "A review on applications of capacitive displacement sensing for capacitive proximity sensor," *IEEE Access*, vol. 8, pp. 45325-45342 %@ 2169-3536, 2020.

[30] J. C. Maxwell, *A treatise on electricity and magnetism*. Clarendon press, 1873.

[31] S. Yao and Y. Zhu, "Wearable multifunctional sensors using printed stretchable conductors made of silver nanowires," *Nanoscale*, vol. 6, no. 4, pp. 2345-2352, 2014.

[32] A. Merdassi, P. Yang, and V. P. Chodavarapu, "A wafer level vacuum encapsulated capacitive accelerometer fabricated in an unmodified commercial MEMS process," *Sensors,* vol. 15, no. 4, pp. 7349-7359, 2015.

[33] S. Gong *et al.*, "A wearable and highly sensitive pressure sensor with ultrathin gold nanowires," *Nat. Commun.,* vol. 5, p. 3132, 2014, doi: https://doi.org/10.1038/ncomms4132.

[34] J. Yeow and J. She, "Carbon nanotube-enhanced capillary condensation for a capacitive humidity sensor," *Nanotechnology,* vol. 17, no. 21, p. 5441, 2006.

[35] Z. Spitalsky, D. Tasis, K. Papagelis, and C. Galiotis, "Carbon nanotube–polymer composites: chemistry, processing, mechanical and electrical properties," *Prog. Polym. Sci.,* vol. 35, no. 3, pp. 357-401 0079-6700, 2010, doi: https://doi.org/10.1016/j.progpolymsci.2009.09.003.

[36] S. Pourteimoor and H. Haratizadeh, "Performance of a fabricated nanocomposite-based capacitive gas sensor at room temperature," *Journal of Materials Science: Materials in Electronics,* vol. 28, no. 24, pp. 18529-18534, 2017.

[37] M. Kang, J. Kim, B. Jang, Y. Chae, J.-H. Kim, and J.-H. Ahn, "Graphene-based three-dimensional capacitive touch sensor for wearable electronics," *ACS nano,* vol. 11, no. 8, pp. 7950-7957, 2017, doi: https://doi.org/10.1021/acsnano.7b02474.

[38] K. Arapov, E. Rubingh, R. Abbel, J. Laven, G. de With, and H. Friedrich, "Conductive Screen Printing Inks by Gelation of Graphene Dispersions," *Adv. Funct. Mater.,* vol. 26, no. 4, pp. 586-593, 2016, doi: https://doi.org/10.1002/adfm.201504030.

[39] I. A. Kinloch, J. Suhr, J. Lou, R. J. Young, and P. M. Ajayan, "Composites with carbon nanotubes and graphene: An outlook," *Science,* vol. 362, no. 6414, pp. 547-553, 2018, doi: 10.1126/science.aat7439.

[40] Y. Abdi, A. Ebrahimi, S. Mohajerzadeh, and M. Fathipour, "High sensitivity interdigited capacitive sensors using branched treelike carbon nanotubes on silicon membranes," *Appl. Phys. Lett.,* vol. 94, no. 17, p. 173507, 2009, doi: https://doi.org/10.1063/1.3127533.

[41] S. K. Jindal, Y. K. Agarwal, S. Priya, A. Kumar, and S. K. Raghuwanshi, "Design and analysis of MEMS pressure transmitter using Machق│ôZehnder interferometer and artificial neural networks," *IEEE Sensors Journal,* vol. 18, no. 17, pp. 7150-7157 %@ 1530-437X, 2018.

[42] B. George, H. Zangl, T. Bretterklieber, and G. Brasseur, "A combined inductive–capacitive proximity sensor for seat occupancy detection," *IEEE transactions on instrumentation and measurement*, vol. 59, no. 5, pp. 1463-1470, 2010.

[43] R. Moheimani, N. Aliahmad, N. Aliheidari, M. Agarwal, and H. Dalir, "Thermoplastic polyurethane flexible capacitive proximity sensor reinforced by CNTs for applications in the creative industries," *Scientific reports*, vol. 11, no. 1, pp. 1-12, 2021.

[44] X. Sun *et al.*, "Flexible Tactile Electronic Skin Sensor with 3D Force Detection Based on Porous CNTs/PDMS Nanocomposites," *Nano-Micro Letters*, journal article vol. 11, no. 1, p. 57, July 16 2019, doi: 10.1007/s40820-019-0288-7.

[45] S. Khan, S. Tinku, L. Lorenzelli, and R. S. Dahiya, "Flexible tactile sensors using screen-printed P (VDF-TrFE) and MWCNT/PDMS composites," *IEEE Sens. J.*, vol. 15, no. 6, pp. 3146-3155, 2014, doi: 10.1109/JSEN.2014.2368989.

[46] H. Guo *et al.*, "A highly sensitive, self-powered triboelectric auditory sensor for social robotics and hearing aids," *Science Robotics*, vol. 3, no. 20, p. eaat2516, 2018, doi: 10.1126/scirobotics.aat2516.

[47] T. Kohama and S. Tsuji, "Tactile and proximity measurement by 3D tactile sensor using self-capacitance measurement," in *2015 IEEE SENSORS*, 2015: IEEE, pp. 1-4.

[48] A. Braun, R. Wichert, A. Kuijper, and D. W. Fellner, "Capacitive proximity sensing in smart environments," *Journal of Ambient Intelligence and Smart Environments*, vol. 7, no. 4, pp. 483-510, 2015.

[49] B. Zhang *et al.*, "Dual functional transparent film for proximity and pressure sensing," *Nano Research*, vol. 7, no. 10, pp. 1488-1496, 2014.

[50] K. Koibuchi, K. Sawa, T. Honma, T. Hayashi, K. Ueda, and H. Sasaki, "Loss estimation and sensing property enhancement for eddy-current-type proximity sensor," *IEEE transactions on magnetics*, vol. 42, no. 4, pp. 1447-1450, 2006.

[51] P. L. Fulmek, F. Wandling, W. Zdiarsky, G. Brasseur, and S. P. Cermak, "Capacitive sensor for relative angle measurement," *IEEE Transactions on Instrumentation and Measurement*, vol. 51, no. 6, pp. 1145-1149 %@ 0018-9456, 2002.

[52] M. Kalantari and M. Shayman, "Design optimization of multi-sink sensor networks by analogy to electrostatic theory," in *IEEE Wireless Communications and Networking Conference, 2006. WCNC 2006.*, 2006, vol. 1: IEEE, pp. 431-438.

[53] H. Askari, E. Asadi, Z. Saadatnia, A. Khajepour, M. B. Khamesee, and J. Zu, "A hybridized electromagnetic-triboelectric self-powered sensor for traffic monitoring: concept, modelling, and optimization," *Nano Energy,* vol. 32, pp. 105-116, 2017.

[54] R. Derakhshan, A. Ramiar, and A. Ghasemi, "Numerical investigation into continuous separation of particles and cells in a two-component fluid flow using dielectrophoresis," *Journal of Molecular Liquids,* vol. 310, p. 113211, 2020.

[55] T. Chen and N. Bowler, "Analysis of a capacitive sensor for the evaluation of circular cylinders with a conductive core," *Measurement Science and Technology,* vol. 23, no. 4, p. 045102, 2012.

[56] R. T. Sheldon and N. Bowler, "An interdigital capacitive sensor for nondestructive evaluation of wire insulation," *IEEE Sensors Journal,* vol. 14, no. 4, pp. 961-970, 2014.

[57] A. Rivadeneyra, J. Fernandez-Salmeron, M. Agudo-Acemel, J. A. Lopez-Villanueva, L. F. Capitan-Vallvey, and A. J. Palma, "Printed electrodes structures as capacitive humidity sensors: A comparison," *Sensors and Actuators A: Physical,* vol. 244, pp. 56-65, 2016.

[58] A. Mohd Syaifudin, S. Mukhopadhyay, and P. Yu, "Modelling and fabrication of optimum structure of novel interdigital sensors for food inspection," *International Journal of Numerical Modelling: Electronic Networks, Devices and Fields,* vol. 25, no. 1, pp. 64-81, 2012.

[59] A. I. Zia *et al.*, "Electrochemical impedance spectroscopy based MEMS sensors for phthalates detection in water and juices," in *Journal of Physics: Conference Series*, 2013, vol. 439, no. 1: IOP Publishing, p. 012026.

[60] M. L. Hammock, A. Chortos, B. C. K. Tee, J. B. H. Tok, and Z. Bao, "25th anniversary article: the evolution of electronic skin (e-skin): a brief history, design considerations, and recent progress," *Adv. Mater.*, vol. 25, no. 42, pp. 5997-6038, 2013, doi: https://doi.org/10.1002/adma.201302240.

[61] M. R. Kulkarni *et al.*, "Transparent flexible multifunctional nanostructured architectures for non-optical readout, proximity, and pressure sensing," *ACS Appl. Mater. Interfaces,* vol. 9, no. 17, pp. 15015-15021, 2017, doi: https://doi.org/10.1021/acsami.6b16840.

[62] B. Zhang *et al.*, "Dual functional transparent film for proximity and pressure sensing," *Nano Res.*, vol. 7, no. 10, pp. 1488-1496, 2014, doi: https://doi.org/10.1007/s12274-014-0510-3.

[63] T. D. Nguyen *et al.*, "Characterization and optimization of flexible dual mode sensor based on Carbon Micro Coils," *Materials Research Express,* vol. 5, no. 1, p. 015604, 2018.

[64] T. D. Nguyen *et al.*, "Highly sensitive flexible proximity tactile array sensor by using carbon micro coils," *Sensors and Actuators A: Physical,* vol. 266, pp. 166-177, 2017.

[65] K. K. Sadasivuni, A. Kafy, L. Zhai, H. U. Ko, S. Mun, and J. Kim, "Transparent and flexible cellulose nanocrystal/reduced graphene oxide film for proximity sensing," *Small,* vol. 11, no. 8, pp. 994-1002, 2015.

[66] R. B. Katragadda and Y. Xu, "A novel intelligent textile technology based on silicon flexible skins," *Sens. Actuators, A,* vol. 143, no. 1, pp. 169-174, 2008, doi: https://doi.org/10.1016/j.sna.2007.08.013.

[67] J. Shin *et al.*, "Bioresorbable optical sensor systems for monitoring of intracranial pressure and temperature," *Sci. Adv.,* vol. 5, no. 7, p. eaaw1899, 2019, doi: 10.1126/sciadv.aaw1899.

[68] W. Gao *et al.*, "Fully integrated wearable sensor arrays for multiplexed in situ perspiration analysis," *Nature,* vol. 529, no. 7587, p. 509, 2016, doi: https://doi.org/10.1038/nature16521.

[69] W. He *et al.*, "Integrated textile sensor patch for real-time and multiplex sweat analysis," *Sci. Adv.,* vol. 5, no. 11, p. eaax0649, 2019, doi: 10.1126/sciadv.aax0649.

[70] H. Guo *et al.*, "A highly sensitive, self-powered triboelectric auditory sensor for social robotics and hearing aids," *Sci. Rob.,* vol. 3, no. 20, p. eaat2516, 2018, doi: 10.1126/scirobotics.aat2516.

[71] R. F. Shepherd *et al.*, "Multigait soft robot," *Proc. Natl. Acad. Sci. U.S.A.,* vol. 108, no. 51, pp. 20400-20403, 2011, doi: https://doi.org/10.1073/pnas.1116564108.

[72] P. A. Schmidt, E. Maël, and R. P. Würtz, "A sensor for dynamic tactile information with applications in human–robot interaction and object exploration," *Rob. Auton. Syst.,* vol. 54, no. 12, pp. 1005-1014, 2006, doi: 10.1016/j.robot.2006.05.013.

[73] J. Park *et al.*, "Tactile-direction-sensitive and stretchable electronic skins based on human-skin-inspired interlocked microstructures," *ACS nano,* vol. 8, no. 12, pp. 12020-12029, 2014, doi: https://doi.org/10.1021/nn505953t.

[74] J. Kim *et al.*, "Stretchable silicon nanoribbon electronics for skin prosthesis," *Nat. Commun.,* vol. 5, p. 5747, 2014, doi: https://doi.org/10.1038/ncomms6747.

[75] B.-C. Zhang *et al.*, "Large-scale assembly of highly sensitive Si-based flexible strain sensors for human motion monitoring," *Nanoscale,* vol. 8, no. 4, pp. 2123-2128, 2016, doi: 10.1039/C5NR07546G.

[76] A. Atalay *et al.*, "Batch fabrication of customizable silicone-textile composite capacitive strain sensors for human motion tracking," *Adv. Mater. Technol.,* vol. 2, no. 9, p. 1700136, 2017, doi: https://doi.org/10.1002/admt.201700136.

[77] D. Y. Choi *et al.*, "Highly stretchable, hysteresis-free ionic liquid-based strain sensor for precise human motion monitoring," *ACS Appl. Mater. Interfaces,* vol. 9, no. 2, pp. 1770-1780, 2017, doi: https://doi.org/10.1021/acsami.6b12415.

[78] Y. Wu *et al.*, "A skin-inspired tactile sensor for smart prosthetics," *Sci. Rob.,* vol. 3, no. 22, p. eaat0429, 2018, doi: 10.1126/scirobotics.aat0429.

[79] S. Y. Kim, S. Park, H. W. Park, D. H. Park, Y. Jeong, and D. H. Kim, "Highly Sensitive and Multimodal All-Carbon Skin Sensors Capable of Simultaneously Detecting Tactile and Biological Stimuli," *Adv. Mater.,* vol. 27, no. 28, pp. 4178-4185, 2015, doi: https://doi.org/10.1002/adma.201501408.

[80] C. Yeom, K. Chen, D. Kiriya, Z. Yu, G. Cho, and A. Javey, "Large-area compliant tactile sensors using printed carbon nanotube active-matrix backplanes," *Adv. Mater.,* vol. 27, no. 9, pp. 1561-1566, 2015, doi: https://doi.org/10.1002/adma.201404850.

[81] S. Harada, K. Kanao, Y. Yamamoto, T. Arie, S. Akita, and K. Takei, "Fully printed flexible fingerprint-like three-axis tactile and slip force and temperature sensors for artificial skin," *ACS nano,* vol. 8, no. 12, pp. 12851-12857, 2014.

[82] I.-J. Cho, H.-K. Lee, S.-I. Chang, and E. Yoon, "Compliant ultrasound proximity sensor for the safe operation of human friendly robots integrated with tactile sensing capability," *J. Electr. Eng. Technol.,* vol. 12, no. 1, pp. 310-316, 2017, doi: https://doi.org/10.5370/JEET.2017.12.1.310.

[83] H.-K. Lee, S.-I. Chang, and E. Yoon, "Dual-mode capacitive proximity sensor for robot application: Implementation of tactile and proximity sensing capability on a single polymer platform using shared electrodes," *IEEE Sens. J.,* vol. 9, no. 12, pp. 1748-1755, 2009, doi: 10.1109/JSEN.2009.2030660.

[84] S. Tsuji and T. Kohama, "Proximity Skin Sensor using Time-of-flight Sensor for Human Collaborative Robot," *IEEE Sens. J.,* 2019, doi: 10.1109/JSEN.2019.2905848.

[85] K. Koibuchi, K. Sawa, T. Honma, T. Hayashi, K. Ueda, and H. Sasaki, "Loss estimation and sensing property enhancement for eddy-current-type proximity sensor," *IEEE Sens. J.*, vol. 42, no. 4, pp. 1447-1450, 2006, doi: 10.1109/TMAG.2006.871421.

[86] H. Zhang and J. A. Rogers, "Recent advances in flexible inorganic light emitting diodes: From materials design to integrated optoelectronic platforms," *Adv. Opt. Mater.*, vol. 7, no. 2, p. 1800936, 2019, doi: 10.1002/adom.201800936.

[87] L.-Y. Zhou, Q. Gao, J.-F. Zhan, C.-Q. Xie, J.-Z. Fu, and Y. He, "Three-dimensional printed wearable sensors with liquid metals for detecting the pose of snakelike soft robots," *ACS Appl. Mater. Interfaces*, vol. 10, no. 27, pp. 23208-23217, 2018, doi: https://doi.org/10.1021/acsami.8b06903.

[88] O. O. Ojuroye, R. N. Torah, A. O. Komolafe, and S. P. Beeby, "Embedded capacitive proximity and touch sensing flexible circuit system for electronic textile and wearable systems," *IEEE Sens. J.*, vol. 19, no. 16, pp. 6975-6985, 2019, doi: 10.1109/JSEN.2019.2911561.

[89] N. Aliheidari, N. Aliahmad, M. Agarwal, and H. Dalir, "Electrospun Nanofibers for Label-Free Sensor Applications," *Sensors*, vol. 19, no. 16, p. 3587, 2019, doi: http://dx.doi.org/10.1155/2015/140716.

[90] G. Langfelder, A. F. Longoni, A. Tocchio, and E. Lasalandra, "MEMS motion sensors based on the variations of the fringe capacitances," *IEEE Sens. J.*, vol. 11, no. 4, pp. 1069-1077, 2010, doi: 10.1109/JSEN.2010.2078499.

[91] C.-Y. Lee, G.-W. Wu, and W.-j. Hsieh, "Fabrication of micro sensors on a flexible substrate," *Sens. Actuators, A*, vol. 147, no. 1, pp. 173-176, 2008, doi: https://doi.org/10.1016/j.sna.2008.05.004.

[92] C.-X. Liu and J.-W. Choi, "Patterning conductive PDMS nanocomposite in an elastomer using microcontact printing," *J. Micromech. Microeng.*, vol. 19, no. 8, p. 085019, 2009, doi: https://doi.org/10.1088/0960-1317/19/8/085019.

[93] C. L. Choong *et al.*, "Highly stretchable resistive pressure sensors using a conductive elastomeric composite on a micropyramid array," *Adv. Mater.*, vol. 26, no. 21, pp. 3451-3458, 2014, doi: https://doi.org/10.1002/adma.201305182.

[94] L. Pan *et al.*, "An ultra-sensitive resistive pressure sensor based on hollow-sphere microstructure induced elasticity in conducting polymer film," *Nat. Commun.,* vol. 5, p. 3002, 2014, doi: https://doi.org/10.1038/ncomms4002.

[95] H. Vandeparre, D. Watson, and S. Lacour, "Extremely robust and conformable capacitive pressure sensors based on flexible polyurethane foams and stretchable metallization," *Appl. Phys. Lett.,* vol. 103, no. 20, p. 204103, 2013, doi: https://doi.org/10.1063/1.4832416.

[96] A. Daneshkhah, S. Vij, A. P. Siegel, and M. Agarwal, "Polyetherimide/carbon black composite sensors demonstrate selective detection of medium-chain aldehydes including nonanal," *Chem. Eng. J.,* p. 123104, 2019, doi: https://doi.org/10.1016/j.cej.2019.123104.

[97] S.-R. Kim, J.-H. Kim, and J.-W. Park, "Wearable and transparent capacitive strain sensor with high sensitivity based on patterned Ag nanowire networks," *ACS applied materials & interfaces,* vol. 9, no. 31, pp. 26407-26416, 2017.

[98] N. Hu, H. Fukunaga, S. Atobe, Y. Liu, and J. Li, "Piezoresistive strain sensors made from carbon nanotubes based polymer nanocomposites," *Sensors,* vol. 11, no. 11, pp. 10691-10723, 2011, doi: 10.3390/s111110691.

[99] M. Kim, J. Jung, S. Jung, Y. H. Moon, D.-H. Kim, and J. H. Kim, "Piezoresistive Behaviour of Additively Manufactured Multi-Walled Carbon Nanotube/Thermoplastic Polyurethane Nanocomposites," *Materials,* vol. 12, no. 16, p. 2613, 2019, doi: https://doi.org/10.3390/ma12162613.

[100] E. El Shafee, M. El Gamal, and M. Isa, "Electrical properties of multi walled carbon nanotubes/poly (vinylidene fluoride/trifluoroethylene) nanocomposites," *Journal of Polymer Research,* vol. 19, no. 1, p. 9805, 2012.

[101] H. Sun *et al.,* "Interfacial polarization and dielectric properties of aligned carbon nanotubes/polymer composites: The role of molecular polarity," *Composites Science and Technology,* vol. 154, pp. 145-153, 2018.

[102] S. Tsuji and T. Kohama, "Proximity Skin Sensor using Time-of-flight Sensor for Human Collaborative Robot," *IEEE Sensors Journal,* 2019.

[103] I.-J. Cho, H.-K. Lee, S.-I. Chang, and E. Yoon, "Compliant ultrasound proximity sensor for the safe operation of human friendly robots integrated with tactile sensing capability," *Journal of Electrical Engineering and Technology,* vol. 12, no. 1, pp. 310-316, 2017.

[104] M. S. Sarwar, Y. Dobashi, C. Preston, J. K. M. Wyss, S. Mirabbasi, and J. D. W. Madden, "Bend, stretch, and touch: Locating a finger on an actively deformed transparent sensor array," *Science Advances,* vol. 3, no. 3, p. e1602200, 2017, doi: 10.1126/sciadv.1602200.

[105] P. A. Schmidt, E. Maël, and R. P. Würtz, "A sensor for dynamic tactile information with applications in human–robot interaction and object exploration," *Robotics and Autonomous Systems,* vol. 54, no. 12, pp. 1005-1014, 2006.

[106] J. Shin *et al.*, "Bioresorbable optical sensor systems for monitoring of intracranial pressure and temperature," *Science Advances,* vol. 5, no. 7, p. eaaw1899, 2019, doi: 10.1126/sciadv.aaw1899.

[107] A. Atalay *et al.*, "Batch fabrication of customizable silicone-textile composite capacitive strain sensors for human motion tracking," *Advanced Materials Technologies,* vol. 2, no. 9, p. 1700136, 2017.

[108] Y. Wu *et al.*, "A skin-inspired tactile sensor for smart prosthetics," *Science Robotics,* vol. 3, no. 22, p. eaat0429, 2018, doi: 10.1126/scirobotics.aat0429.

[109] C. L. Choong *et al.*, "Highly stretchable resistive pressure sensors using a conductive elastomeric composite on a micropyramid array," *Advanced materials,* vol. 26, no. 21, pp. 3451-3458, 2014.

[110] S. Y. Kim, S. Park, H. W. Park, D. H. Park, Y. Jeong, and D. H. Kim, "Highly Sensitive and Multimodal All-Carbon Skin Sensors Capable of Simultaneously Detecting Tactile and Biological Stimuli," *Advanced materials,* vol. 27, no. 28, pp. 4178-4185, 2015.

[111] O. O. Ojuroye, R. N. Torah, A. O. Komolafe, and S. P. Beeby, "Embedded capacitive proximity and touch sensing flexible circuit system for electronic textile and wearable systems," *IEEE Sensors Journal,* vol. 19, no. 16, pp. 6975-6985, 2019.

[112] R. Matsuzaki and A. Todoroki, "Wireless flexible capacitive sensor based on ultra-flexible epoxy resin for strain measurement of automobile tires," *Sensors and Actuators A: Physical,* vol. 140, no. 1, pp. 32-42, 2007.

[113] G. Langfelder, A. F. Longoni, A. Tocchio, and E. Lasalandra, "MEMS motion sensors based on the variations of the fringe capacitances," *IEEE Sensors Journal,* vol. 11, no. 4, pp. 1069-1077, 2010.

[114] H.-K. Lee, S.-I. Chang, and E. Yoon, "Dual-mode capacitive proximity sensor for robot application: Implementation of tactile and proximity sensing capability on a single polymer platform using shared electrodes," *IEEE sensors journal,* vol. 9, no. 12, pp. 1748-1755, 2009.

[115] Z. Chen and R. C. Luo, "Design and implementation of capacitive proximity sensor using microelectromechanical systems technology," *IEEE Transactions on Industrial Electronics,* vol. 45, no. 6, pp. 886-894, 1998.

[116] X. Hu and W. Yang, "Planar capacitive sensors–designs and applications," *Sensor Review,* 2010.

[117] R. C. Luo and Z. Chen, "Modeling and implementation of an innovative micro proximity sensor using micromachining technology," in *Proceedings of 1993 IEEE/RSJ International Conference on Intelligent Robots and Systems (IROS'93)*, 1993, vol. 3: IEEE, pp. 1709-1716.

[118] R. C. Joy and E. Schlig, "Thermal properties of very fast transistors," *IEEE Transactions on Electron Devices,* vol. 17, no. 8, pp. 586-594, 1970.

[119] J. L. Novak and J. J. Wiczer, "A high resolution capacitive imaging sensor for manufacturing applications," Sandia National Labs., Albuquerque, NM (USA), 1990.

[120] B. Noltingk, N. BE, and N. AET, "THEORY AND APPLICATION OF A PROXIMITY GAUGE USING FRINGING CAPACITANCE," 1976.

[121] W.-C. Chuang, C.-W. Wang, W.-C. Chu, P.-Z. Chang, and Y.-C. Hu, "The fringe capacitance formula of microstructures," *Journal of micromechanics and microengineering*, vol. 22, no. 2, p. 025015, 2012.

[122] D. Y. Choi *et al.*, "Highly stretchable, hysteresis-free ionic liquid-based strain sensor for precise human motion monitoring," *ACS Appl. Mater. Interfaces* vol. 9, no. 2, pp. 1770-1780, 2017.

[123] E. MacDonald and R. Wicker, "Multiprocess 3D printing for increasing component functionality," *Science,* vol. 353, no. 6307, p. aaf2093, 2016.

[124] K. B. Perez and C. B. Williams, "Combining additive manufacturing and direct write for integrated electronics—a review," in *24th International Solid Freeform Fabrication Symposium—An Additive Manufacturing Conference, SFF*, 2013, pp. 962-979.

[125] T. Rahman, L. Renaud, D. Heo, M. Renn, and R. Panat, "Aerosol based direct-write micro-additive fabrication method for sub-mm 3D metal-dielectric structures," *Journal of Micromechanics and Microengineering*, vol. 25, no. 10, p. 107002, 2015.

[126] D. Espalin, D. W. Muse, E. MacDonald, and R. B. Wicker, "3D Printing multifunctionality: structures with electronics," *The International Journal of Advanced Manufacturing Technology*, vol. 72, no. 5-8, pp. 963-978, 2014.

[127] C. Kim *et al.*, "3D printed electronics with high performance, multi-layered electrical interconnect," *IEEE Access*, vol. 5, pp. 25286-25294, 2017.

[128] A. Panesar, M. Abdi, D. Hickman, and I. Ashcroft, "Strategies for functionally graded lattice structures derived using topology optimisation for additive manufacturing," *Additive Manufacturing*, vol. 19, pp. 81-94, 2018.

[129] S.-I. Park, D. W. Rosen, S.-k. Choi, and C. E. Duty, "Effective mechanical properties of lattice material fabricated by material extrusion additive manufacturing," *Additive Manufacturing*, vol. 1, pp. 12-23, 2014.

[130] J. H. Low *et al.*, "Hybrid tele-manipulation system using a sensorized 3-D-printed soft robotic gripper and a soft fabric-based haptic glove," *IEEE Robotics and Automation Letters*, vol. 2, no. 2, pp. 880-887, 2017.

[131] A. Hussein, L. Hao, C. Yan, R. Everson, and P. Young, "Advanced lattice support structures for metal additive manufacturing," *Journal of Materials Processing Technology*, vol. 213, no. 7, pp. 1019-1026, 2013.

[132] C. Chu, G. Graf, and D. W. Rosen, "Design for additive manufacturing of cellular structures," *Computer-Aided Design and Applications*, vol. 5, no. 5, pp. 686-696, 2008.

[133] A. Du Plessis, I. Yadroitsava, I. Yadroitsev, S. le Roux, and D. Blaine, "Numerical comparison of lattice unit cell designs for medical implants by additive manufacturing," *Virtual and Physical Prototyping*, vol. 13, no. 4, pp. 266-281, 2018.

[134] L. Hao, D. Raymont, C. Yan, A. Hussein, and P. Young, "Design and additive manufacturing of cellular lattice structures," in *The International Conference on Advanced Research in Virtual and Rapid Prototyping (VRAP). Taylor & Francis Group, Leiria*, 2011, pp. 249-254.

[135] M. Maghsoudi-Ganjeh, L. Lin, X. Wang, and X. Zeng, "Bioinspired design of hybrid composite materials," *International Journal of Smart and Nano Materials,* vol. 10, no. 1, pp. 90-105, 2019.

[136] V. Andalib and J. Sarkar, "A System with Two Spare Units, Two Repair Facilities, and Two Types of Repairers," *Mathematics,* vol. 10, no. 6, p. 852, 2022.

[137] S. Joshi and S. Boyd, "Sensor selection via convex optimization," *IEEE Transactions on Signal Processing,* vol. 57, no. 2, pp. 451-462, 2008.

[138] L. Fraleigh, M. Guay, and J. Forbes, "Sensor selection for model-based real-time optimization: relating design of experiments and design cost," *Journal of Process Control,* vol. 13, no. 7, pp. 667-678, 2003.

[139] H. Jin *et al.*, "Computational simulation using machine learning models in prediction of CO2 absorption in environmental applications," *Journal of Molecular Liquids,* p. 119159, 2022.

[140] M. A. Adly, M. H. Arafa, and H. A. Hegazi, "Modeling and optimization of an inertial triboelectric motion sensor," *Nano Energy,* vol. 85, p. 105952, 2021.

[141] X. Fu, P. Pace, G. Aloi, L. Yang, and G. Fortino, "Topology optimization against cascading failures on wireless sensor networks using a memetic algorithm," *Computer Networks,* vol. 177, p. 107327, 2020.

[142] S. Wang, M. Bi, Z. Cao, and X. Ye, "Linear freestanding electret generator for harvesting swinging motion energy: optimization and experiment," *Nano Energy,* vol. 65, p. 104013, 2019.

[143] C. Kim, M. Choi, T. Park, M. Kim, K. Seo, and H. Kim, "Optimization of yield monitoring in harvest using a capacitive proximity sensor," *Engineering in agriculture, environment and food,* vol. 9, no. 2, pp. 151-157, 2016.

[144] K. P. Ferentinos and T. A. Tsiligiridis, "Adaptive design optimization of wireless sensor networks using genetic algorithms," *Computer Networks,* vol. 51, no. 4, pp. 1031-1051, 2007.

[145] E. Masazade, R. Rajagopalan, P. K. Varshney, G. K. Sendur, and M. Keskinoz, "Evaluation of local decision thresholds for distributed detection in wireless sensor networks using multiobjective optimization," in *2008 42nd Asilomar Conference on Signals, Systems and Computers,* 2008: IEEE, pp. 1958-1962.

[146] M. Iqbal, M. Naeem, A. Anpalagan, A. Ahmed, and M. Azam, "Wireless sensor network optimization: Multi-objective paradigm," *Sensors*, vol. 15, no. 7, pp. 17572-17620, 2015.

[147] C.-F. Hu, W.-S. Su, and W. Fang, "Development of patterned carbon nanotubes on a 3D polymer substrate for the flexible tactile sensor application," *J. Micromech. Microeng.*, vol. 21, no. 11, pp. 115012 0960-1317, 2011, doi: 10.1109/MEMSYS.2010.5442331.

[148] N. Hu *et al.*, "Investigation on sensitivity of a polymer/carbon nanotube composite strain sensor," *Carbon*, vol. 48, no. 3, pp. 680-687 0008-6223, 2010, doi: https://doi.org/10.1016/j.carbon.2009.10.012.

[149] R. Moheimani, A. Pasharavesh, M. Agarwal, and H. Dalir, "Mathematical Model and Experimental Design of Nanocomposite Proximity Sensors," *IEEE Access*, vol. 8, pp. 153087-153097, 2020.

[150] A. Ehsani and H. Dalir, "Multi-objective optimization of composite angle grid plates for maximum buckling load and minimum weight using genetic algorithms and neural networks," *Composite Structures*, vol. 229, p. 111450, 2019.

[151] S. N. Naserabad, R. Rafee, S. Saedodin, and P. Ahmadi, "A novel approach of tri-objective optimization for a building energy system with thermal energy storage to determine the optimum size of energy suppliers," *Sustainable Energy Technologies and Assessments*, vol. 47, p. 101379, 2021.